Vibroacoustic modelling of a dowelled-joist timber floor using finite element methods

Thesis submitted in accordance with the requirements of the University of Liverpool for the degree of Master of Philosophy

by

Marios Filippoupolitis

School of Architecture, University of Liverpool

September 2014

Abstract

Timber floor systems are often used as separating floors between dwellings in multi-storey buildings as they are a sustainable, economical, lightweight solution. However, compared to concrete floors, typical timber joist floor systems tend to provide lower impact sound insulation in the low-frequency range (below 200 Hz).

The research in this thesis forms part of a project funded by the Swiss National Science Foundation to develop a new dowelled-joist timber floor using Swiss hardwood with the aim of improving the impact sound insulation below 200Hz. This floor consists of dowel-connected joists that form an assembly which can then be connected to other assemblies using metal screws. It is sufficiently complex that numerical models are required to give insight into its dynamic response and its sound radiation; hence in this thesis, finite element models are developed and validated to carry out this modelling.

Finite element models have been developed and validated against experimental modal analysis in terms of eigen-frequencies and mode shapes for individual beam assemblies and a complete dowelled-joist timber floor formed from three assemblies. Models of increasing complexity have been developed to find an approach that provides good agreement with experimental results. This has resulted in a model that use spring connections at the dowel positions combined with precise modelling of the boundary conditions at the two ends of the assemblies. Close agreement has been achieved between this model and results from experimental modal analysis with the differences between the eigen-frequencies in the majority of the mode pairs being less than 10 %. Close agreement has also been achieved in terms of modeshapes with MAC values greater than 80 % for the majority of the mode pairs.

For sound radiation from a rectangular plate into a rectangular room, a finite element model has been developed for fluid-structure interaction. The finite element model has been validated against a normal mode model for both a 140 mm and 180 mm concrete plate. This validated approach to modelling has then been used to predict sound radiation from the dowelled-joist timber floor into a rectangular room. In order to accommodate a finite element model of the dowelled-joist floor which had ‘virtual gaps’ between the joists it was necessary to introduce a ‘transfer plate’ to transfer the motion from the dowelled-joist timber floor to the acoustic medium. This approach appears to be novel as no mention of it has been found in the literature. Use of this transfer plate was validated in terms of both vibration and sound radiation. Compared to the concrete floors the dowelled-joist floor was found to have significant sound radiation around the 16Hz band (near the lowest eigen-frequency). The

work carried out in this thesis will enable future research to make a more detailed assessment of the impact sound insulation for the dowelled-joist timber floor.

For Iris,

Acknowledgments

I would like to thank my supervisor, Professor Carl Hopkins, for his support, advice and guidance during this year. I would like to acknowledge the opportunity he gave me to enter into the world of acoustics.

I would like also to thank Dr Gary Seiffert for his support and his positive vibe throughout my time in the Acoustics Research Unit.

Special thanks to my colleagues in the Acoustics Research Unit, especially Nuno Ferreira for our discussions about vibroacoustics and other various topics.

I would like to gratefully acknowledge the funding provided by the Swiss National Science Foundation (SNF) and the industrial partner of the project, Nägeli AG for providing the experimental specimens.

I thank Professor Ulrich Schanda, Raphael Völtl, Dr Jeffrey Mahn and Dr Lubos Krajci for providing me with all the experimental data needed for my research and for our positive cooperation in this project.

Finally, I would like to thank my parents and my brother, Dr Avgoustinos Filippoupolitis for their support and encouraging during my studies. Last but not least, I would like to thank my partner, Iris for her support and patience.

Contents

List of figures

List of tables

1. Introduction

1.1 Background and aim of the thesis

Timber floor systems are often used as separating floors between dwellings in multi-storey buildings as they are a sustainable, economical, lightweight solution. In Europe and North America these are typically timber joist floors with a floating floor and a resiliently suspended ceiling as shown in Figure 1-1. However, one disadvantage of typical timber joist floor systems can be the impact noise that is produced in the room below the floor from everyday activities such as walking. Concrete floors often have higher impact sound insulation than standard timber floor systems in the low frequency range (50-200 Hz) as indicated in Figure 1-2 (Hopkins, 2007).

A recent survey has shown that more occupants of timber frame buildings describe impact noise as causing considerable disturbance compared to those in concrete buildings even though they have been measured and rated to have similar impact sound insulation (Simmons, et al., 2011). For many decades it has been known that the use of the ISO tapping machine to measure impact sound insulation has problems, particularly with the rating of timber floors for footsteps and heavy impacts such as children running and jumping (see review in Hopkins, 2007). However, there is evidence that timber floors do produce significantly higher impact sound pressure levels from footsteps than concrete floors below 50Hz (Hopkins, 2007).

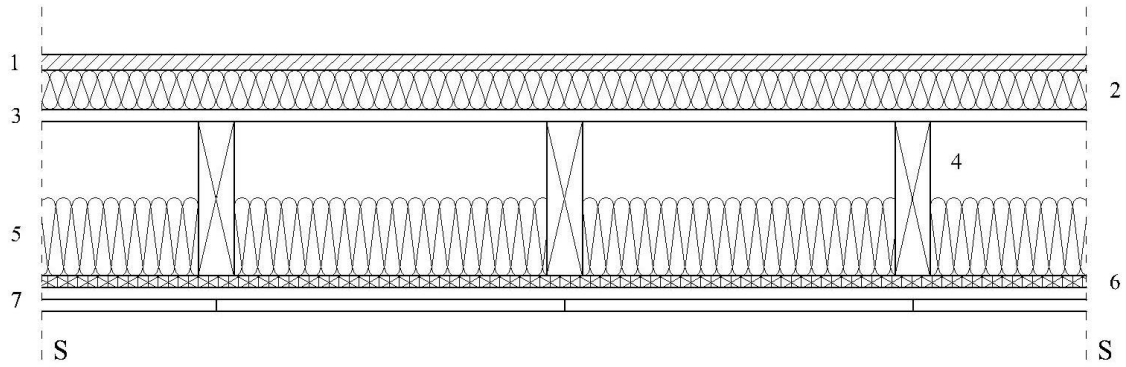

Figure 1-1 Typical timber joist floor (1) Timber board, (2) Mineral wool, (3) Timber board, (4) Timber joist, (5) Mineral wool, (6) Resilient bar (7) Plaster boards (two layers)

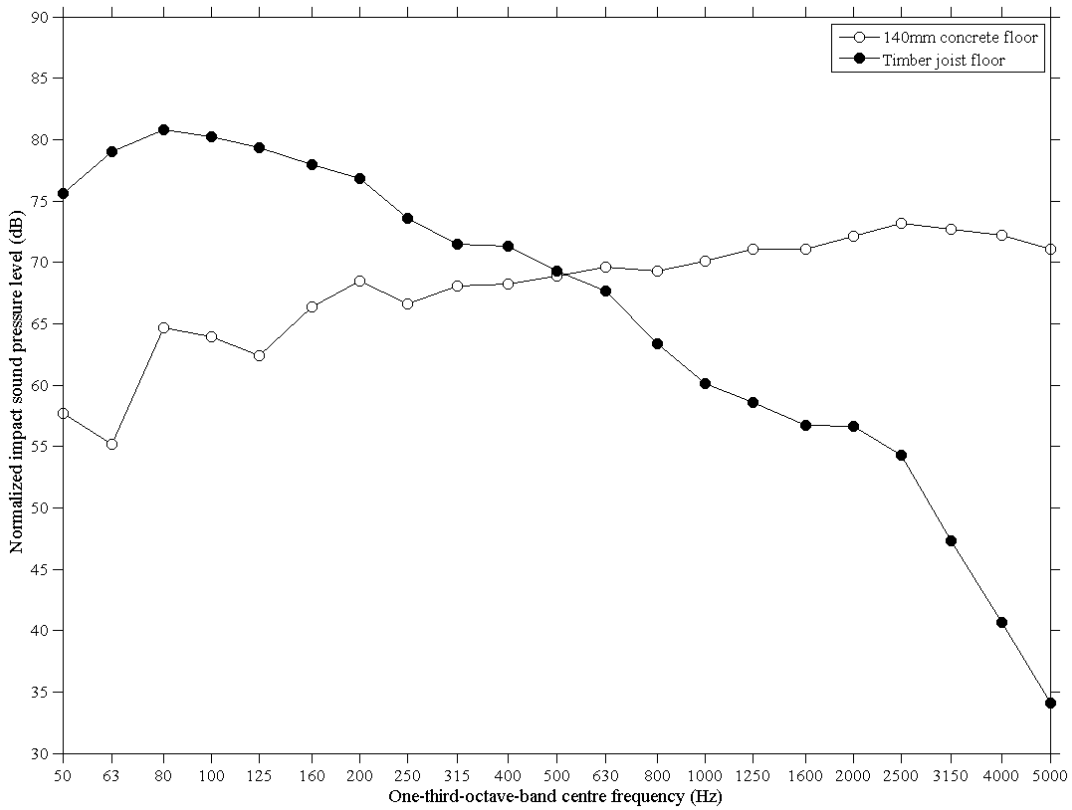

Figure 1-2 Comparison of impact sound insulation for a timber joist floor and concrete floor (both floors are without floating floor). Measured data taken from Hopkins, 2007.

The research in this thesis forms part of a project that was funded by the Swiss National Science Foundation to develop a new type of timber floor from Swiss hardwood which has improved impact sound insulation below 200Hz. This is a dowelled-joist timber floor.

There are two main aims in this thesis. The first is to develop and validate finite element models to assess the dynamic response of a dowelled-joist timber floor in terms of its local modes. The second is to validate finite element models for sound radiation from the floor under point force excitation on its surface, such as would occur with footsteps or the ISO tapping machine used for impact sound insulation measurements.

The dowelled-joist timber floor has a thickness of 200 mm and consists of individual assemblies of joists. Each assembly has a maximum width of 1250 mm and consists of joists (45 x 200 mm) connected using two rows of timber dowels (see Figure 1-3). The dowels are solid cylindrical rods that are used to hold parts together in a fixed alignment. The dowels have a diameter of 16 mm, follow a zigzag pattern and have a spacing of 250 mm in each row (see Figure 1-4). The assemblies are joined together using 240 mm metal screws with an angle of insertion approximately equal to 45 degrees and an average spacing of 313 mm.

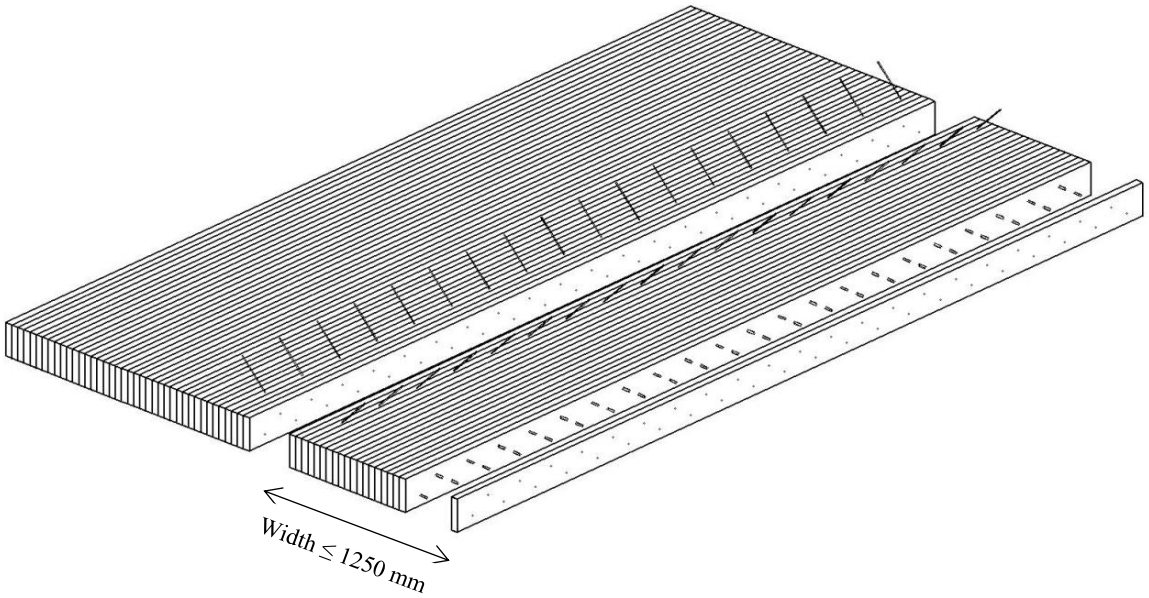

Figure 1-3 Dowelled-joist timber floor system comprised of individual assemblies joined together using metal screws

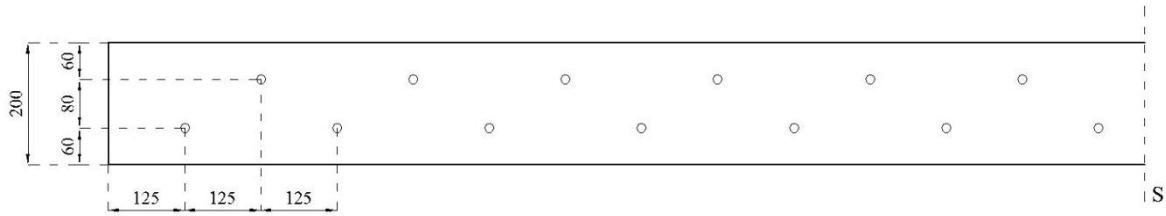

Figure 1-4 Side view of the joist (45 mm wide) showing the dowel pattern (units: millimetres)

Three individual assemblies (900 mm x 5500 mm) and one dowelled-joist timber floor formed from the three assemblies were provided by the industrial partner of the project, Nägeli and tested at the Rosenheim University of Applied Sciences in Germany in order to determine their material properties and their dynamic characteristics (i.e. eigen-frequencies and modeshapes).

Finite element models will be developed in the finite element software, Abaqus (Hibbitt et al., 2012) for the three individual assemblies and the dowelled-joist timber floor. The results of the experimental procedure will be used for the validation of the finite element models in terms of eigen-frequencies and modeshapes. The next step will be to validate Abaqus for the prediction of sound radiation from a plate into a room against a normal mode model. Then, the validated finite element model of the dowelled-joist timber floor will be used for the prediction of sound radiation from the floor into a room under point force excitation on its surface, using a vibroacoustic finite element model developed in Abaqus.

1.2 Outline of the thesis

The thesis structure is organised as follows.

Chapter 2 contains the literature review on the prediction of vibration and impact sound insulation of timber floors using finite element methods.

Chapter 3 contains the development and validation of finite element models for the structural modes of (1) a single beam, (2) three individual beam assemblies and (3) a dowelled-joist timber floor formed from the three assemblies.

Chapter 4 contains the validation of the finite element method against a normal mode model for the prediction of sound radiation from a 140mm and 180mm thick concrete plate into a box-shaped room.

Chapter 5 contains the development of a finite element model for the prediction of sound radiation from a dowelled-joist timber floor into a 'standard' room and the direct comparison with a 140 mm and 180 mm thick concrete plate in terms of sound radiation.

Chapter 6 contains the conclusions of this thesis and proposals for future work.

2. Theoretical background for the Finite Element Method

2.1 Introduction

The finite element method (FEM) is a computational technique used to obtain approximate solutions of boundary value problems in engineering (Hutton, 2004). The method was first applied in the late 1940s for sophisticated analysis of airframe structures. During the 1960s and 1970s it was extended to applications in plate bending, shell bending, pressure vessels and general three-dimensional problems in elastic structural analysis as well as to fluid flow and heat transfer (Hutton, 2004). More recently the method was extended to cover multiphysics (Khennane, 2013).

The fundamental concept is to divide the domain of interest (e.g. a structure) into a finite number of simple sub-domains (elements) and uses numerical methods (interpolation and integration) to construct an approximation of the solution over the collection of sub-domains (Mac Donald, 2013). With this approach, problems with complex geometry, complex boundary conditions or other complexities are possible to find an approximate solution whereas this was not possible before using analytical methods. Figure 2-1 shows the steps for finite element analysis as defined by Mac Donald (2013).

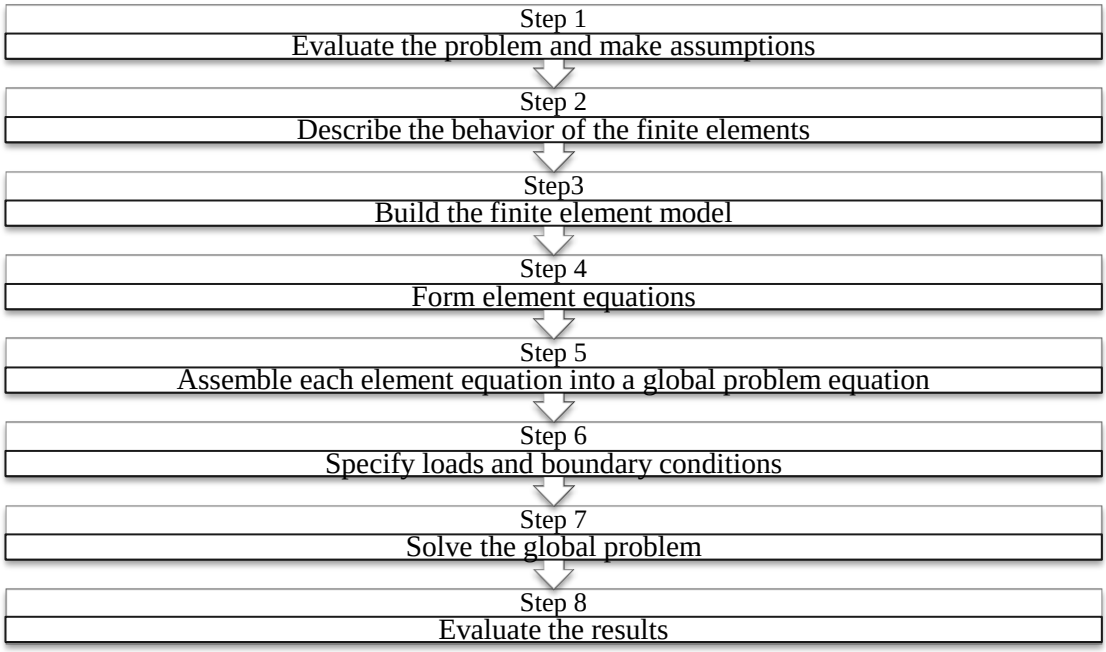

Figure 2-1 Steps in a finite element analysis (Mac Donald, 2013)

Today, many commercial finite element analysis software packages are available for use on personal computers to obtain solutions to large problems in static and dynamic analysis, heat transfer, fluid flow, electromagnetics, seismic response and acoustics. For the finite element models of this thesis the finite element software Abaqus was used and especially the programs Abaqus/Standard and Abaqus/CAE.

Abaqus is a suite of engineering software, based on the finite element method that can solve problems ranging from simple linear analyses to complex non-linear simulations (Hibbitt et al., 2012). Abaqus/standard is a general-purpose analysis program that can solve a wide range of linear and nonlinear problems involving the static, dynamic, thermal, electrical, and electromagnetic response of components (Hibbitt et al., 2012). Abaqus/CAE is an interactive environment used to create finite element models, submit Abaqus analyses, monitor and diagnose jobs, and evaluate results (Hibbitt et al., 2012).

2.2 Validation of finite element models

A perfectly computed finite element solution is of absolutely no value if it corresponds to the wrong problem (Hutton, 2004). For this reason it is necessary to validate any finite element model using experimental results or analytical solutions.

A well-known procedure for the validation of finite element models is the comparison of their dynamic characteristics (i.e. eigen-frequencies and mode shapes) with data acquired from a vibration test (Friswell & Mottershead, 1995). For the comparison of mode shapes the most wide used correlation criteria are the modal assurance criterion (MAC) and the coordinate modal assurance criterion (CoMAC).

2.2.1 Modal assurance criterion (MAC)

MAC is a commonly used method for assessing the degree of correlation between any two vectors and provides a measure of the least-squares deviation of the points from the straight line correlation. It is calculated using (Ewins, 2000),

$$MAC(X_i, A_j) = \frac{\left|\{X_i\}^T\{A_j\}\right|^2}{\left[(\{X_i\}^T\{X_i\}) * \left(\{A_j\}^T\{A_j\}\right)\right]} \quad (1)$$

where X_i is the number of the experimental mode shape, A_j is the number of the computational mode shape, $\{X_i\}$ is the matrix of the correlation points from the experimental data and $\{A_j\}$ is the matrix of the correlation points from the numerical data.

Application of equation (1) results a scalar number between 0 and 1. MAC values close to 1 indicate well correlated modes while MAC values close to 0 indicate uncorrelated modes (Ewins, 2000).

2.2.2 Coordinate modal assurance criterion (CoMAC)

The coordinate modal assurance criterion (CoMAC) is an extension of the modal assurance criterion that gives an indication of the contribution of each correlation point to the MAC values. In other words, CoMAC tries to identify where the mode shapes of a structure from two sets of data do not correlate. It is calculated using (Heylen & Avitabile, 1998),

$$CoMAC(k) = \frac{(|\{X_k\}||\{A_k\}|)^2}{[(\{X_k\}^T\{X_k\}) * (\{A_k\}^T\{A_k\})]} \quad (2)$$

where k is the number of the correlation point, $\{X_k\}$ is the matrix of the experimental modal coefficients for the correlation point k and $\{A_k\}$ is the matrix of the computational modal coefficients for the correlation point k.

Application of equation (2) results a scalar number between 0 and 1. CoMAC values close to 1 indicate high correlation while values close to 0 indicate low correlation (Heylen & Avitabile, 1998).

2.3 Analysis methods for the prediction of vibrations in floor systems

2.3.1 Eigenvalue analysis

The eigenvalue analysis is a computationally inexpensive analysis method that extracts the natural frequencies and mode shapes of vibration of a mechanical system, using the elastic (stiffness, K) and inertia (mass, M) characteristics of the system (Hutton, 2004).

It is a valuable tool in the hands of engineers since the results of the eigenvalue analysis (i.e. eigenfrequencies and mode shapes) are often used for the validation and updating of the finite element models.

For a multi-degree of freedom system (*N*-DOF), such as a floor structure, the eigenvalue problem can be written as (Chopra, 2006),

$$\left[[K] - {\omega_n}^2[M]\right]\{\Phi_n\} = 0 \tag{3}$$

where $[K]$ is the stiffness matrix of the system, $[M]$ is the mass matrix of the system, ω_n is the natural circular frequencies of vibration and $\{\Phi_n\}$ is the matrix of the natural modes of vibration.

The natural circular frequencies of an *N*-DOF system can be obtained by solving equation (4), (Chopra, 2006). This equation has *N* roots and each root corresponds to one independent natural circular frequency, ω_n of the system.

$$det\left[[K] - {\omega_n}^2[M]\right] = 0 \tag{4}$$

By replacing in equation (3) the *N* natural circular frequencies, ω_n of the system, we obtain *N* independent vectors of the natural modes of vibration, $\{\Phi_n\}$. The natural modes, $\{\Phi_n\}$ and $\{\Phi_r\}$ corresponding to different natural circular frequencies, ω_n and ω_r must satisfy the following orthogonality criterion (Chopra, 2006),

$$\left\{{\Phi_n}^T\right\}[K]\{\Phi_r\} = 0 \qquad \left\{{\Phi_n}^T\right\}[M]\{\Phi_r\} = 0 \tag{5}$$

Orthogonality makes the modal solutions independent and the corresponding modeshapes normal. It also makes the infinite set of modal solutions a complete set, or a basis, so that any arbitrary response can be formed as a linear combination of these normal mode solutions (de Silva, 2005).

In Abaqus/Standard there are three eigenvalue extraction methods: a) Lanczos, b) Automatic multi-level substructuring (AMS) and c) Subspace iteration. Lanczos is the default eigensolver in Abaqus/Standard and is the only one which allows structural-acoustic coupling (Hibbitt et al., 2012). For this reason, Lanczos is used throughout this thesis.

2.3.2 Steady-state dynamic analysis

Steady-state dynamic analysis provides the steady-state amplitude and phase of the response of a system due to harmonic excitation at a given frequency. Usually such analysis is done as

a frequency sweep by applying the loading at a series of different frequencies and recording the response (Hibbitt et al., 2012).

For a multi degree of freedom system that exhibits harmonic excitation, the equation of motion can be written as (Petyt, 2010),

$$[M]\{\ddot{u}\} + [C]\{\dot{u}\} + [K]\{u\} = \{f\}\exp(i\omega t) \quad (6)$$

where $\{u\}$ is the column matrix of nodal displacements, $[M]$ is the mass matrix, $[C]$ is the damping matrix, $[K]$ is the stiffness matrix, $\{f\}\exp(i\omega t)$ is the column matrix of equivalent harmonic nodal forces and ω is the circular frequency of the harmonic forces.

In Abaqus/Standard there are three methods for solving steady-state dynamic analysis problems: a) the direct-solution, b) the mode-based and c) the subspace-based steady-state dynamic analysis (Hibbitt et al., 2012). However, in this thesis only the first two methods are used as significant errors occurred with method (c).

2.3.2.1 Direct-solution steady-state dynamic analysis

In a direct-solution steady-state analysis the steady-state harmonic response is calculated directly in terms of the physical degrees of freedom of a system using the mass, $[M]$, damping, $[C]$, and stiffness matrices of the system, $[K]$.

The solution of equation (6) is (Petyt, 2010),

$$\{u\} = \left[[K] - \omega^2[M] + i\omega[C]\right]^{-1}\{f\}\exp(i\omega t) \quad (7)$$

The advantage of this method is that the eigen-frequencies and eigen-modes of the system do not have to be calculated prior to the response analysis (Petyt, 2010). However, this type of analysis is computationally more expensive than the mode-based steady-state dynamic analysis. When frequency-dependent material damping is involved the direct- solution steady-state analysis offers more accurate solutions (Hibbitt et al., 2012).

2.3.2.2 Mode-based steady-state dynamic analysis

In a mode-based steady-state dynamic analysis the response is based on modal superposition techniques where the modes of the system must first be extracted using the eigenfrequency extraction procedure.

The modal mass matrix, $[\bar{M}]$, the modal damping matrix, $[\bar{C}]$ and the modal stiffness matrix, $[\bar{K}]$ of the system are given by (Petyt, 2010),

$$\begin{aligned}[\bar{M}] &= [\Phi^T][M][\Phi] \\ [\bar{C}] &= [\Phi^T][C][\Phi] \\ [\bar{K}] &= [\Phi^T][K][\Phi]\end{aligned} \tag{8}$$

where $[\Phi]$ is the matrix of the eigenmodes, $[M]$ is the mass matrix, $[C]$ is the damping matrix and $[K]$ is the stiffness matrix of the system.

If equation (5) is satisfied and using the formulas of equation (8) the solution of equation (6) can be expressed in the form (Petyt, 2010),

$$\{u\} = [\Phi]\left[[\Lambda] - \omega^2[I] + i\omega[\bar{C}]\right]^{-1}[\Phi]^T\{f\}\exp(i\omega t) \tag{9}$$

where $\{u\}$ is the column matrix of nodal displacements, [Φ] is the matrix of the eigenmodes, [Λ] is the diagonal matrix of the circular frequencies of the system equal to $[\bar{K}]$, $[I]$ is the unit matrix, $[\bar{C}]$ is the modal damping matrix, ω is the circular frequency of the harmonic forces and $\{f\}\exp(i\omega t)$ is the column matrix of equivalent harmonic nodal forces.

In a mode-based steady-state analysis the number of modes extracted must be sufficient to model the dynamic response of the system adequately. This type of analysis is computationally cheaper than the direct-solution steady-state dynamic analysis. However, when frequency-dependent material damping is involved the mode- based steady-state analysis offers less accurate solutions (Hibbitt et al., 2012).

2.4 Coupled fluid-structure analysis for the prediction of sound radiation from a structure

When a flexible plate is vibrating into a rectangular cavity, the acoustic field in the cavity is influenced by the motion of the plate and the vibration of the plate is perturbed by the fluid pressure loading (Fahy & Gardonio, 2007).

When finite element methods are used for the analysis of this system the acoustic medium of the cavity is modelled using three dimensional acoustic elements whereas the plate is modelled using two-dimensional structural shell elements (Fahy & Gardonio, 2007).

The equation of motion for a forced vibrational behaviour of a coupled fluid-structural system is described by (Fahy & Gardonio, 2007),

$$\begin{bmatrix} \boldsymbol{M} & \boldsymbol{0} \\ -\boldsymbol{S^T} & \boldsymbol{Q} \end{bmatrix} \begin{Bmatrix} \ddot{\boldsymbol{u}}(t) \\ \ddot{\boldsymbol{p}}(t) \end{Bmatrix} + \begin{bmatrix} \boldsymbol{C} & \boldsymbol{0} \\ \boldsymbol{0} & \boldsymbol{D} \end{bmatrix} \begin{Bmatrix} \dot{\boldsymbol{u}}(t) \\ \dot{\boldsymbol{p}}(t) \end{Bmatrix} + \begin{bmatrix} \boldsymbol{K} & \boldsymbol{S} \\ \boldsymbol{0} & \boldsymbol{H} \end{bmatrix} \begin{Bmatrix} \boldsymbol{u}(t) \\ \boldsymbol{p}(t) \end{Bmatrix} = \begin{Bmatrix} \boldsymbol{f}(t) \\ \boldsymbol{q}(t) \end{Bmatrix} \tag{10}$$

where $\boldsymbol{M}$ is the mass matrix of the plate, $\boldsymbol{C}$ is the damping matrix of the plate, $\boldsymbol{K}$ is the stiffness matrix of the plate, $\boldsymbol{Q}$ is the acoustic inertia matrix, $\boldsymbol{D}$ is the acoustic damping matrix, $\boldsymbol{H}$ is the acoustic stiffness matrix, $\boldsymbol{S}$ is the structural-acoustic coupling matrix, $\boldsymbol{p}(t)$ is the column matrix of the nodal sound pressures in the acoustic medium, $\boldsymbol{u}(t)$ is the column matrix of the nodal displacements on the plate, $\boldsymbol{f}(t)$ is the column matrix of the nodal forces on the plate and $\boldsymbol{q}(t)$ is the column matrix of the nodal excitations generated by the volumetric sources in the acoustic medium.

If the coupled fluid-structure system of Equation (10) is subjected to harmonic excitation then its response can be calculated using steady-state analysis methods (Hibbitt et al., 2012).

2.5 Summary

This chapter reviewed the theoretical background of the finite element methods used in this thesis. After a brief introduction to the historical background and the basic concepts of the method, an overview was given for the finite element approach using the software, Abaqus. Two correlation criteria were introduced for the validation stages that use experimental or analytical solutions: these were the modal assurance criterion and the coordinate modal assurance criterion. Analysis methods for the prediction of vibration in floor systems were introduced as well as basic concepts of the eigenvalue analysis, and two methods for performing steady-state dynamic analysis. For the latter these methods were the direct-solution and mode-based steady-state analysis. At the end of chapter, a brief introduction was given to the coupled fluid-structure analysis for the prediction of sound radiation from a structure using the finite element method.

3. Finite element modelling of experimental specimens and validation against experimental results

3.1 Introduction

This chapter discusses the development and validation of finite element models using Abaqus (Hibbitt et al., 2012) for a) a beech beam, b) three individual spruce beam assemblies and c) a dowelled-joist timber floor formed from the three assemblies. The validation of the models was carried out by assessing the eigen-frequencies and mode shapes with results from the experimental work carried out by the project partners at the Rosenheim University of Applied Sciences in Germany. This experimental work is described in this chapter. A sequence of finite element models of increasing complexity is assessed which result in the use of spring connections at the dowel positions combined with precise modelling of the boundary conditions (supports) at the two ends of the assemblies. From the three spruce assemblies, Assembly A was chosen for the model updating procedure. Assembly A forms the mid-assembly when the three assemblies are connected (Figure 3-1). Once the model was finalised and validated on Assembly A, models were also made for Assemblies B and C and validated against experimental results. Finally, the three validated finite element models were joined together to form a finite element model for a complete floor system. This complete floor was also validated against modal analysis measurements.

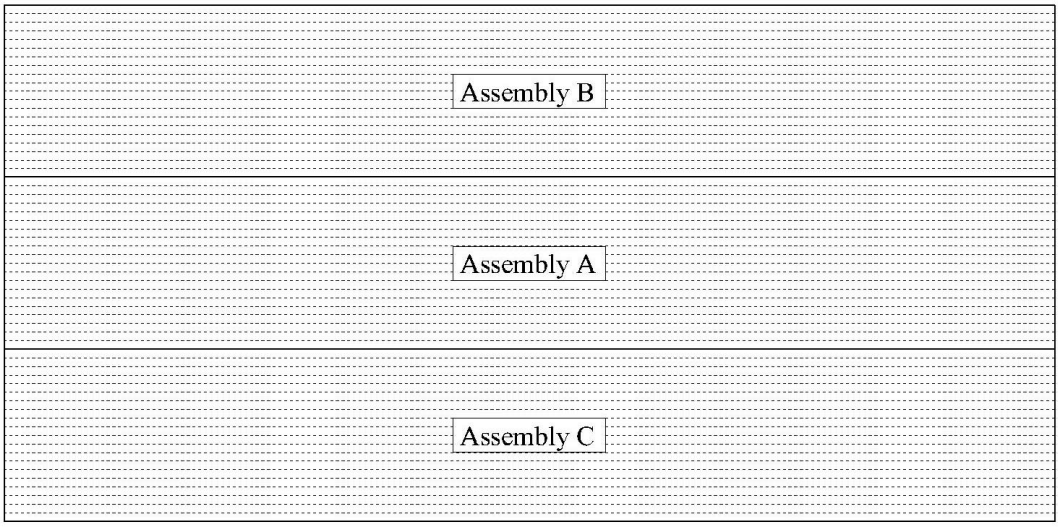

Figure 3-1 Assemblies numbering system

3.2 Experimental work

All the experimental work was carried out by the project partners in the acoustics laboratories at the Rosenheim University of Applied Sciences in Germany and included a) one beech beam, b) three individual spruce assemblies and c) a dowelled – joist timber floor system formed from the three assemblies. All the experimental specimens were provided by the industrial partner Nägeli AG. Modal tests were carried out to identify the material properties and the dynamic characteristics of the experimental specimens. The results of the experimental procedure were necessary for the development and validation of the finite element models.

3.2.1 Beech beam

The beech beam (Project ID code BS3) with dimensions 5004 mm x 81mm x 45 mm and a mass of 13.1 kg was suspended by wires and accelerometers were attached in positions along the largest dimension of the beam (Figure 3-2). The beam was excited using an impact hammer in locations along the same line as the accelerometers and the response was measured at each accelerometer. This resulted in a large number of transfer functions between the source and the receiver positions.

Figure 3-2 Experimental modal analysis setup

3.2.2 Individual spruce assemblies

The industrial partner, Nägeli AG, provided three spruce assemblies with dimensions 5500 x 900 x 200mm (Figure 3-3). Each assembly was made from 20 beams (45 mm x 200 mm) which were connected together using two rows of Φ16 mm dowels with a spacing of ≈ 250 mm in each row. The dowels followed a zigzag pattern as indicated in Figure 3-4.

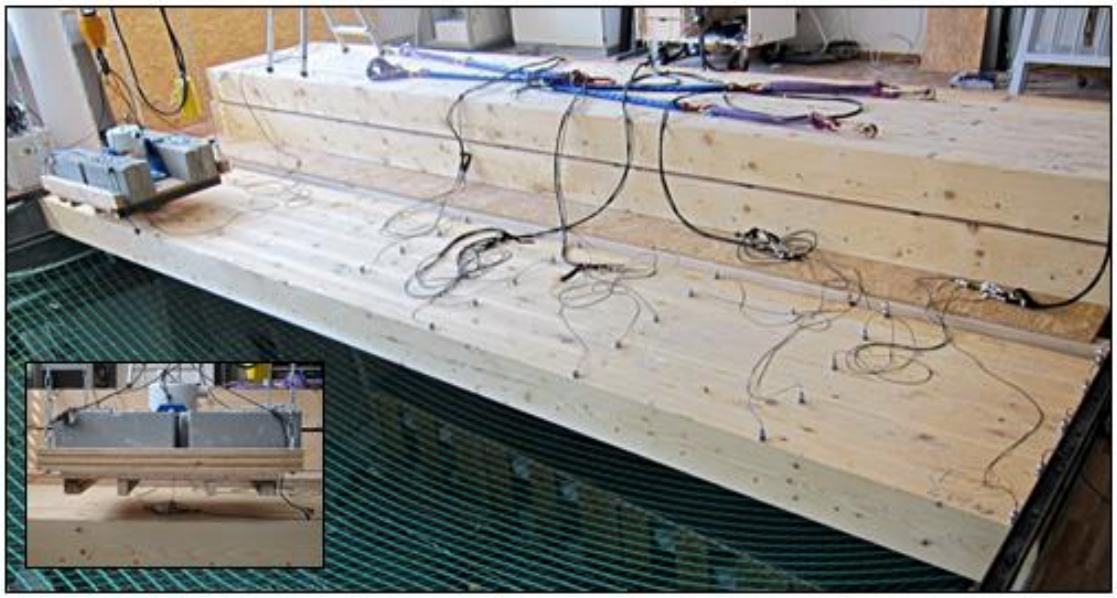

Figure 3-3 The three spruce assemblies that were provided by the industrial partner, Nägeli AG. The grid of accelerometers and the electrodynamic shaker that were used during the modal test can be seen in the photo as well as the stinger that connects the shaker to the assemblies.

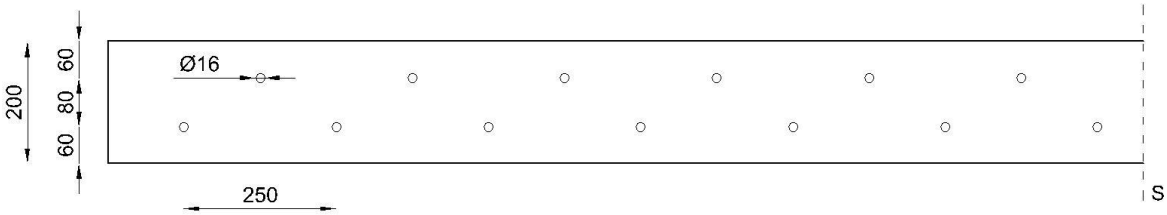

Figure 3-4 Zigzag pattern of the dowels (dimensions in mm)

In order to approximate pinned boundary conditions at the two ends of the assemblies, elastomeric material was used above and below the edges of the assemblies. Figure 3-5 shows in detail this support condition. The intention was for translational degrees of freedom to be restrained due to the metal rod but for the elastomer layers to allow the rotation of each assembly.

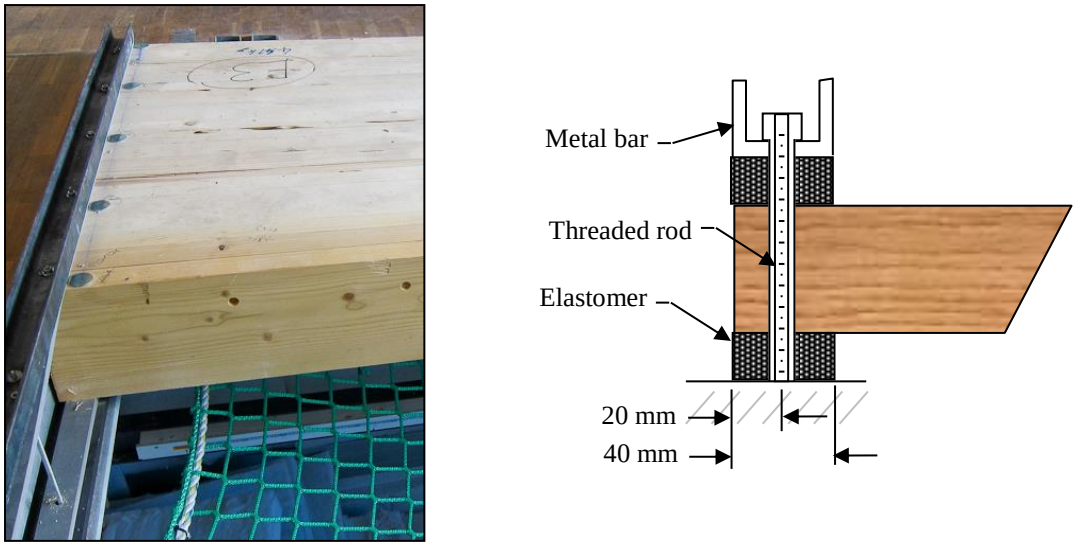

(a) (b)

Figure 3-5 (a) The edge of the assembly resting on the ledge on the side of the test aperture, (b) Cross section of the edge conditions of the assemblies.

Modal tests were carried out to identify the material properties and the modal characteristics of the three spruce assemblies. The assemblies were excited using an electrodynamic shaker which was suspended above each assembly and connected to it via a stinger (Figure 3-3). Swept sine excitation was used from 4.3Hz to 200Hz. The input impedance was measured by a force transducer and an accelerometer. The response of the assembly was measured using a grid of 45 accelerometer positions (five rows by nine columns).

3.2.3 Dowelled-joist timber floor system

In order to create a dowelled-joist timber floor system the spruce assemblies were connected together using metal screws at 300 mm centres (Figure 3-6). These screws have a length of 240 mm and were inserted at an angle of approximately 45° (Figure 3-7).

Modal tests were carried out to identify the modal characteristics of the dowelled-joist timber floor. Figure 3-6 shows the setup of the modal test. Following the same procedure as for the individual assemblies the floor was excited using an electrodynamic shaker and the response was captured in different positions using a grid of accelerometers.

Figure 3-6 The dowelled – joist timber floor system during the modal test

Figure 3-7 Metal screws used to join the individual spruce assemblies

3.3 Finite element modelling and validation of a beech beam

In this section, two finite element models of the beech beam (5004 mm x 81 mm x 45 mm) are developed and validated using the experimental data (see Section 3.2.1). The beam was modelled using shell elements in the YZ plane as indicated in Figure 3-8. The only difference between the two models was the finite element that was selected from the element library of the Abaqus/Standard (Hibbitt et al., 2012) for the meshing of each model. The general-purpose conventional shell element S4R, with four nodes and linear interpolation functions, was selected for the model B1 and the thick conventional shell element S8R, with eight nodes and quadratic interpolation functions, for the model B2. Both elements have six degrees of freedom per node. Thick shells are needed in cases where transverse shear flexibility is important while for general purpose shell elements the transverse shear deformation becomes very small as the shell thickness decreases (Hibbitt et al., 2012). Table 3-1 summarizes the data of the finite element analyses.

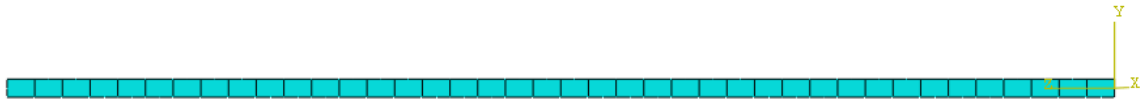

Figure 3-8 Finite element model of the beech beam

Table 3-1 Analysis summary

Model	B1	B2
Element type	S4R	S8R
	4-nodes	8-nodes
	Linear interpolation	Quadratic interpolation
Support conditions	Free-free	Free-free
Analysis type	Eigenvalue	Eigenvalue
Eigenvalue extraction method	Lanczos	Lanczos

Table 3-2 shows the material properties of the beech beam. The Young's modulus was calculated using the fundamental experimental eigen-frequency, according to the procedure described in Section 3.4. The value for the Poisson ratio was taken from the literature (Dahl, 2009).

Table 3-2 Material properties of the beech beam

Timber type	Density, ρ [kg/m^3]	Young's modulus, E [MPa]	Poisson ratio, v
Beech	735,3	14400	0,37

Table 3-3 compares the numerical with the experimental results for models B1 and B2. It is clear that model B2 shows close agreement in terms of frequencies with the experimental results. However, this is not the case for model B1which shows large errors. As result, the following finite element models use the finite element S8R.

Table 3-3 Comparison between experimental and numerical results

Experimental model [Hz]	FEM Model B1 [Hz]	Difference [%]	FEM Model B2 [Hz]	Difference [%]
14.9	4.09	72.6	14.70	1.3
40.4	11.30	72.0	40.44	-0.1
78.0	22.21	71.5	79.08	-1.4
128.2	36.82	71.3	130.26	-1.6
188.2	55.20	70.7	193.80	-3.0
256.9	77.43	69.9	269.29	-4.8

3.4 Physical and mechanical properties of spruce assemblies

The Young's modulus of the spruce assemblies in the x-direction along the beam length was calculated according to (Blevins, 1995),

$$E_X = \frac{m}{I_X}\left(\frac{2f_1\pi L^2}{{\lambda_1}^2}\right)^2 \tag{11}$$

where E_X is the modulus of elasticity in the X-direction, I_X is the second moment of inertia in the X-direction, f_1 is the fundamental frequency (taken from the experimental results), L is the length of each assembly and λ_1 is a constant based on the boundary conditions. For a pinned-pinned supports the constant λ_1 is equal to π and for free-free supports is equal to 1.5π.

In the finite element models, the whole length of the assemblies (equal to 5.5 m) has been considered and used in equation (11). Table 3-4 shows the resulting estimates of the Young's moduli, the densities and Poisson ratios for the assemblies used in the models in this report. The value of the Poisson ratio was taken from the literature (Dahl, 2009).

Table 3-4 Material properties for the assemblies used in the finite element analysis

	Density, ρ [kg/m^3]	Young's modulus, E [N/mm^2]	Poisson ratio, v
Assembly A	473	11700	0.37
Assembly B	459	11650	0.37
Assembly C	449	10218	0.37

3.5 Finite element modelling and updating of Assembly A

3.5.1 Model updating procedure

The model updating procedure was carried out for Assembly A (Figure 3-9). The results of the eigenvalue analysis from each finite element model were compared with the experimental results in terms of eigen-frequencies and mode shapes. The agreement was assessed using as criteria the percentage of the difference, for the eigen-frequencies and the MAC value, for the mode shapes (Table 3-5).

Table 3-5 Agreement criteria between numerical and experimental results

	Close	Reasonable	Weak
Frequency - Difference [%]	0 – 10	10 – 15	> 15
Mode shapes – MAC [%]	80 – 100	70 – 80	< 70

The initial approach was to model this assembly as an isotropic plate (Model 1) with pinned ends. This approach was unsuccessful since the results of the modal analysis (frequencies and mode shapes) were in poor agreement with the experimental results. It is noted that the errors in the eigen-frequencies were up to346 %. The next step was to update the model of the isotropic plate by introducing elastic springs acting in the vertical direction (Model 2) to model the elastic supports (elastomers) at the ends of the assemblies. This procedure was again unsuccessful and at this point it was evident that it was not possible to model this complex floor system as a homogeneous, isotropic plate.

A new finite element model was developed for Assembly A which consisted of twenty beams connected at the position of the dowels using coupling constraints and with elastic supports at both ends of each beam (Model 3). Only the translational degrees of freedom were coupled. Using this approach, good agreement between numerical and experimental results was achieved for the majority of the mode pairs in terms of frequencies and mode shapes. An alternative version of this model was produced by replacing the coupling constraints with join connectors that constraint the translational degrees of freedom between two nodes (Model 4). This approach was also successful and it produced smoother mode shapes than the previous one. However, even better agreement was achieved by replacing the coupling constraints at each dowel position with three springs, one for each translational degree of freedom (Model 5).

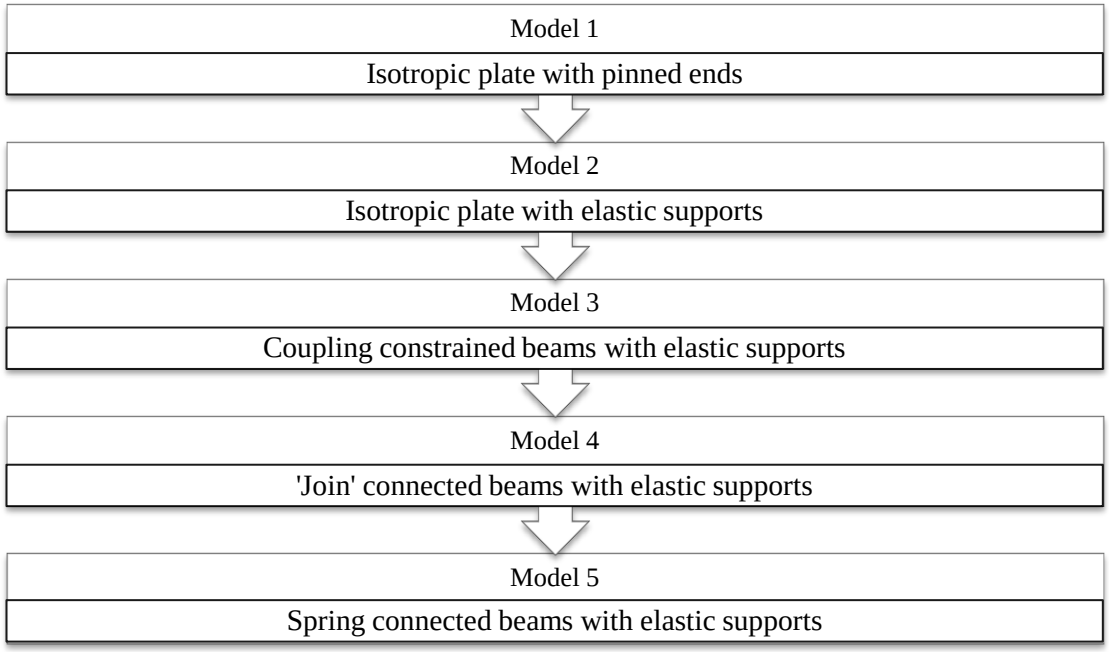

Figure 3-9 Model updating procedure

3.5.2 Model 1: Isotropic plate

Description of the model

In this model, Assembly A was assumed to act as a homogeneous isotropic plate with dimensions 5500 mm x 200 mm m x 45 mm. Table 3-6 summarises the data of the finite element analysis.

Boundary conditions

The assembly was assumed to be pinned ($U_X = U_Y = U_Z = 0$) along the two short edges (Figure 3-10)

Meshing

The second order Abaqus/Standard thick shell element S8R (Hibbitt et al., 2012) was used for the meshing of the isotropic plate (Figure 3-10). This 8–node element has 6 degrees of freedom per node, uses quadratic interpolation functions and takes into account transverse shear flexibility.

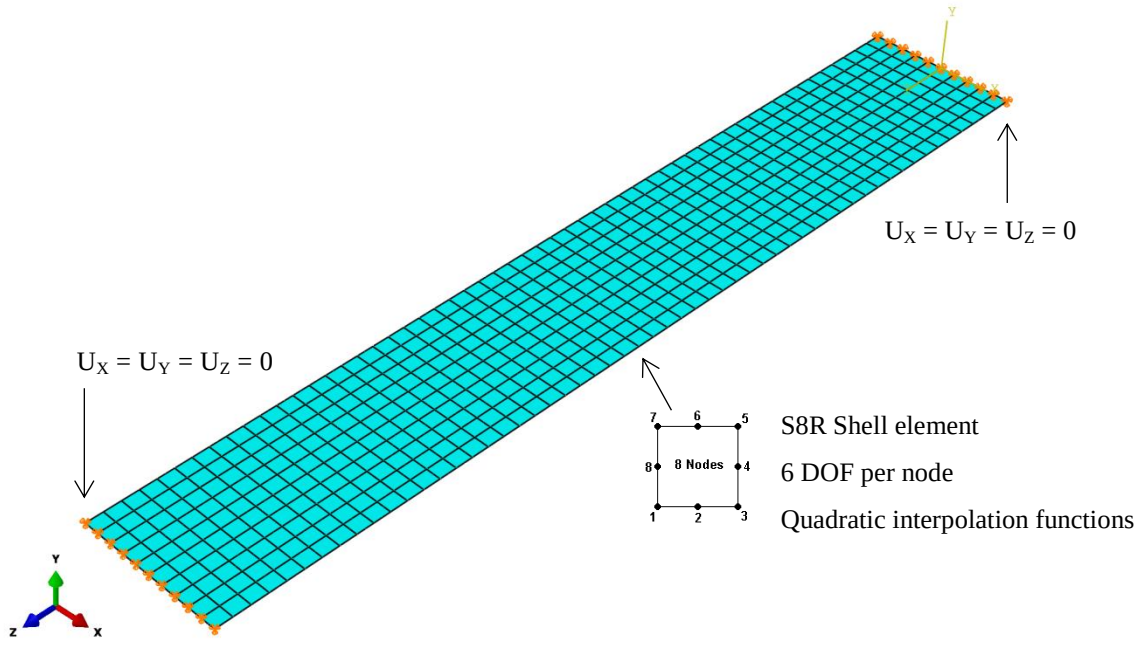

Figure 3-10 Finite element model of an individual assembly

Table 3-6 Analysis summary

Model	Homogeneous isotropic plate
Element type	S8R
	8-nodes
	Quadratic interpolation
Support conditions	Pinned-pinned
Analysis type	Eigenvalue
Eigenvalue extraction method	Lanczos

Modal analysis results

Table 3-7 compares the results of the numerical analysis with the results of the experimental modal analysis. Excluding the first mode, all modes are significantly different in terms of frequency. It is concluded that Assembly A cannot be simulated as a pinned - pinned homogeneous plate and a more advanced finite element model is required.

Note that the eigenvalue analysis produces modes that are not observed in the experimental modal analysis. For that reason, the numerical modes were numbered according to the number of the experimental mode with which they correspond.

Table 3-7 Comparison between experimental and FEM results

Experimental modal analysis	Finite element analysis	Difference [%]
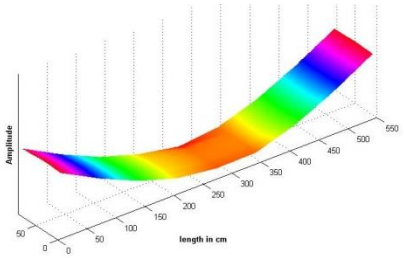	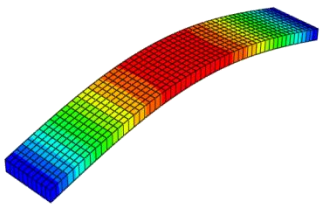	*Close agreement in terms of frequency*
Mode 1: 15.0 Hz	Mode 1: 14.9 Hz	0.7

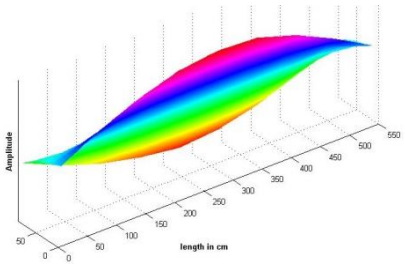	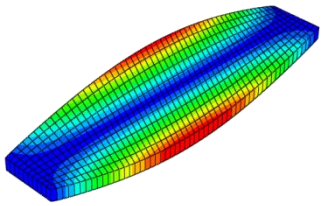	*Weak agreement in terms of frequency*
Mode 2: 24.1 Hz	Mode 2: 107.6 Hz	-346.4
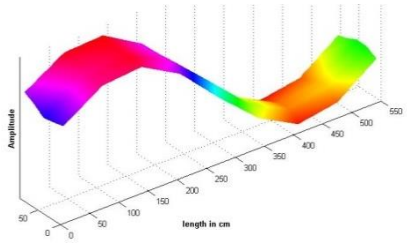	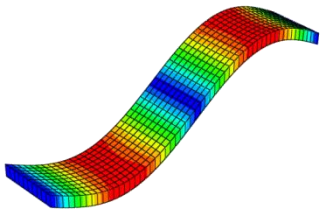	*Reasonable agreement in terms of frequency*
Mode 3: 52.6 Hz	Mode 3: 59.4 Hz	-12.8
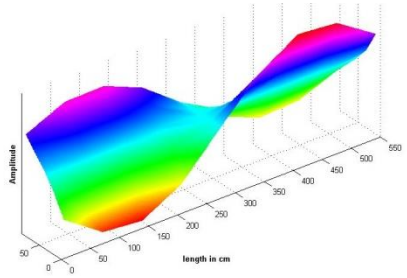	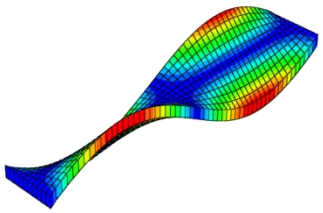	*Weak agreement in terms of frequency*
Mode 4: 59.8 Hz	Mode 4: 219.6 Hz	-267.2
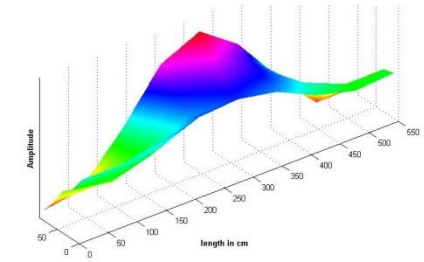	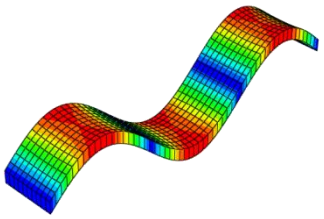	*Weak agreement in terms of frequency*
Mode 5: 97.4 Hz	Mode 5: 132.6 Hz	-36.1
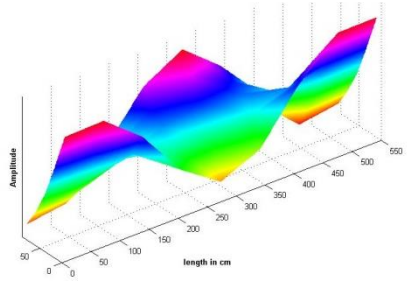	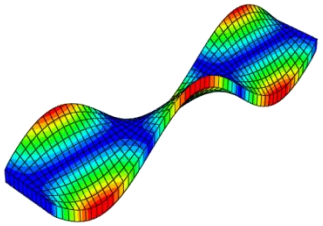	*Weak agreement in terms of frequency*
Mode 6: 103.7 Hz	Mode 6: 339.8 Hz	-227.7

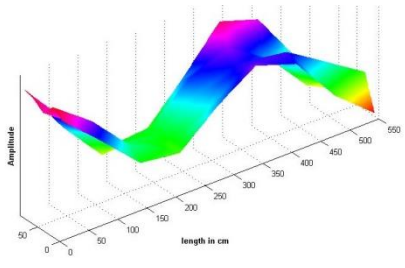	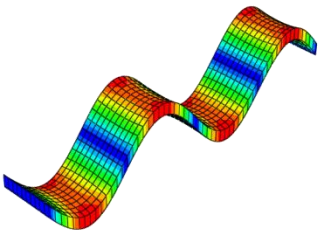	*Weak agreement in terms of frequency*
Mode 7: 137.4 Hz	Mode 7: 233.2 Hz	-69.8
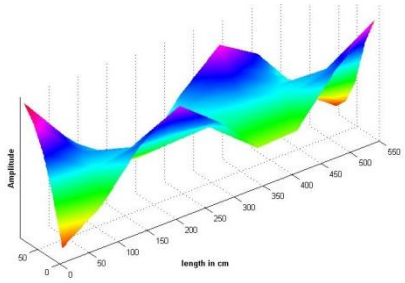	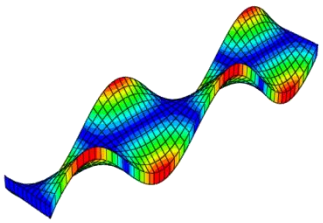	*Weak agreement in terms of frequency*
Mode 8: 150.3 Hz	Mode 8: 471.0 Hz	-213.4
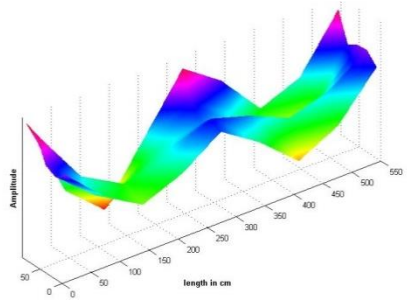	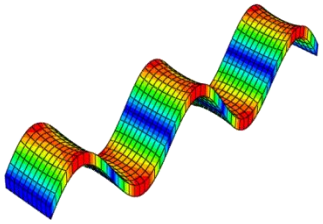	*Weak agreement in terms of frequency*
Mode 9: 188.6 Hz	Mode 9: 359.0 Hz	-90.3

3.5.3 Model 2: Isotropic plate with elastic supports

Description of the model

Model 2 was produced by taking Model 1 and introducing elastic springs in the vertical direction (Y–direction) at the end supports of the plate (Figure 3-11). In this way an attempt was made to simulate the elastomer supports around the edges of the test aperture (Figure 3-5). In the other two directions the boundary conditions remained pinned – pinned. Table 3-8 summarizes the data of the finite element analysis.

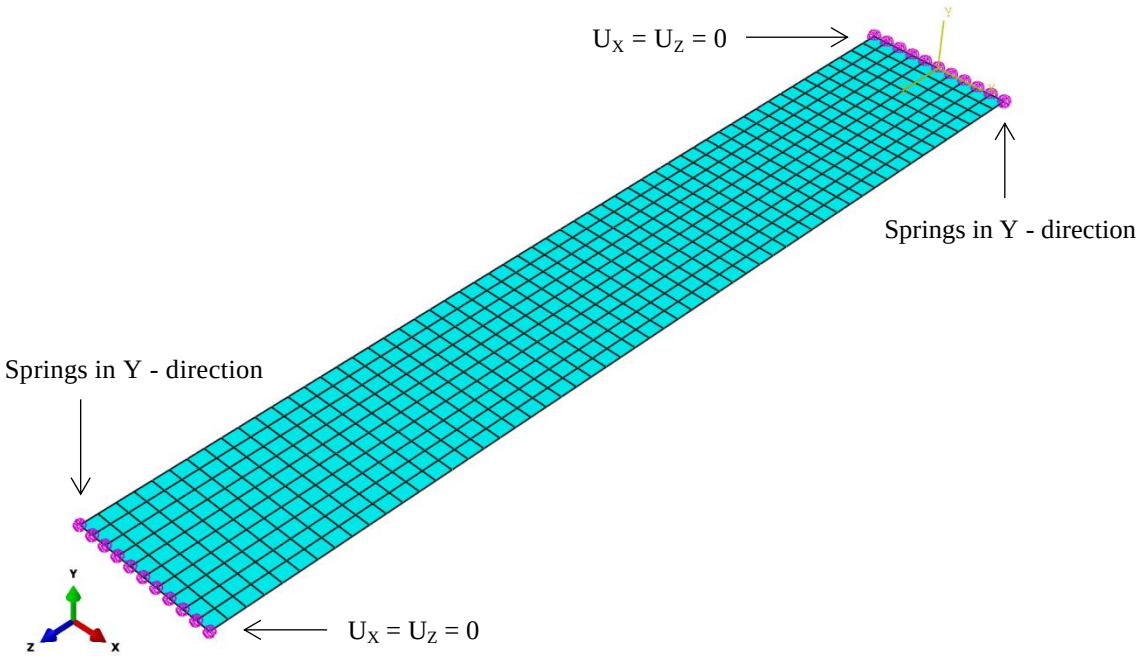

Figure 3-11 Vertical springs (Y-direction) located at both ends of the isotropic plate

Meshing

The second order Abaqus/Standard thick shell element S8R was used to mesh the plate (Figure 3-11). The Spring1(S) element was chosen from the element library of Abaqus (Hibbitt et al., 2012) to represent the elastic support conditions. This is a spring between a node and a ‘ground’ or ‘earth’ point, acting in a fixed direction (Figure 3-12).

Figure 3-12 Spring1(S) element ((Hibbitt et al., 2012))

Spring stiffness

The spring stiffness was calculated using the elastomer manufacturer's datasheet (Getzner, 2012). Each one of the 22 springs of the supports was assigned a stiffness of 2356 N/mm corresponding to the stiffness of the two layers of elastomer. Specifically, the spring stiffness, k_{spr} , was calculated according to,

$$k_{spr} = \left(\frac{F b_{el} b_{pl}}{N_{spr}}\right) N_{el} \tag{12}$$

where: F is the specific load of the elastomer in N/mm^2, for 1.0 mm of deflection

b_{el} is the width of the elastomer, (mm)

b_{pl} is width of the plate, (mm)

N_{spr} is the number of springs in each end of the assembly

N_{el} is the number of elastomer layers

Table 3-8 Analysis summary

Model	Isotropic plate with elastic supports	
Element type	Plate	S8R
	Support in Y-direction	Spring(1)S
Support conditions	Pinned-pinned (X and Z directions)	
	Elastic supports in Y-direction	
Analysis type	Eigenvalue	
Eigenvalue extraction method	Lanczos	

Modal analysis results

Table 3-9 compares the results of the numerical analysis with the results of the experimental modal analysis. The replacement of the pinned – pinned support in the Y – direction in Model 1 with springs in Model 2, resulted in the good agreement in terms of frequencies between numerical and experimental results for all the bending modes. However, all the other modes show significant differences in frequency. Therefore Assembly A cannot be simulated as a pinned - pinned homogeneous plate with elastic supports hence a more advanced finite element model is considered in the next section.

Table 3-9 Comparison between experimental and FEM results

Experimental modal analysis	Finite element analysis	Difference [%]
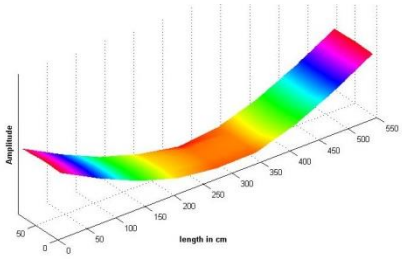	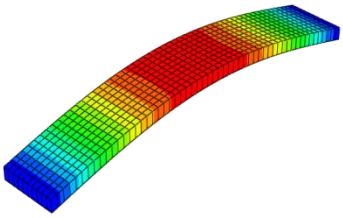	*Close agreement in terms of frequency*
Mode 1: 15.0 Hz	Mode 1: 14.4 Hz	3.8
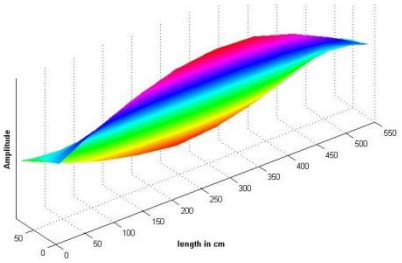	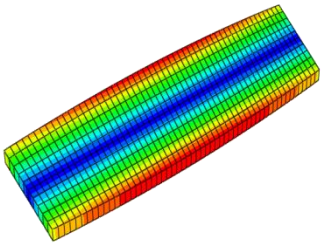	*Weak agreement in terms of frequency*
Mode 2: 24.1 Hz	Mode 2: 50.8 Hz	-111.0
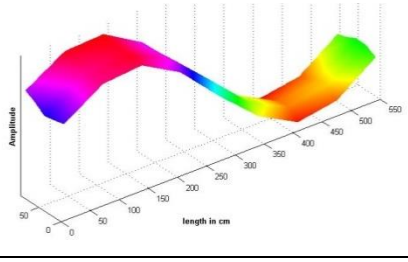	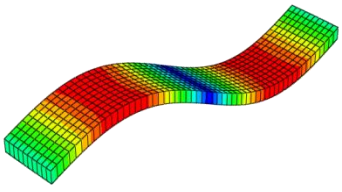	*Close agreement in terms of frequency*
Mode 3: 52.6 Hz	Mode 3: 52.2 Hz	0.8

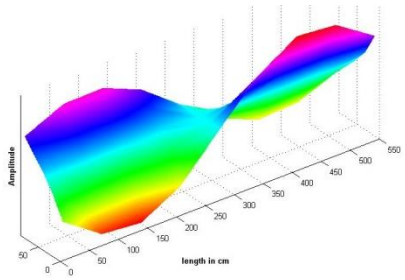	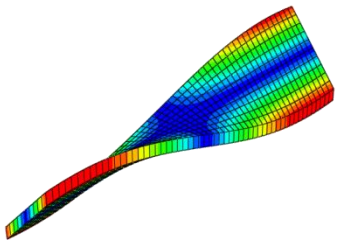	*Weak agreement in terms of frequency*
Mode 4: 59.8 Hz	Mode 4: 134.0 Hz	-124.1
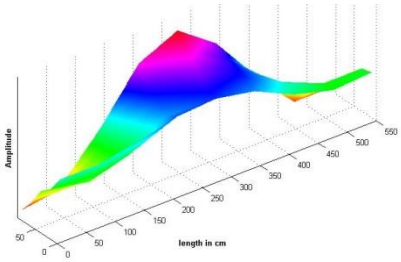	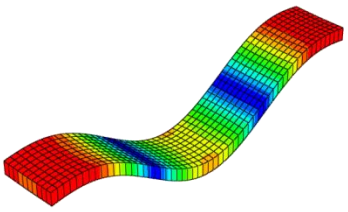	*Close agreement in terms of frequency*
Mode 5: 97.4 Hz	Mode 5: 98.9 Hz	-1.5
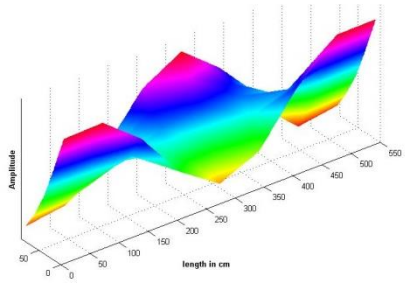	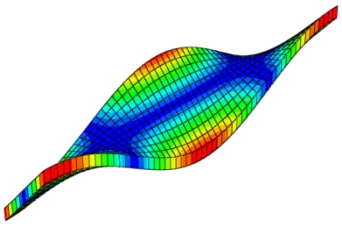	*Weak agreement in terms of frequency*
Mode 6: 103.7 Hz	Mode 6: 238.8 Hz	-130.2
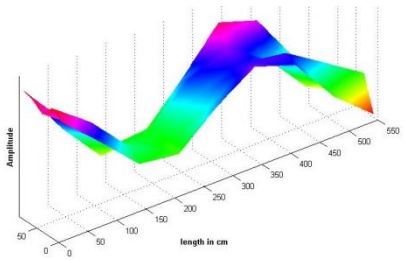	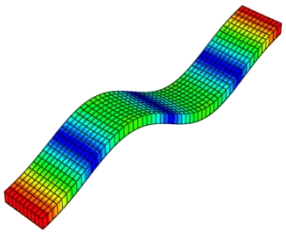	*Close agreement in terms of frequency*
Mode 7: 137.4 Hz	Mode 7: 147.5 Hz	-7.4
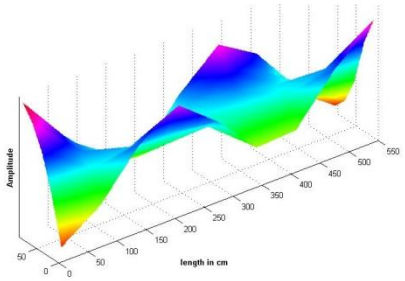	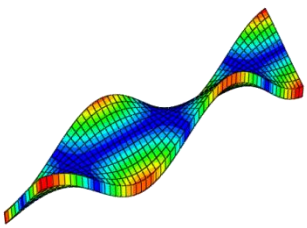	*Weak agreement in terms of frequency*
Mode 8: 150.3 Hz	Mode 8: 354.6 Hz	-136.0

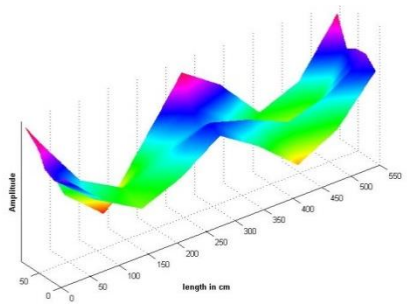	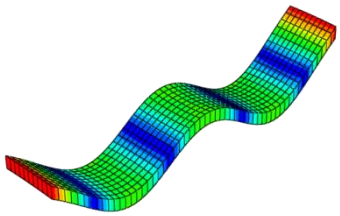	*Reasonable agreement in terms of frequency*
Mode 9: 188.6 Hz	Mode 9: 213.9 Hz	-13.4

3.5.4 Model 3: Coupled constrained beams with elastic supports

Description of the model

In this finite element model, Assembly A was modelled as twenty beams connected at the position of the dowels (Figure 3-13). Each beam has 200 mm height, 45 mm thickness and 5500 mm length. At the dowel positions, only the translational degrees of freedom (U_X, U_Y, U_Z) were coupled so that there was continuity of displacement but no continuity for the rotational degrees of freedom. This condition is described as a 'coupling constraint' although it effectively just couples the displacements at each dowel connection.

Two rows of constraints along each beam were used in order to model the actual dowel pattern with a vertical distance of 80 mm between them. In each row, the horizontal distance was 250 mm between each 'coupling constraint'.

In order to consider the elastomers, each beam of the assembly was assigned two vertical springs at the top and bottom nodes of both ends (Figure 3-14). These springs act only in the Y- direction. Table 3-10 summarizes the data of the finite element analysis.

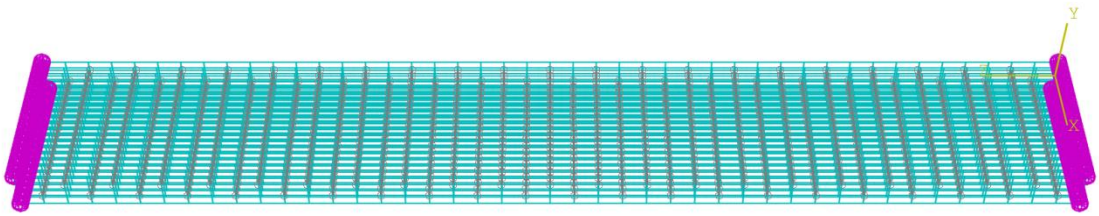

Figure 3-13 Coupling constraints at the position of the dowels indicated using brown arrows

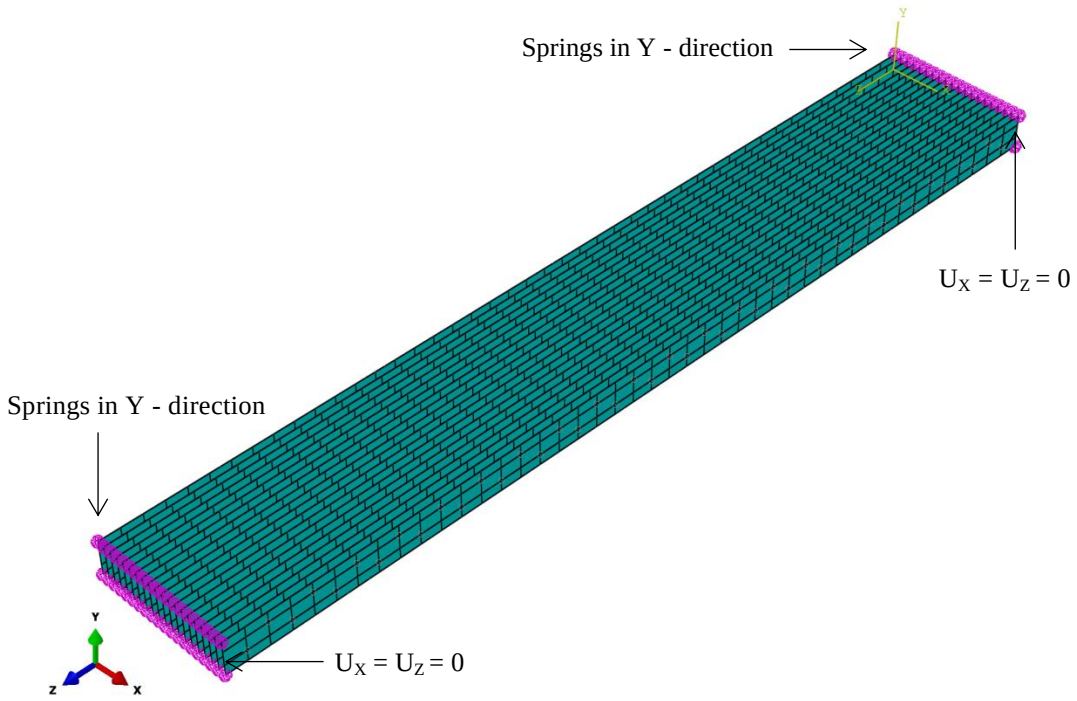

Figure 3-14 Finite element model of an individual assembly

Boundary conditions

Each beam of the assembly was pinned ($U_X = U_Z = 0$) at the mid-nodes of both ends (Figure 3-14).

Meshing

The second order Abaqus/Standard thick shell element S8R was used to mesh the beams (Figure 3-14). This 8–node element has 6 degrees of freedom per node and use quadratic interpolation functions.

The Spring1(S) element was chosen from the element library of Abaqus (Hibbitt et al., 2012) to represent the elastic support conditions (Figure 3-14). Note that this is a spring between a node and a 'ground' or 'earth' point, acting in a fixed direction.

Spring stiffness

The spring stiffness was calculated using the elastomer manufacturer's datasheet (Getzner, 2012). Each one of the 80 springs of the supports was assigned a stiffness of 650 N/mm corresponding to the stiffness of one layer of elastomer. Specifically, the spring stiffness, k_{spr}, was calculated according to,

$$k_{spr} = Fb_{el}t_b \quad (13)$$

where: F is Specific load of the elastomer [N/mm^2], for 1.0 mm of deflection

b_{el} is width of the elastomer [mm]

t_b is thickness of each beam [mm]

Table 3-10 Analysis summary

Model	Coupled constrained beams with elastic supports	
Element type	Beams	S8R
	Support in Y-direction	Spring(1)S
Support conditions	Pinned-pinned (X and Z directions)	
	Elastic supports in Y-direction	
Interaction	Coupling constraints at the position of the dowels	
Analysis type	Eigenvalue	
Eigenvalue extraction method	Lanczos	

Modal analysis results

Table 3-11 compares the results of the numerical analysis with the results of the experimental modal analysis. The results of the finite element model show good agreement in terms of frequencies with the majority of the experimental modes. At this point it is important to notice that good agreement in terms of frequencies is a difference less than 10%. However, the difference between the second experimental and the third FEM mode is quite high, so again, an improved model is sought in the next section.

Table 3-11 Comparison between experimental and FEM results

Experimental modal analysis	Finite element analysis	Difference [%]
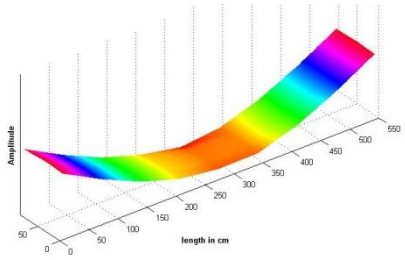	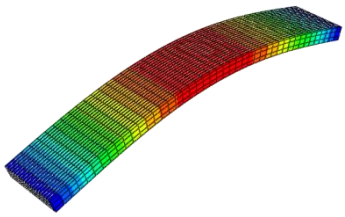	*Close agreement in terms of frequency*
Mode 1: 15.0 Hz	Mode 1: 14.4 Hz	3.9
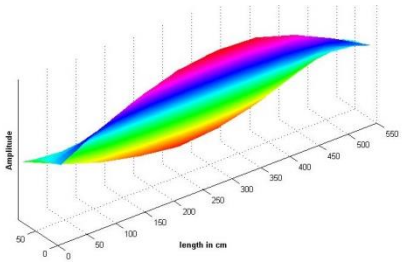	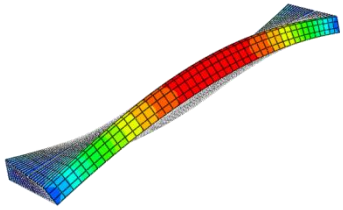	*Reasonable agreement in terms of frequency*
Mode 2: 24.1 Hz	Mode 2: 20.4 Hz	15.2
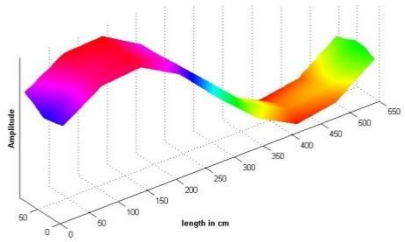	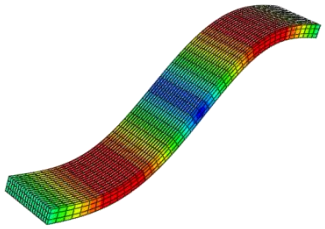	*Close agreement in terms of frequency*
Mode 3: 52.6 Hz	Mode 3: 52.0 Hz	1.1
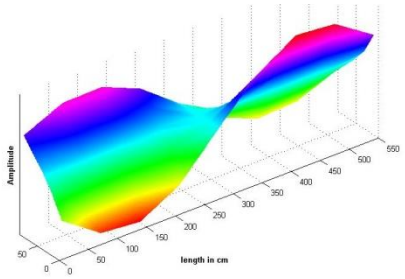	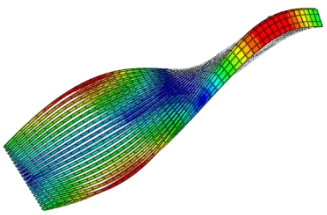	*Close agreement in terms of frequency*
Mode 4: 59.8 Hz	Mode 4: 58.1 Hz	2.8

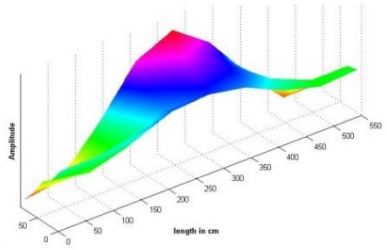	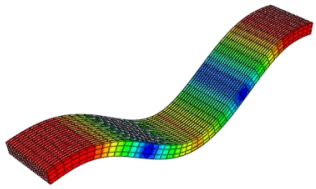	*Close agreement in terms of frequency*
Mode 5: 97.4 Hz	Mode 5: 98.5Hz	-1.1
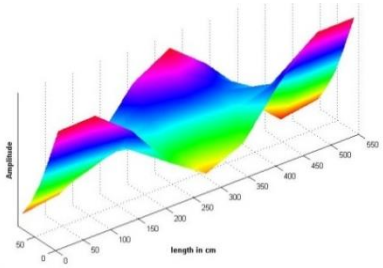	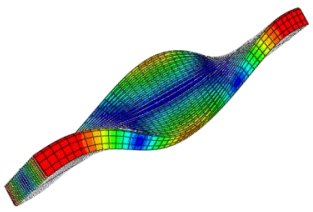	*Close agreement in terms of frequency*
Mode 6: 103.7 Hz	Mode 6: 104.2 Hz	-0.5
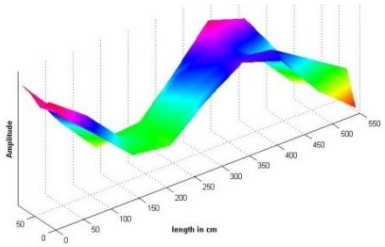	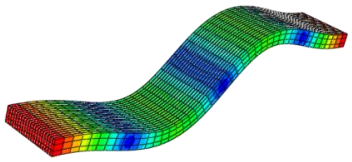	*Close agreement in terms of frequency*
Mode 7: 137.4 Hz	Mode 7: 146.9 Hz	-6.9
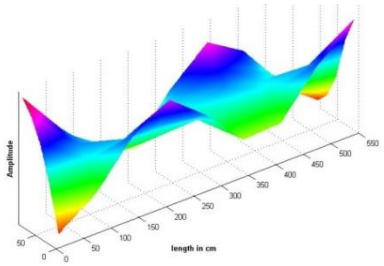	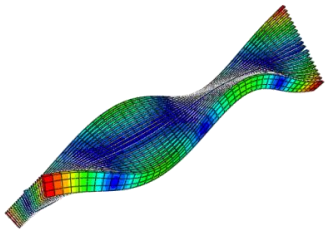	*Close agreement in terms of frequency*
Mode 8: 150.3 Hz	Mode 8: 152.9 Hz	-1.8
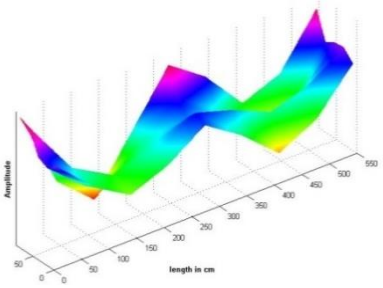	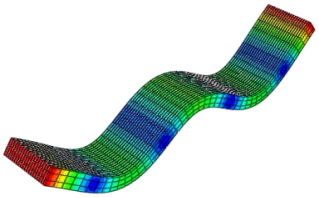	*Reasonable agreement in terms of frequency*
Mode 9: 188.6 Hz	Mode 9: 212.4 Hz	-12.6

3.5.5 Model 4: 'Join' connected beams with elastic supports

Description of the model

In this section, Model 3 was updated by using Abaqus 'join connectors' instead of coupling constraints to connect the twenty beams at the dowel positions. A join connection (Figure 3-15) is a kinematic constraint that makes the position of two nodes the same (Hibbitt et al., 2012). Table 3-12 summarises the data of the finite element analysis.

Figure 3-15 Abaqus 'Join' connection (Hibbitt et al., 2012)

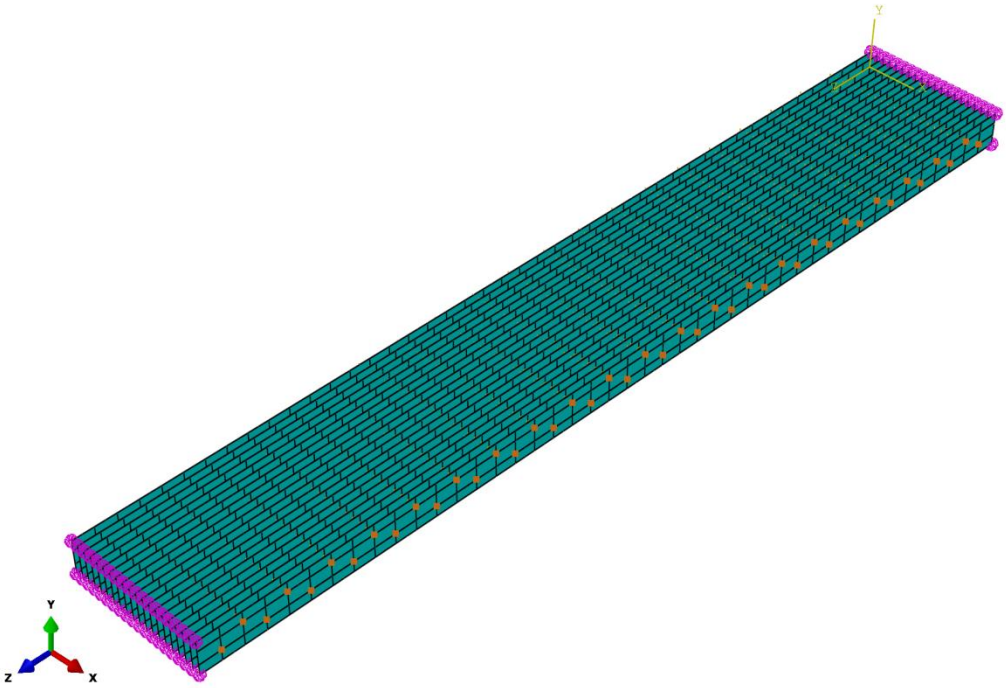

Figure 3-16 Finite element model of an individual assembly using 'join' connected beams with elastic supports

Table 3-12 Analysis summary

Model	'Join' connected beams with elastic supports	
Element type	Beams	S8R
	Support in Y-direction	Spring(1)S
Support conditions	Pinned-pinned (X and Z directions)	
	Elastic supports in Y-direction	
Interaction	'Join' connectors at the position of the dowels	
Analysis type	Eigenvalue	
Eigenvalue extraction method	Lanczos	

Modal analysis results

Table 3-13 compares the results of the numerical analysis with the results of the experimental modal analysis. The results of the finite element model show good agreement with the experimental modes since the difference in terms of frequencies is less than 10% for the majority of the mode pairs.

Table 3-13 Comparison between experimental and FEM results

Experimental modal analysis	**Finite element analysis**	**Difference [%]**
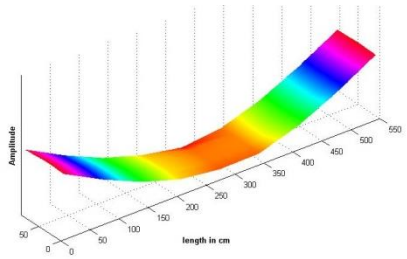	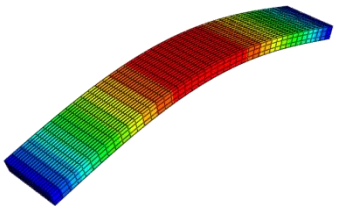	*Close agreement in terms of frequency*
Mode 1: 15.0 Hz	Mode 1: 14.4 Hz	3.9

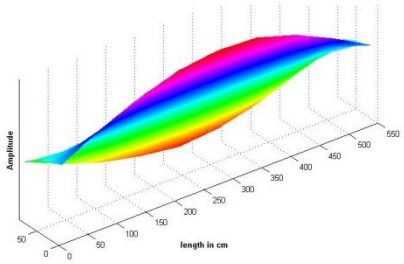	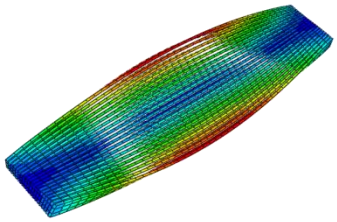	*Close agreement in terms of frequency*
Mode 2: 24.1 Hz	Mode 2: 26.2 Hz	-8.9
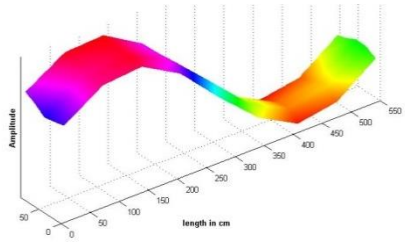	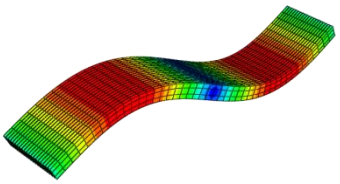	*Close agreement in terms of frequency*
Mode 3: 52.6 Hz	Mode 3: 52.1 Hz	1.1
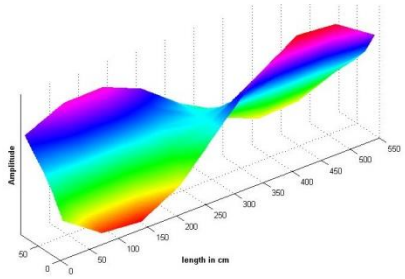	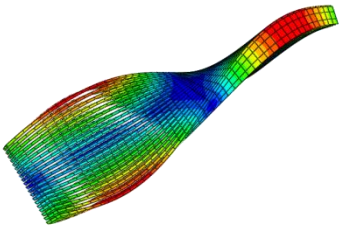	*Close agreement in terms of frequency*
Mode 4: 59.8 Hz	Mode 4: 63.90 Hz	-6.9
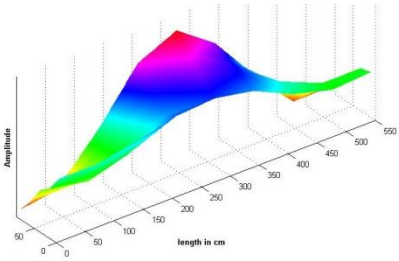	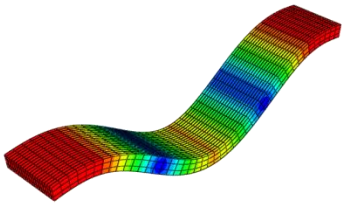	*Close agreement in terms of frequency*
Mode 5: 97.4 Hz	Mode 5: 98.5 Hz	-1.1
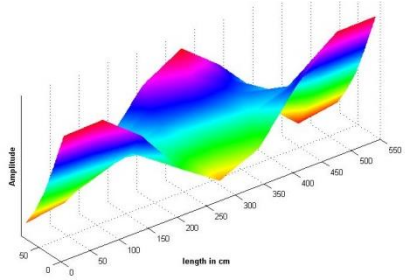	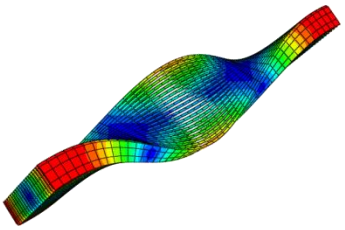	*Close agreement in terms of frequency*
Mode 6: 103.7 Hz	Mode 6: 110.5 Hz	-6.6

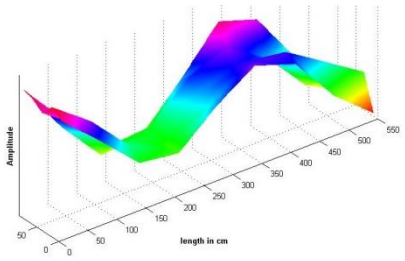	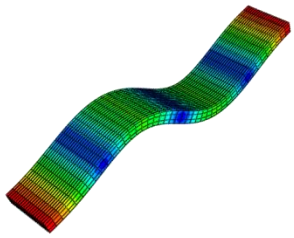	*Close agreement in terms of frequency*
Mode 7: 137.4 Hz	Mode 7: 146.9 Hz	-6.9
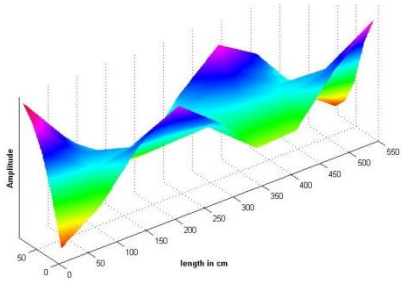	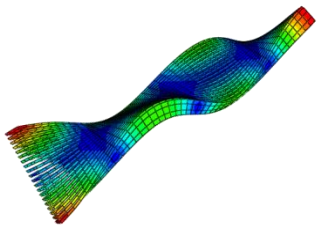	*Close agreement in terms of frequency*
Mode 8: 150.3 Hz	Mode 8: 163.9 Hz	-9.1
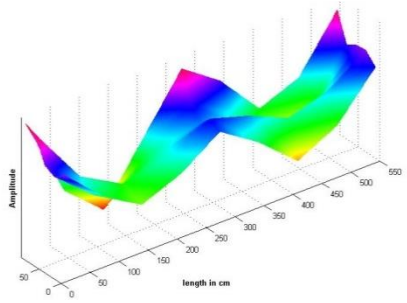	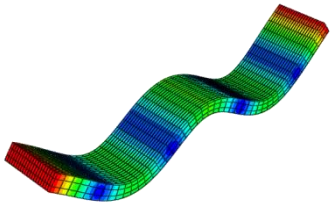	*Reasonable agreement in terms of frequency*
Mode 9: 188.6 Hz	Mode 9: 212.4 Hz	-12.6

3.5.6 Model 5: Spring connected beams with elastic supports

Description of the model

In this finite element model, Assembly A was modelled as twenty beams (200mm x 45mm x 5500mm), with spring elements as connections between the mid-plane of the beam at the individual positions of the dowels (Figure 3-17). Three springs, one in the vertical and two in the horizontal directions, were used to simulate the interaction of each dowel with each pair of beams.

Two rows of springs were considered in order to model the actual dowel pattern with a vertical distance of 80 mm between them. Along the length of the beam the spring spacing in the horizontal direction was 250 mm for each row of dowels.

In order to include the elastomers, each beam of the assembly was assigned two vertical support springs at the top and bottom nodes of both ends (Figure 3-18). These springs act only in the Y- direction. A summary of the analysis data is presented in Table 3-14.

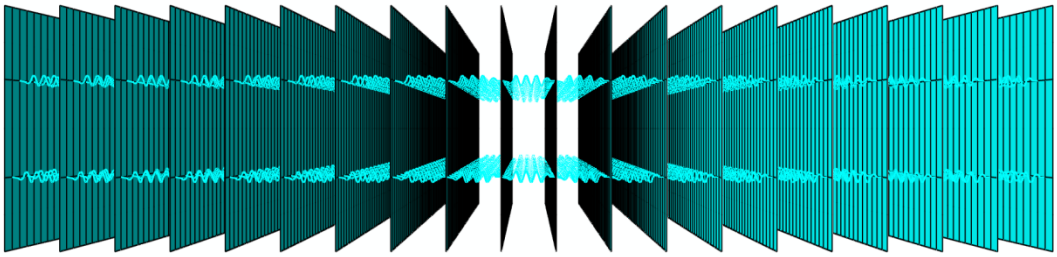

Figure 3-17 Connections between shell and spring elements

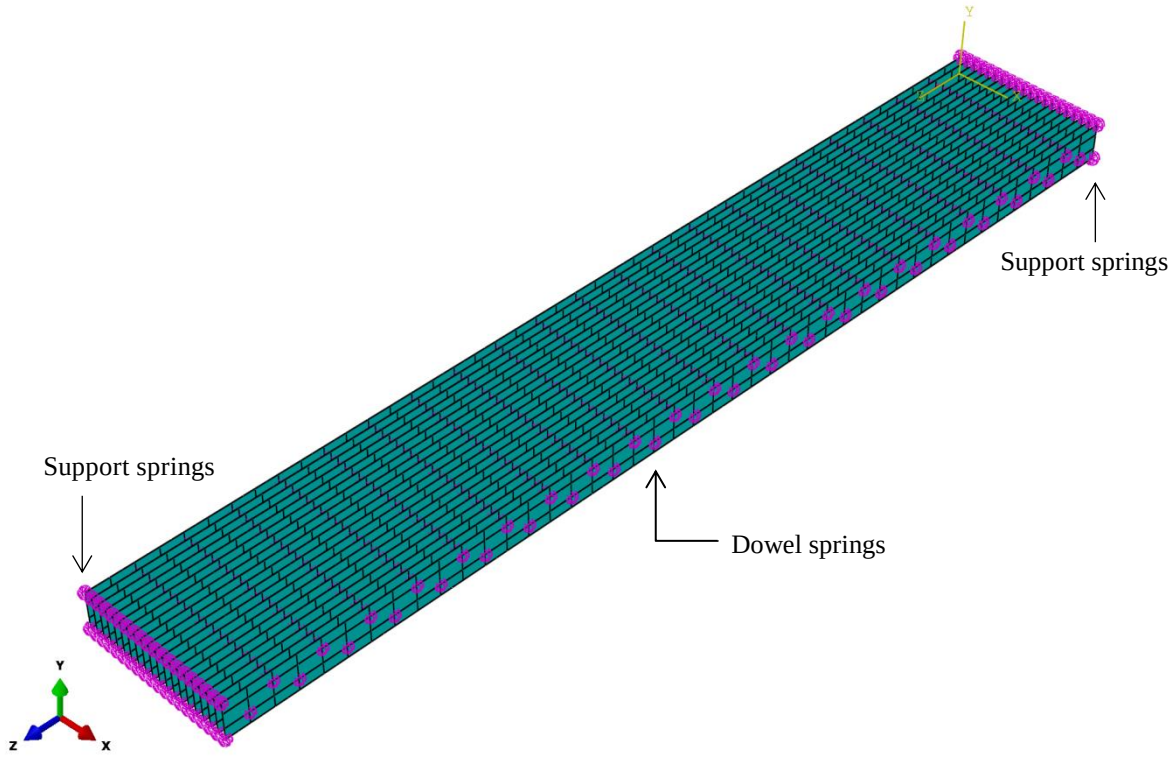

Figure 3-18 Finite element model of an individual assembly and position of the spring elements (purple markers)

Table 3-14 Analysis summary

Model	Spring connected beams with elastic supports	
Element type	Beams	S8R
	Support in Y-direction	Spring(1)S
	Dowels	Spring(2)S
Support conditions	Pinned-pinned (X and Z directions)	
	Elastic supports in Y-direction	
Analysis type	Eigenvalue	
Eigenvalue extraction method	Lanczos	

Boundary conditions

As previously noted, elastic springs were used to simulate the support conditions in the vertical direction (Y–direction), (Figure 3-18). The displacement degrees of freedom for the support nodes in the X and Z – directions were restrained ($U_X = U_Z = 0$).

Meshing

The twenty beams were meshed using the second order Abaqus/Standard thick shell element S8R (Figure 3-18). This 8–node element has 6 degrees of freedom per node, use quadratic interpolation functions and takes into account transverse shear flexibility.

The Spring2(S) element was chosen from the element library of Abaqus (Hibbitt et al., 2012) to represent the beam – dowel interaction. This is a spring between two nodes, acting in a fixed direction (Figure 3-19a). As in the previous models, the Spring1(S) element was chosen from the element library of Abaqus to represent the elastic support conditions. This is a spring between a node and a 'ground' or 'earth' point, acting in a fixed direction (Figure 3-19b).

(a) (b)

Figure 3-19 (a) Spring2(S) element, (b) Spring1(S) element

Spring stiffness

Appropriate values of the dowel spring stiffness were determined by comparing the results of several trial numerical analyses with the experimental data. An initial estimate was made for the stiffness of the springs by considering that the value for k_X should be much larger than k_Y and k_Z since the dowel is expected to have greater stiffness along its longitudinal axis. The spring set up with the closest agreement were adopted as indicated in Table 3-15. The value of the support spring stiffness was maintained equal to 650 N/mm. More information about the calculation of the support spring stiffness can be found in Section 3.5.4.

Table 3-15 Dowel and support spring stiffness properties

	k_X [N/mm]	k_Y [N/mm]	k_Z [N/mm]
Dowel springs	10000	350	350
Support springs	-	650	-

Modal analysis results

Table 3-16, compares the results of the numerical analysis with the results of the experimental modal analysis. The comparison was made in terms of frequencies and mode shapes.

In order to compare the mode shapes we have applied the Modal Assurance Criterion (MAC).

For the calculation of MAC we used the out-of-plane displacements of 45 correlation points. These points were selected as close as possible to the measurement points. Figure 3-20 shows the correlation between the experimental and the numerical mode shapes using a 2D plot. MAC values close to 1 indicate well correlated modes while MAC values close to 0 indicate uncorrelated modes.

Table 3-16 Comparison between experimental and FEM results

Experimental modal analysis	Finite element analysis	Difference [%]	MAC [%]
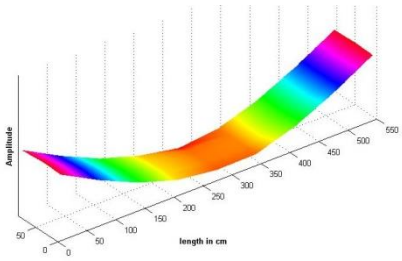	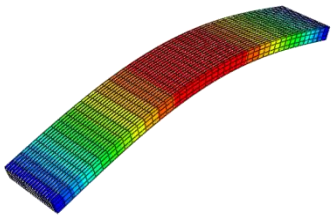	*Close agreement in terms of frequency*	*Close correlation of the mode shapes*
Mode 1: 15.0 Hz	Mode 1: 14.4 Hz	3.9	99.9
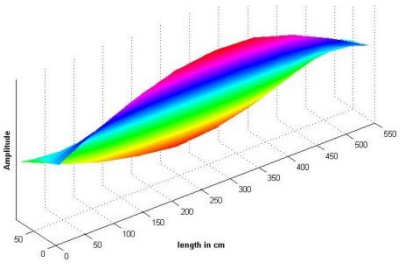	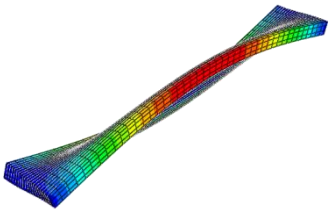	*Close agreement in terms of frequency*	*Close correlation of the mode shapes*
Mode 2: 24.1 Hz	Mode 2: 24.8 Hz	-3.1	97.4
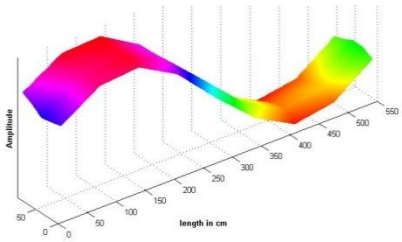	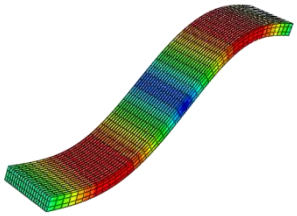	*Close agreement in terms of frequency*	*Close correlation of the mode shapes*
Mode 3: 52.6 Hz	Mode 3: 52.1 Hz	1.1	99.3
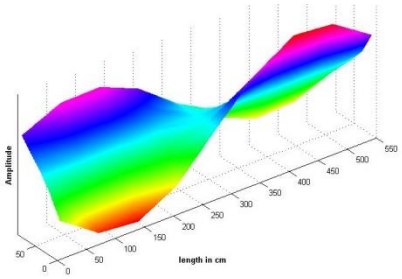	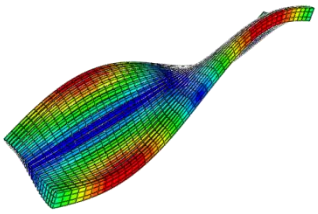	*Close agreement in terms of frequency*	*Close correlation of the mode shapes*
Mode 4: 59.8 Hz	Mode 4: 55.8 Hz	6.7	94.2

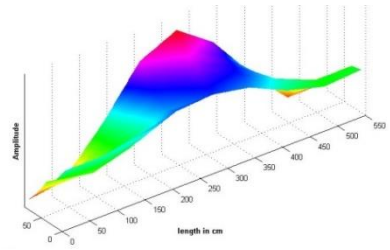	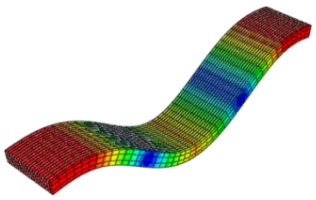	*Close agreement in terms of frequency*	*Close correlation of the mode shapes*
Mode 5: 97.4 Hz	Mode 5: 98.5 Hz	-1.1	82.5
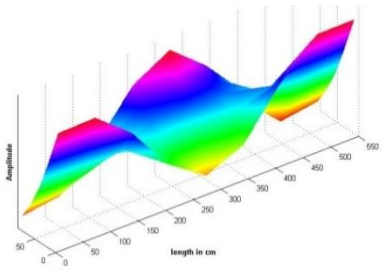	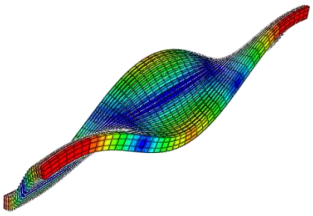	*Close agreement in terms of frequency*	*Close correlation of the mode shapes*
Mode 6: 103.7 Hz	Mode 6: 100.5 Hz	3.1	92.6
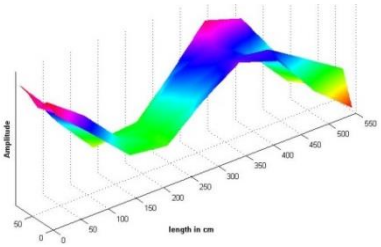	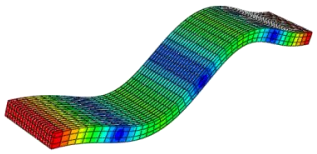	*Close agreement in terms of frequency*	*Close correlation of the mode shapes*
Mode 7: 137.4 Hz	Mode 7: 146.9 Hz	-6.9	90.1
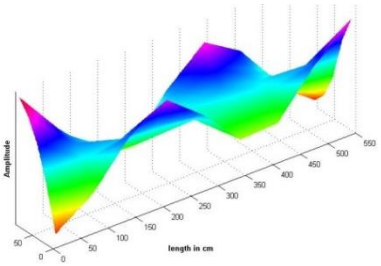	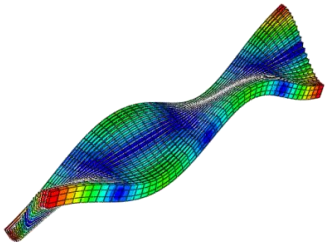	*Close agreement in terms of frequency*	*Close correlation of the mode shapes*
Mode 8: 150.3 Hz	Mode 8: 148.1 Hz	1.4	86.9
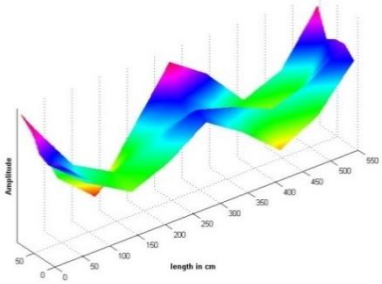	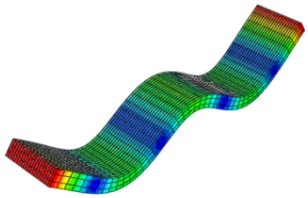	*Reasonable agreement in terms of frequency*	*Reasonable correlation of the mode shapes*
Mode 9: 188.6 Hz	Mode 9: 212.4 Hz	-12.6	78.6

The results of the finite element model show good agreement with the experimental results in terms of eigenfrequencies and mode shapes. It is concluded that this model is representative of the experimental data; hence the next step is to check the agreement for beam assemblies B and C.

In order to explore the contribution of each correlation point to the MAC values, the coordinate modal assurance criterion (CoMAC) was used.

Figure 3-21 shows the CoMAC value of each of the 45 correlation points as bar chart, including in the calculation of CoMAC all the mode pairs (9 pairs) in the frequency range (0<f<200 Hz). CoMAC values close to 1 indicate high correlation while values close to 0 indicate low correlation. Figure 3-22 shows an alternative way to present CoMAC as contour plot. The benefit of using this plot is that it visualizes the location of each correlation point in the assembly and indicates with colors the areas that show high or low correlation between FEM and experimental mode pairs.

CoMAC results for Assembly A indicate that the correlation points that are located near the supports have the lowest CoMAC values (bellow 0.7). This is indicative of the complexity in modeling accurately the boundary in FEM. However, the majority of the correlation points show a high degree of correlation with CoMAC values between 0.75 and 0.95.

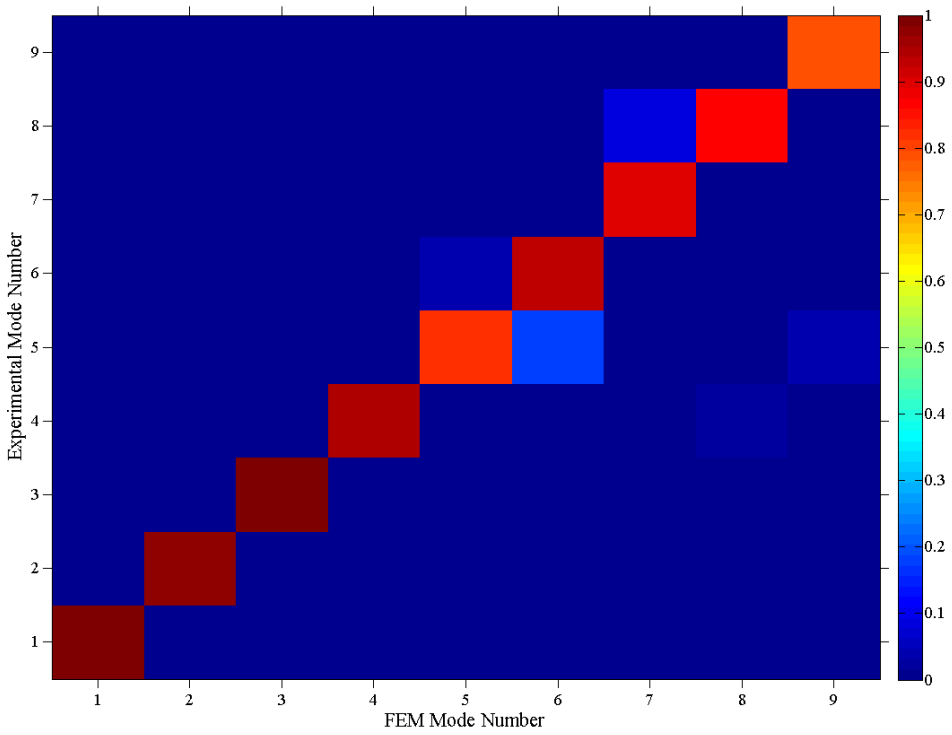

Figure 3-20 2-D presentation of MAC values (out-of-plane displacements)

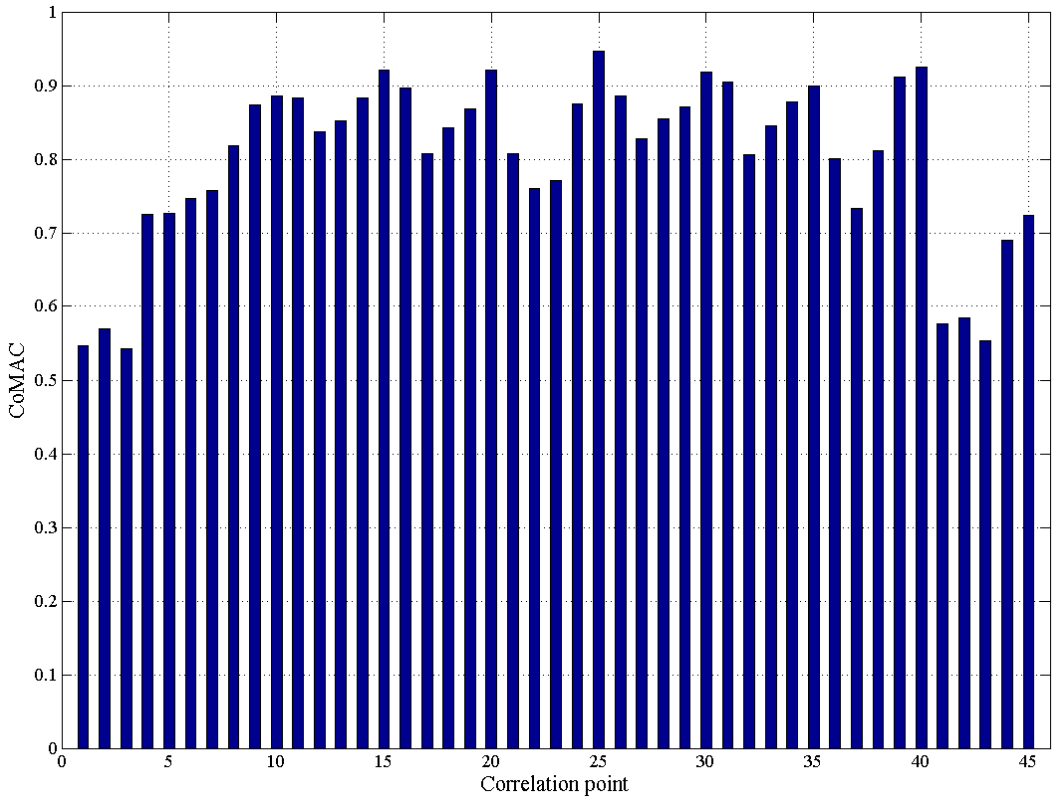

Figure 3-21 CoMAC values of each correlation point (Out-of-plane displacements)

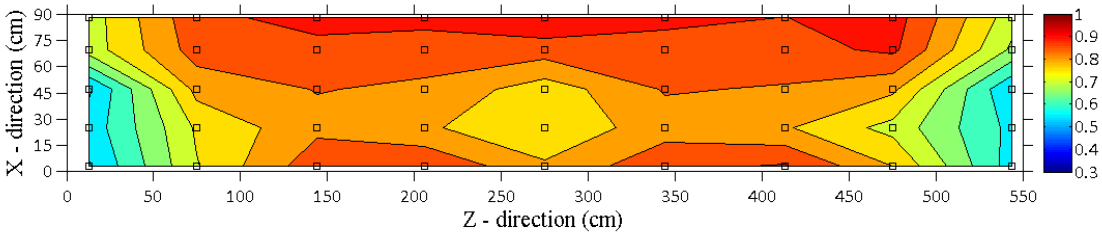

Figure 3-22 Presentation of CoMAC as contour plot (the square dots indicate the location of each correlation point)

3.6 Finite element modelling and validation of Assemblies B and C

For the modeling of Assemblies B and C, the validated finite element model from Assembly A is used but with material properties relating specifically to assemblies 1 and 3 (Table 3-4) and dowel spring stiffness (Table 3-17).

Table 3-17 Dowel spring stiffness for Assemblies B and C

	k_x [N/mm]	k_y[N/mm]	k_z [N/mm]
Assembly B	10000	300	300
Assembly C	10000	300	300

3.6.1 Assembly B

Modal analysis results

Table 3-18, compares the results of the numerical analysis with the results of the experimental modal analysis for the Assembly B. The comparison was made in terms of frequencies and mode shapes.

In order to compare the mode shapes, MAC is calculated using the out-of-plane displacements of 45 correlation points. Figure 3-23 shows the correlation between the experimental and the FEM mode shapes using a 2D plot.

For the majority of the mode pairs, close agreement was achieved between experimental and FEM results in terms of eigenfrequencies with differences below 10 % and mode shapes with MAC over 85 %.

In order to explore the contribution of each of the 45 correlation points to the MAC values, the CoMAC was applied. Figure 3-24 shows the CoMAC values of each correlation point as bar chart, including in the calculation of CoMAC all 9 mode pairs in the frequency range (0<f<200 Hz). The contour plot of Figure 3-25 shows that the correlation points that are located near the supports have the lowest CoMAC values (below 0.7). This is indicative of the complexity in modelling accurately the boundary in FEM. However, the majority of the correlation points show a high degree of correlation with CoMAC values close to 0.8.

Table 3-18 Comparison between experimental and FEM results

Experimental modal analysis	Finite element analysis	Difference [%]	MAC [%]
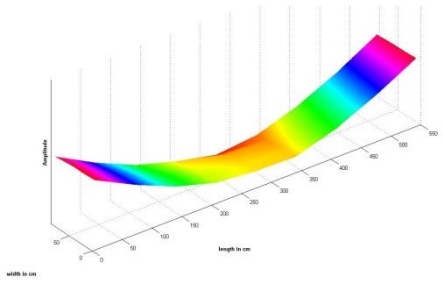	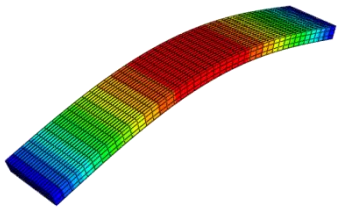	*Close agreement in terms of frequency*	*Close correlation of the mode shapes*
Mode 1: 15.3 Hz	Mode 1: 14.6 Hz	4.2	99.7
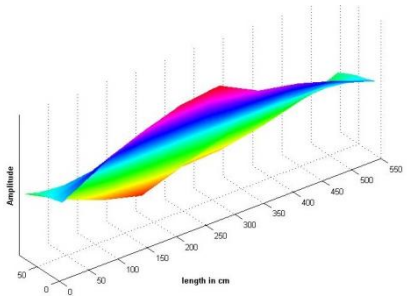	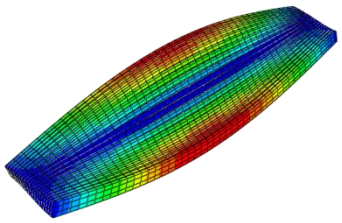	*Close agreement in terms of frequency*	*Close correlation of the mode shapes*
Mode 2: 24.0 Hz	Mode 2: 24.0 Hz	0.0	95.4
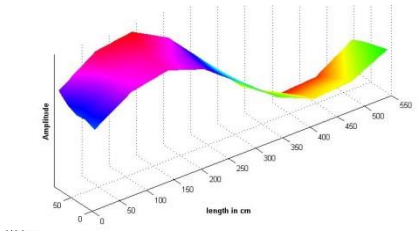	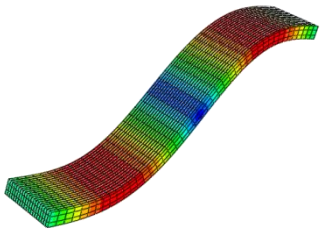	*Close agreement in terms of frequency*	*Close correlation of the mode shapes*
Mode 3: 53.0 Hz	Mode 3: 52.8 Hz	0.5	97.7
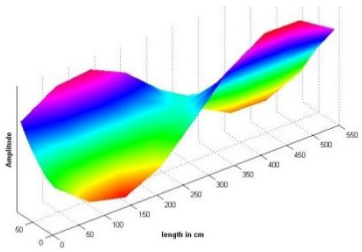	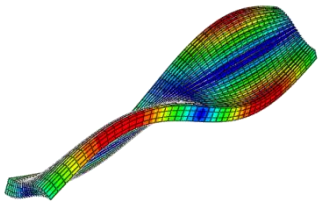	*Close agreement in terms of frequency*	*Close correlation of the mode shapes*
Mode 4: 61.3 Hz	Mode 4: 56.1 Hz	8.6	94.9

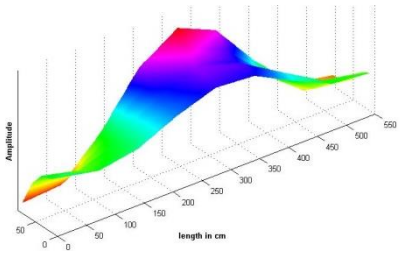	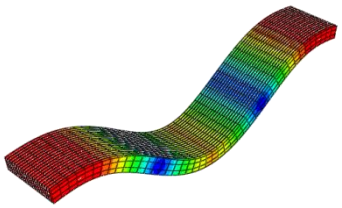	*Close agreement in terms of frequency*	*Close correlation of the mode shapes*
Mode 5: 97.9 Hz	Mode 5: 99.9 Hz	-2.1	86.4
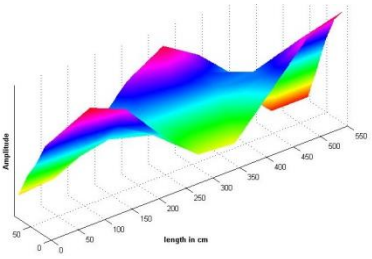	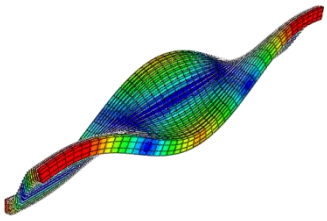	*Close agreement in terms of frequency*	*Close correlation of the mode shapes*
Mode 6: 107.6 Hz	Mode 6: 101.6 Hz	5.6	91.2
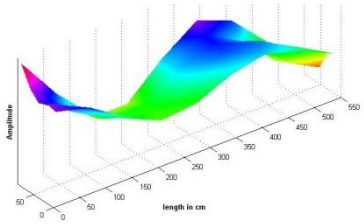	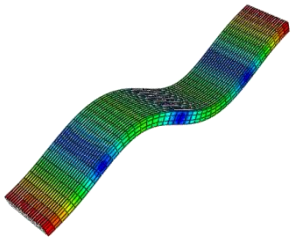	*Close agreement in terms of frequency*	*Close correlation of the mode shapes*
Mode 7: 135.8 Hz	Mode 7: 149.0 Hz	-9.7	85.0
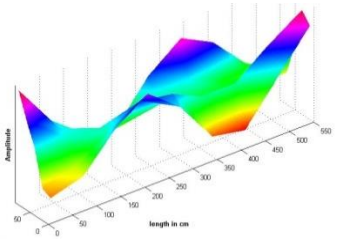	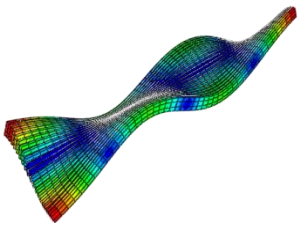	*Close agreement in terms of frequency*	*Reasonable correlation of the mode shapes*
Mode 8: 157.5 Hz	Mode 8: 150.1 Hz	4.7	76.1
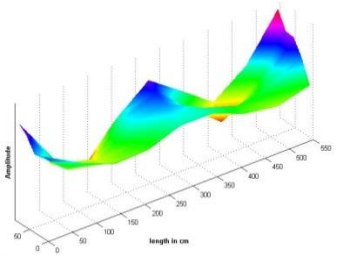	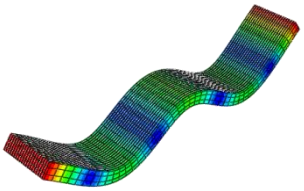	*Reasonable agreement in terms of frequency*	*Reasonable correlation of the mode shapes*
Mode 9: 185.9 Hz	Mode 9: 215.4 Hz	-15.8	72.2

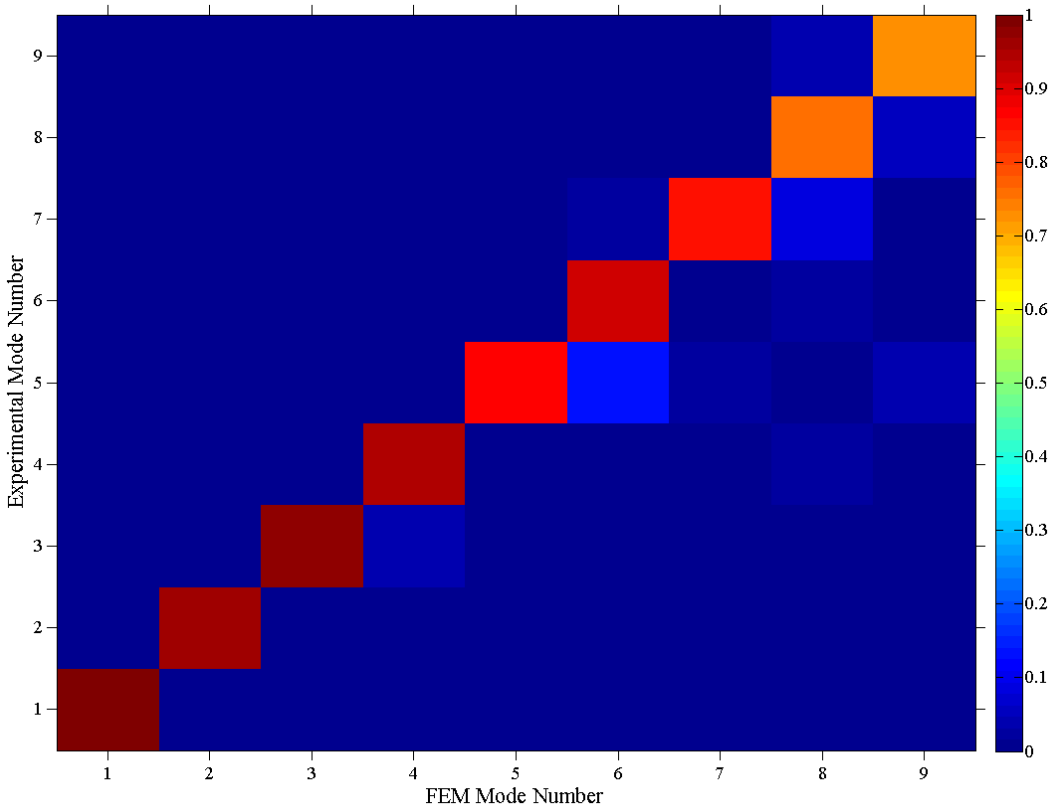

Figure 3-23 2-D presentation of MAC values (out-of-plane displacements)

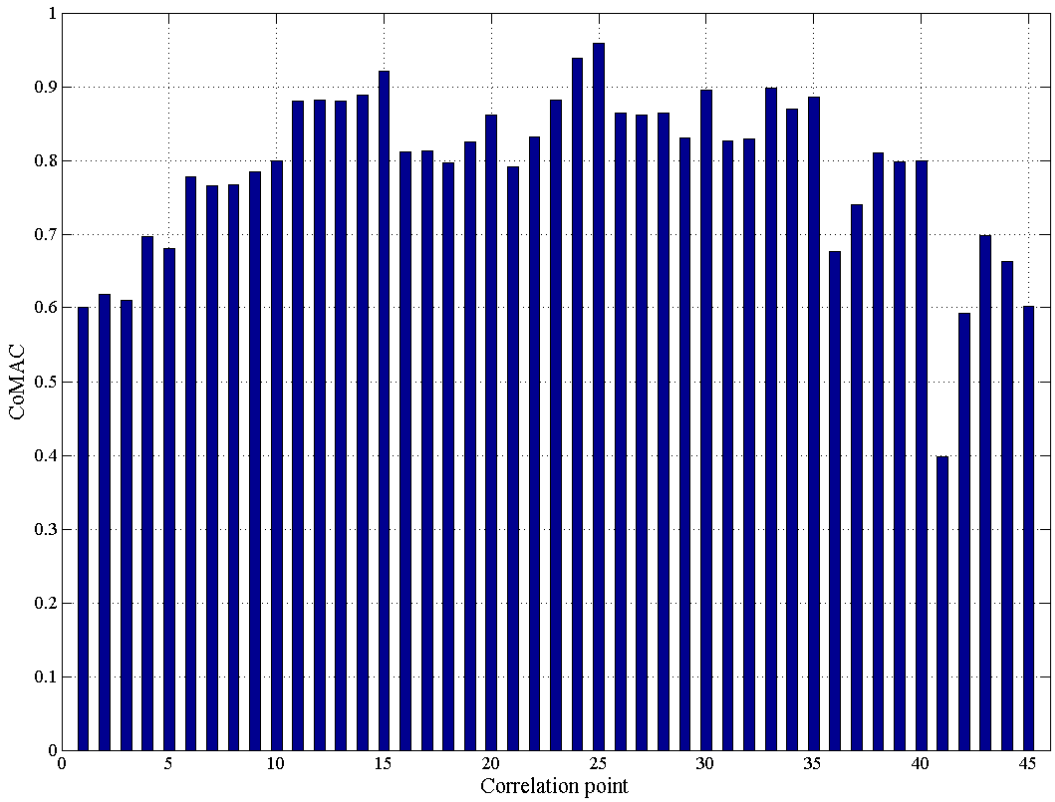

Figure 3-24 CoMAC values of each correlation point (out-of-plane displacements)

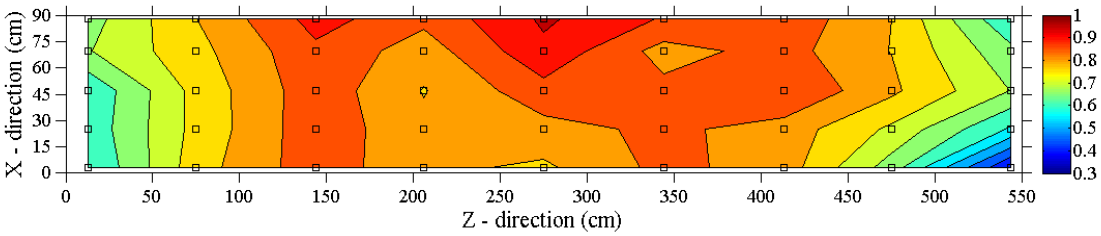

Figure 3-25 Presentation of CoMAC as contour plot (the square dots indicate the location of each correlation point)

3.6.2 Assembly C

Modal analysis results

Table 3-19, compares the results of the numerical analysis with the results of the experimental modal analysis for the Assembly C. The comparison was made in terms of frequencies and mode shapes.

Figure 3-26 present the correlation between the experimental and the FEM mode shapes using a 2D plot.

The results of the finite element model show good agreement with the experimental results in terms of eigenfrequencies and mode shapes. For the majority of the mode pairs, close agreement was achieved between experimental and FEM results in terms of eigenfrequencies with differences below and up to 10 %. For all the mode pairs close agreement was achieved in terms of mode shapes with MAC over 85 %.

Figure 3-27 present the CoMAC value of each correlation point as bar chart, including in the calculation of CoMAC all the 9 mode pairs in the frequency range (0<f<200 Hz). The contour plot of Figure 3-28 shows that the correlation points near the supports have the lowest degree of correlation with CoMAC values from 0.6 to 0.8. This degree of correlation is higher than for Assemblies A and B since the correlation points near the supports of assembly A have CoMAC values between 0.55 and 0.7 and the correlation points near the supports of assembly B have CoMAC values between 0.4 and 0.7. This highlights the degree of inhomogeneity that can occur with assemblies that are assumed to be nominally identical.

Table 3-19 Comparison between experimental and FEM results

Experimental modal analysis	Finite element analysis	Difference [%]	MAC [%]
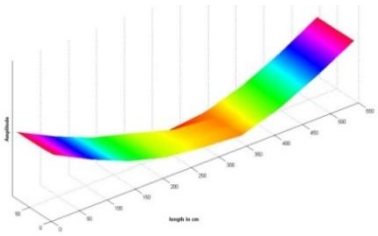	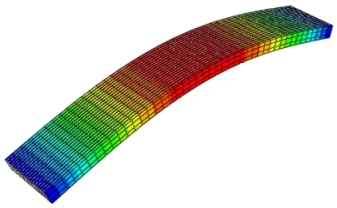	*Close agreement in terms of frequency*	*Close correlation of the mode shapes*
Mode 1: 14.3 Hz	Mode 1: 13.9 Hz	3.0	99.4
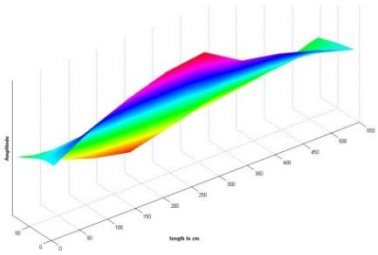	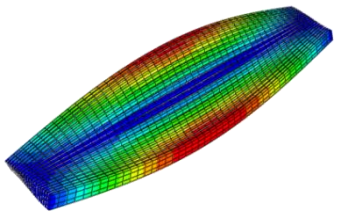	*Close agreement in terms of frequency*	*Close correlation of the mode shapes*
Mode 2: 23.4 Hz	Mode 2: 23.7 Hz	-1.6	93.8
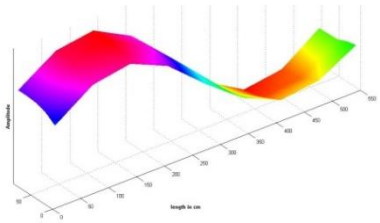	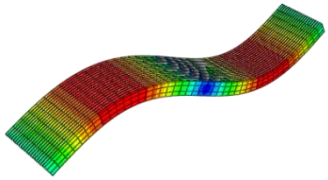	*Close agreement in terms of frequency*	*Close correlation of the mode shapes*
Mode 3: 49.7 Hz	Mode 3: 52.7 Hz	-2.1	98.8
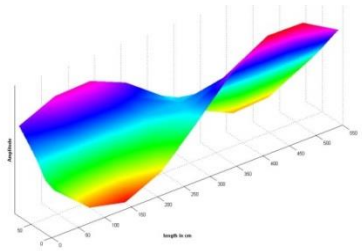	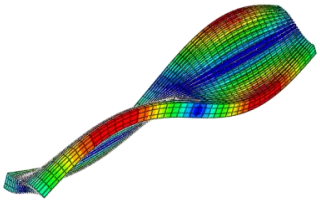	*Close agreement in terms of frequency*	*Close correlation of the mode shapes*
Mode 4: 58.4 Hz	Mode 4: 54.2 Hz	7.1	95.8
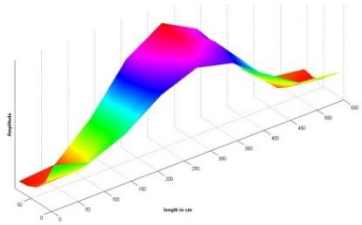	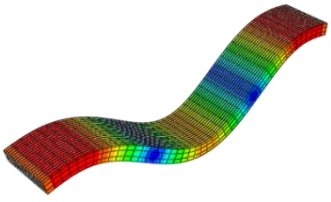	*Close agreement in terms of frequency*	*Close correlation of the mode shapes*
Mode 5: 90.7 Hz	Mode 5: 97.7 Hz	-7.6	95.1

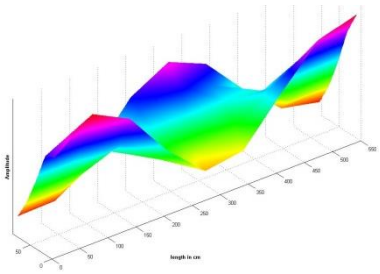	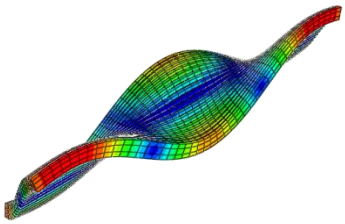	*Close agreement in terms of frequency*	*Close correlation of the mode shapes*
Mode 6: 102.7 Hz	Mode 6: 99.5 Hz	3.1	94.5
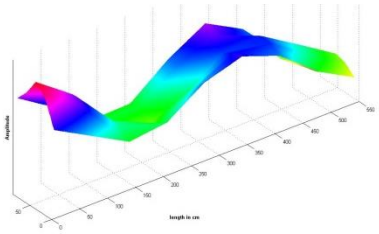	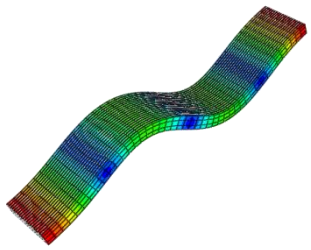	*Close agreement in terms of frequency*	*Close correlation of the mode shapes*
Mode 7: 132.8 Hz	Mode 7: 146.2 Hz	-10.1	87.9
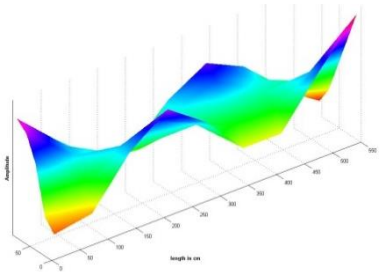	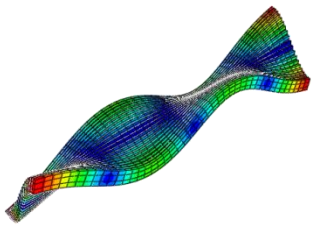	*Close agreement in terms of frequency*	*Close correlation of the mode shapes*
Mode 8: 150.5 Hz	Mode 8: 147.4 Hz	2.0	94.0
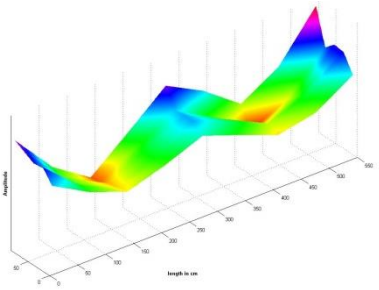	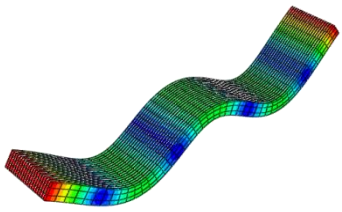	*Reasonable agreement in terms of frequency*	*Close correlation of the mode shapes*
Mode 9: 187.8 Hz	Mode 9: 208.7 Hz	-11.1	85.3

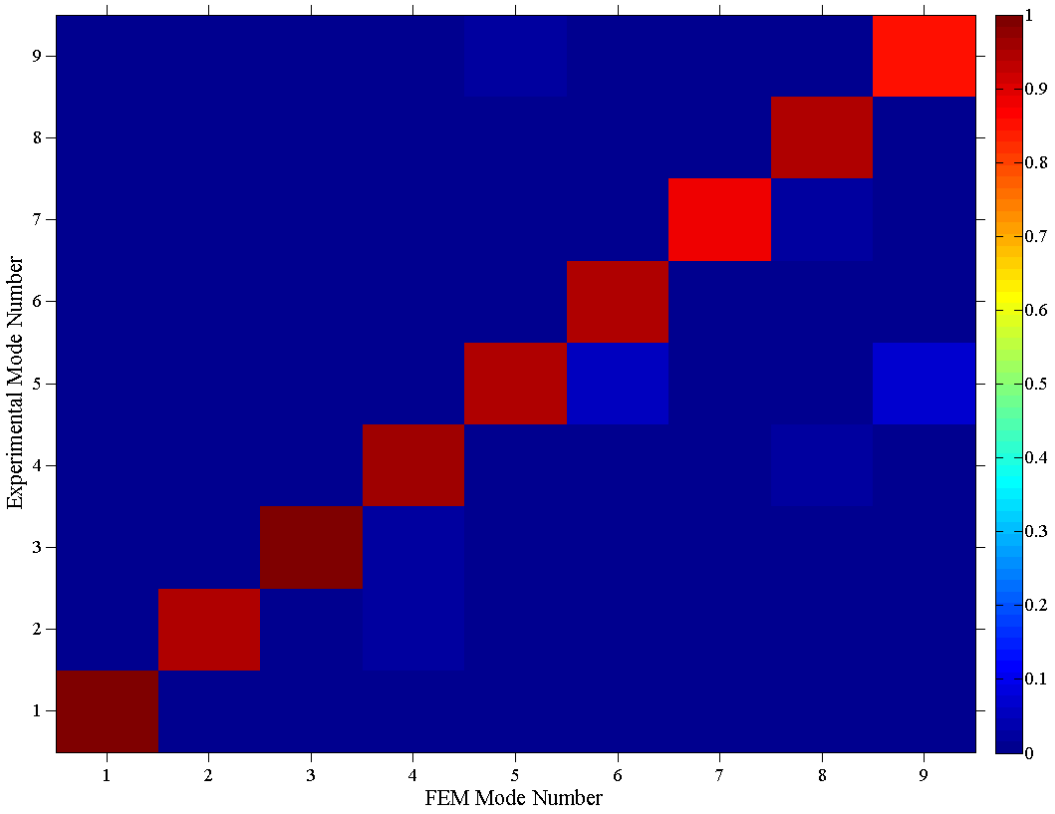

Figure 3-26 2-D presentation of MAC values (out-of-plane displacement)

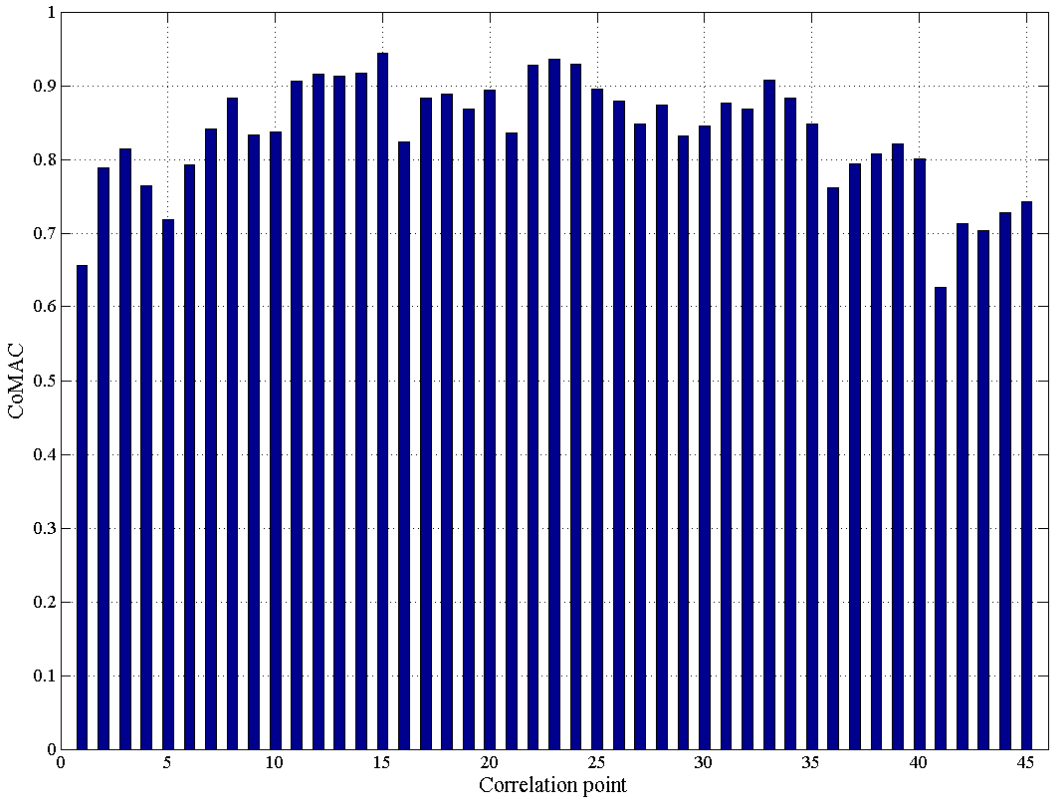

Figure 3-27 CoMAC values of each correlation point (out-of-plane displacement)

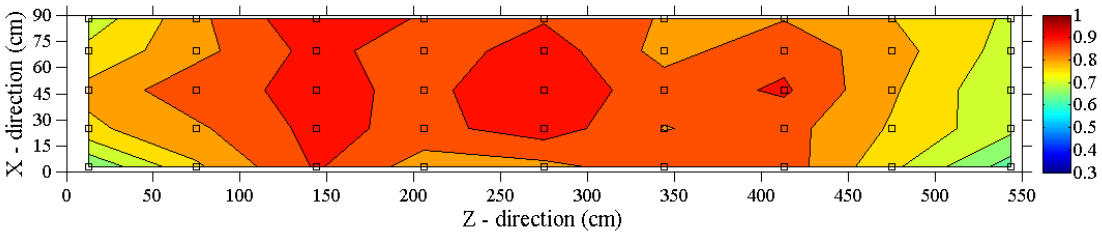

Figure 3-28 Presentation of CoMAC as contour plot (the square dots indicate the location of each correlation point)

3.7 Finite element modelling and validation of the dowelled-joist timber floor system

Description of the model

In this section, the validated finite element models of the three assemblies are joined together to create a finite element model of the dowelled-joist timber floor system (Figure 3-29). The joining of the assemblies is carried out using two connection zones. In each connection zone, the two assemblies are connected using coupling constraints that follow the pattern of the metal screws (Figure 3-30). All degrees of freedom (i.e. translational and rotational) are coupled in each constraint.

Each connection zone consists of six beams with very fine element mesh in order to create the inclined metal screw geometry.

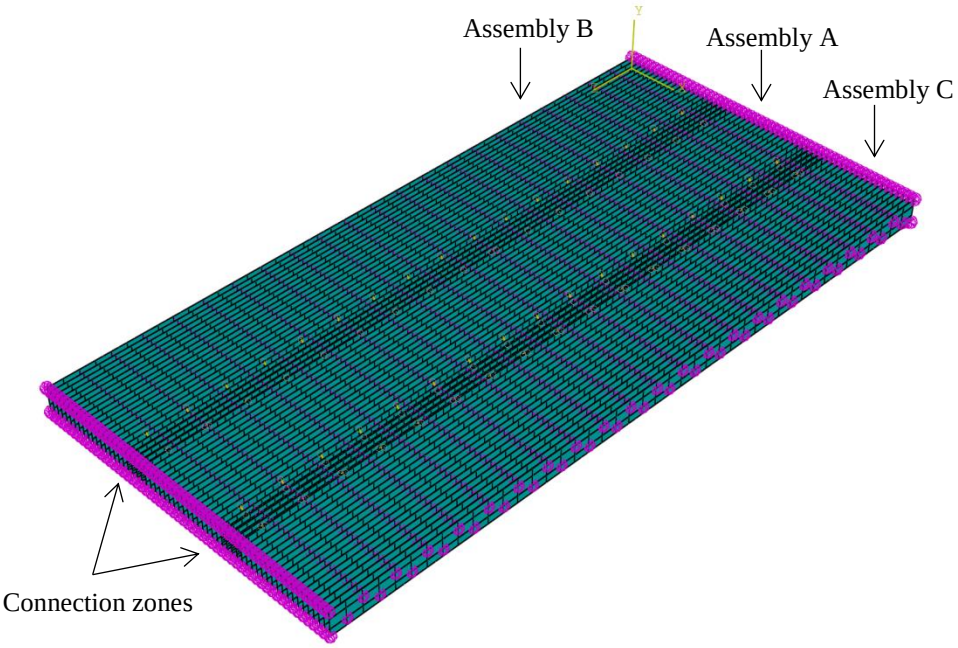

Figure 3-29 Finite element model of the dowelled-joist timber floor system

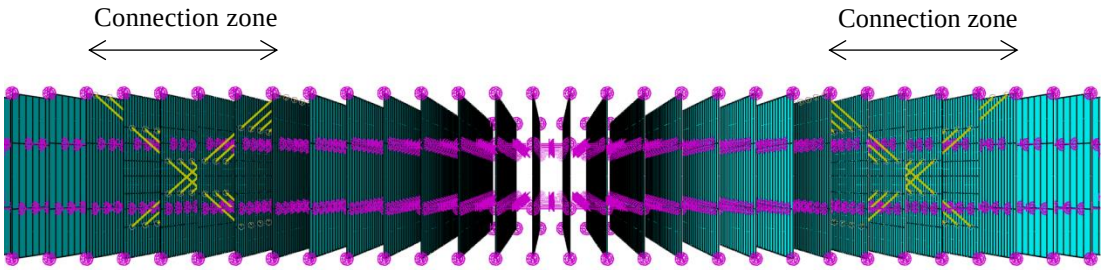

Figure 3-30 Detail of the two connection zones where the metal screws (yellow) act as coupling constraint

Modal analysis results

Table 3-20 compares the results of the finite element analysis with the results of the experimental modal analysis for the complete floor. The comparison was made in terms of frequencies and mode shapes.

In order to compare the mode shapes the Modal Assurance Criterion (MAC) uses the out-of-plane displacements of 117 correlation points. Figure 3-31 show the correlation between the experimental and the FEM mode shapes using a 2D plot.

In general, there is a close agreement between the FEM and the experimental results in terms of frequencies and mode shapes. The only exceptions are experimental mode shapes 8 and 13 which have weak or no correlation with the finite element mode shapes.

Table 3-20 Comparison between experimental and FEM results

Experimental modal analysis	Finite element analysis	Difference [%]	MAC [%]
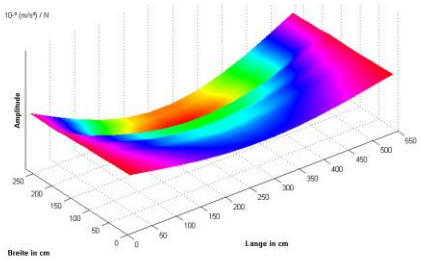	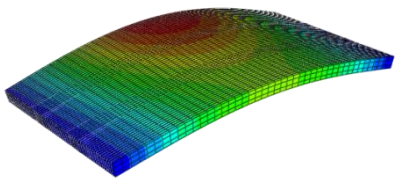	*Close agreement in terms of frequency*	*Close correlation of the mode shapes*
Mode 1: 14.6 Hz	Mode 1: 14.3 Hz	2.3	96.6

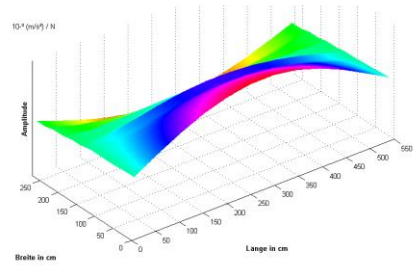	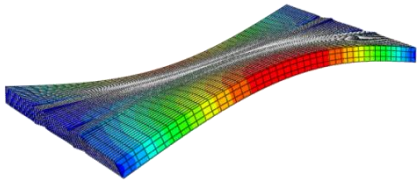	*Close agreement in terms of frequency*	*Close correlation of the mode shapes*
Mode 2: 16.1 Hz	Mode 2: 15.9Hz	1.4	93.0
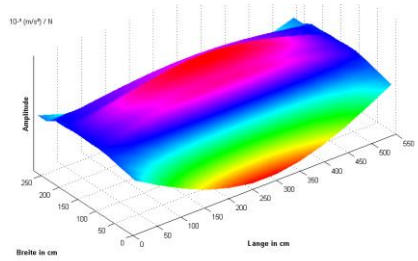	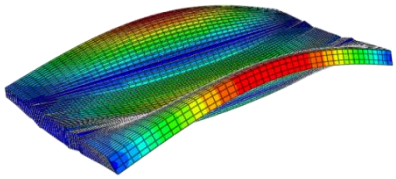	*Close agreement in terms of frequency*	*Close correlation of the mode shapes*
Mode 3: 20.8 Hz	Mode 3: 19.8 Hz	5.0	88.9
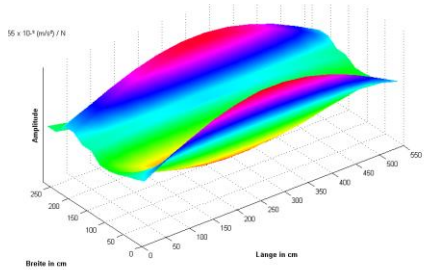	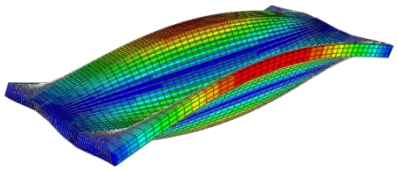	*Reasonable agreement in terms of frequency*	*Reasonable correlation of the mode shapes*
Mode 4: 28.6 Hz	Mode 4: 24.3 Hz	15.0	70.0
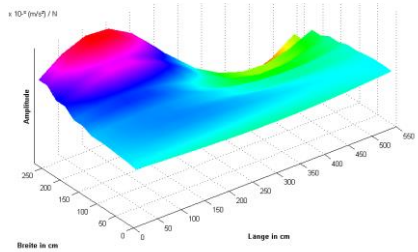	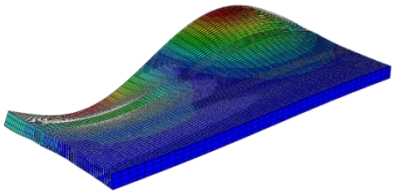	*Close agreement in terms of frequency*	*Close correlation of the mode shapes*
Mode 5: 49.7 Hz	Mode 5: 51.2 Hz	-3.1	96.4
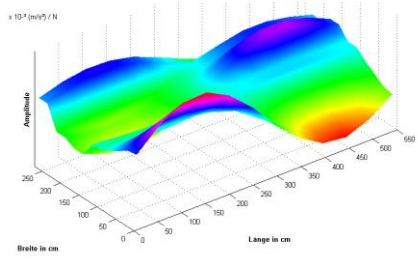	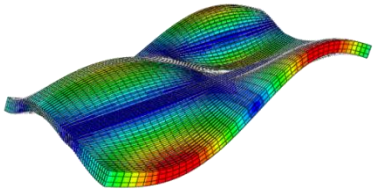	*Close agreement in terms of frequency*	*Close correlation of the mode shapes*
Mode 6: 57.0 Hz	Mode 6: 53.8 Hz	5.6	92.1

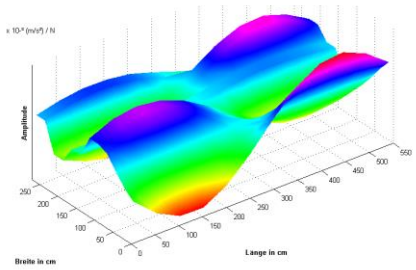	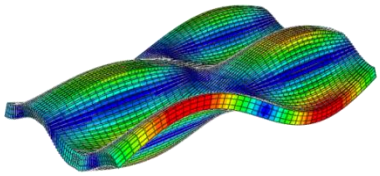	*Reasonable agreement in terms of frequency*	*Close correlation of the mode shapes*
Mode 7: 63.2 Hz	Mode 7: 55.5 Hz	12.1	87.8
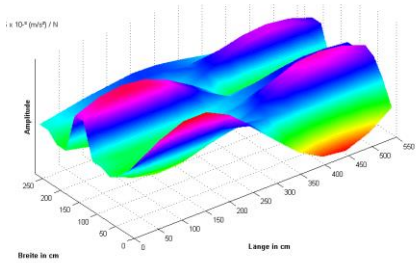	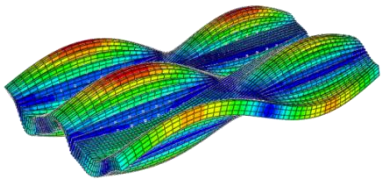	Weak *agreement in terms of frequency*	*Weak correlation of the mode shapes*
Mode 8: 74.0 Hz	Mode 8: 59.7 Hz	19.3	50.9
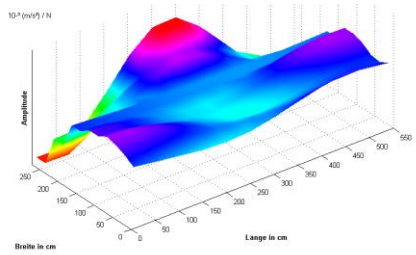	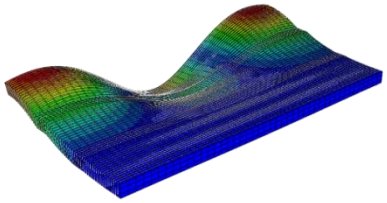	*Close agreement in terms of frequency*	*Reasonable correlation of the mode shapes*
Mode 9: 90.5 Hz	Mode 9: 97.9 Hz	-8.2	69.8
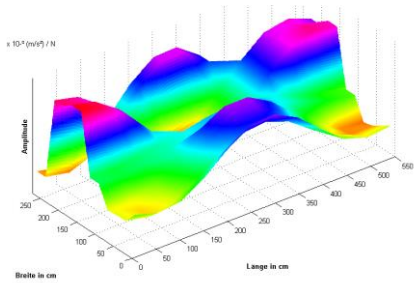	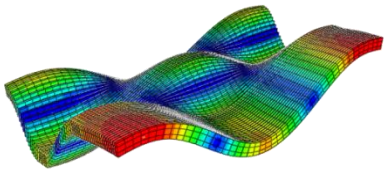	*Close agreement in terms of frequency*	*Reasonable correlation of the mode shapes*
Mode 10: 100.8 Hz	Mode 10: 100.0 Hz	0.8	77.9
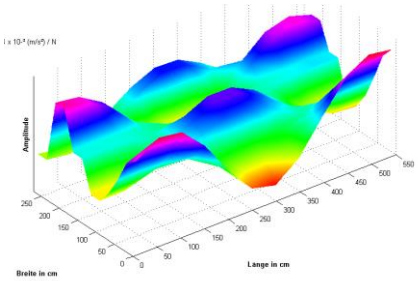	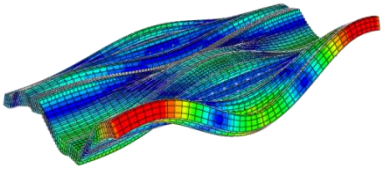	*Close agreement in terms of frequency*	*Reasonable correlation of the mode shapes*
Mode 11: 107.0 Hz	Mode 11: 100.9 Hz	5.7	78.5

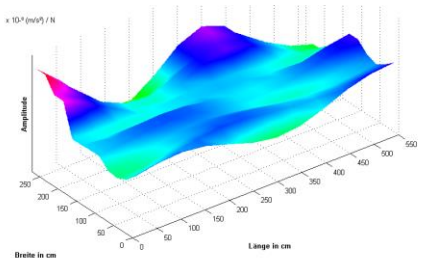	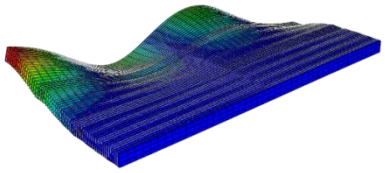	*Reasonable agreement in terms of frequency*	*Reasonable correlation of the mode shapes*
Mode 12: 132.5 Hz	Mode 12: 146.4 Hz	-10.5	77.0
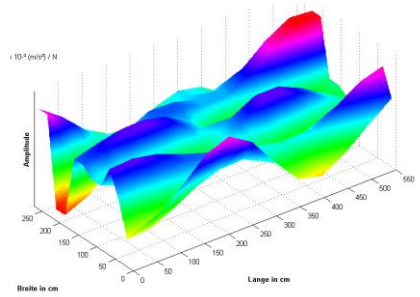	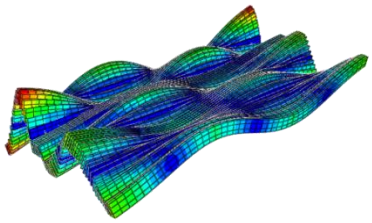	*Close agreement in terms of frequency*	*Uncorrelated mode shapes*
Mode 13: 156.6 Hz	Mode 13: 150.0 Hz	4.2	0.0
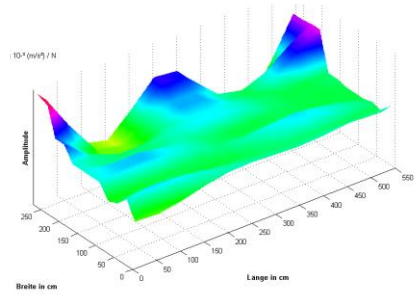	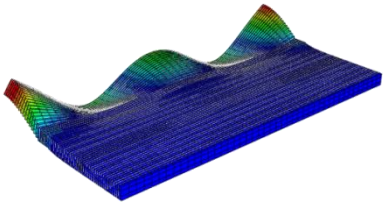	*Reasonable agreement in terms of frequency*	*Close correlation of the mode shapes*
Mode 14: 188.1 Hz	Mode 14: 208.9 Hz	-11.0	80.1

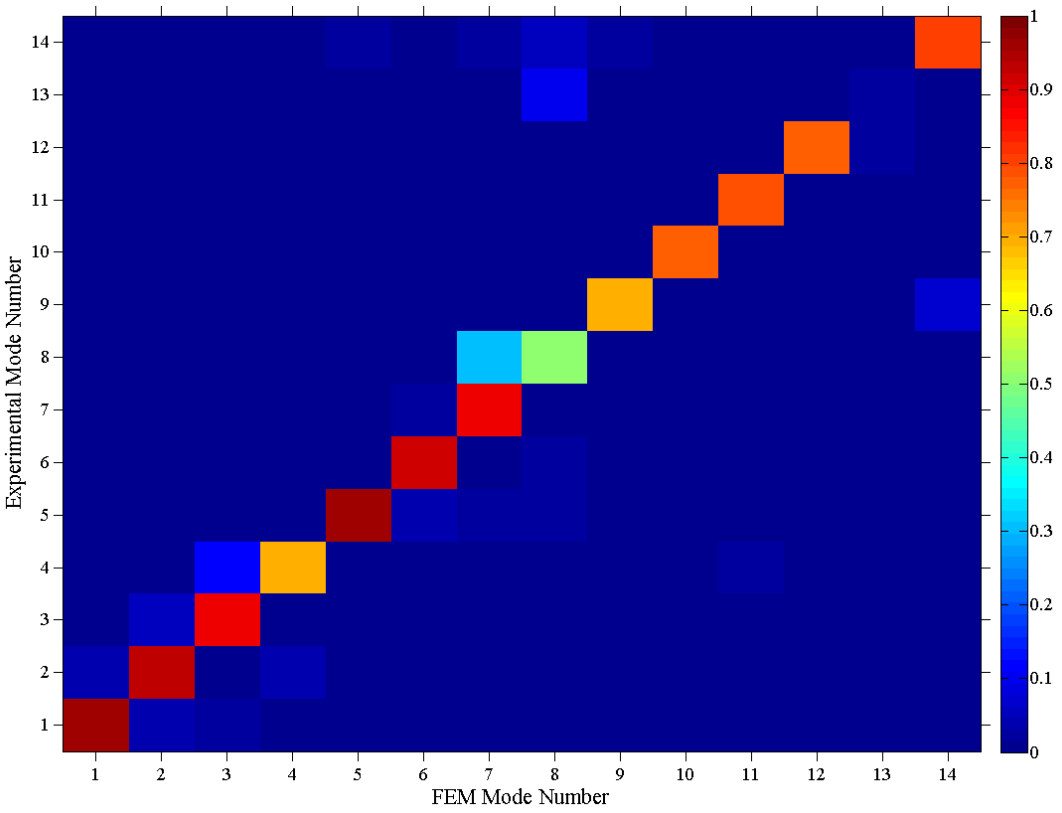

Figure 3-31 2-D presentation of MAC values (out-of-plane displacements)

In order to explore the contribution of each of the 117 correlation points to the MAC values, the coordinate modal assurance criterion (CoMAC) was applied. Figure 3-32 present the CoMAC values of each correlation point as bar chart, including in the calculation of CoMAC all 12 correlated mode pairs in the frequency range (0<f<200 Hz). The contour plot of Figure 3-33 shows that the correlation points near the supports of the assemblies A and B show a lower degree of correlation than the correlation points that are near the supports of the assembly C. Also the correlation points near the connection zones of the assemblies have a lower CoMAC value than the rest correlation points of the floor that show in general high degree of correlation with CoMAC values over 0.7. This indicates the complexity in accurately modelling the boundary conditions and the connection zones.

Figure 3-34 present the CoMAC values of each correlation point as bar chart, including in the calculation of CoMAC all the 8 correlated mode pairs in the frequency range (0<f<100 Hz). Figure 3-35 shows that in this frequency range the majority of the correlation points have a higher CoMAC value than in the frequency range 0<f<200 Hz. However, the correlation points near the connection zones of the assemblies are still showing lower degree of correlation than the rest of the correlation points of the dowelled-joist timber floor.

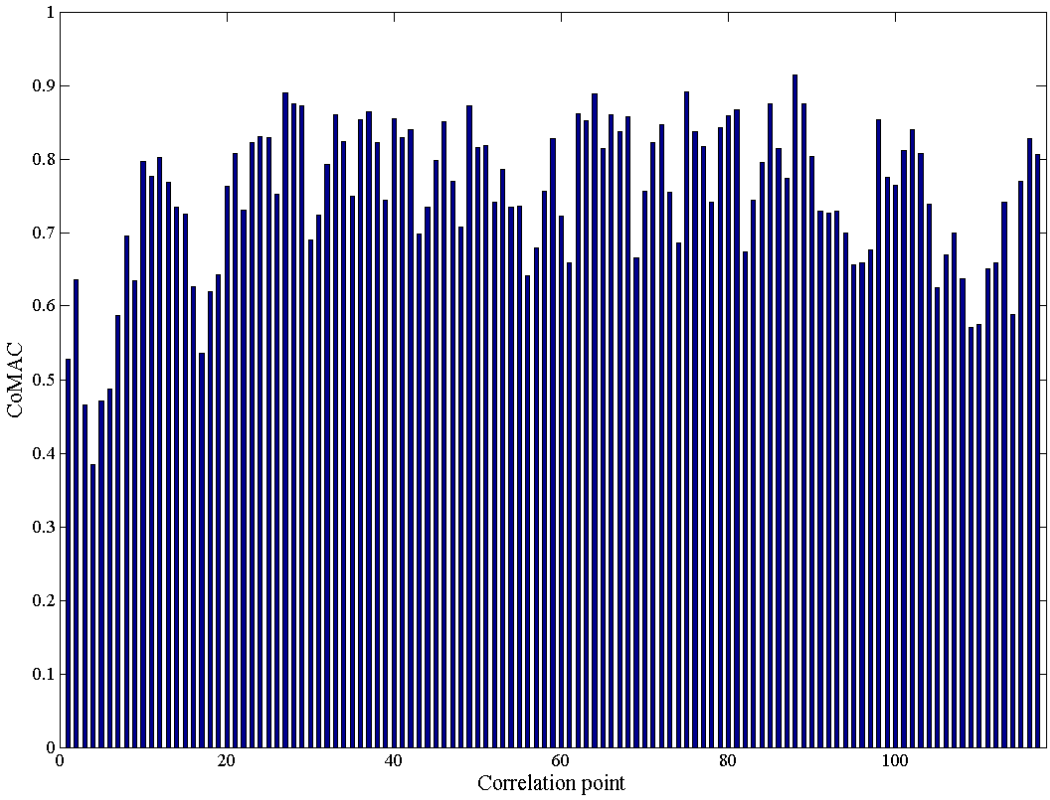

Figure 3-32 CoMAC values of each correlation point for 0<f<200 Hz (out-of-plane displacements)

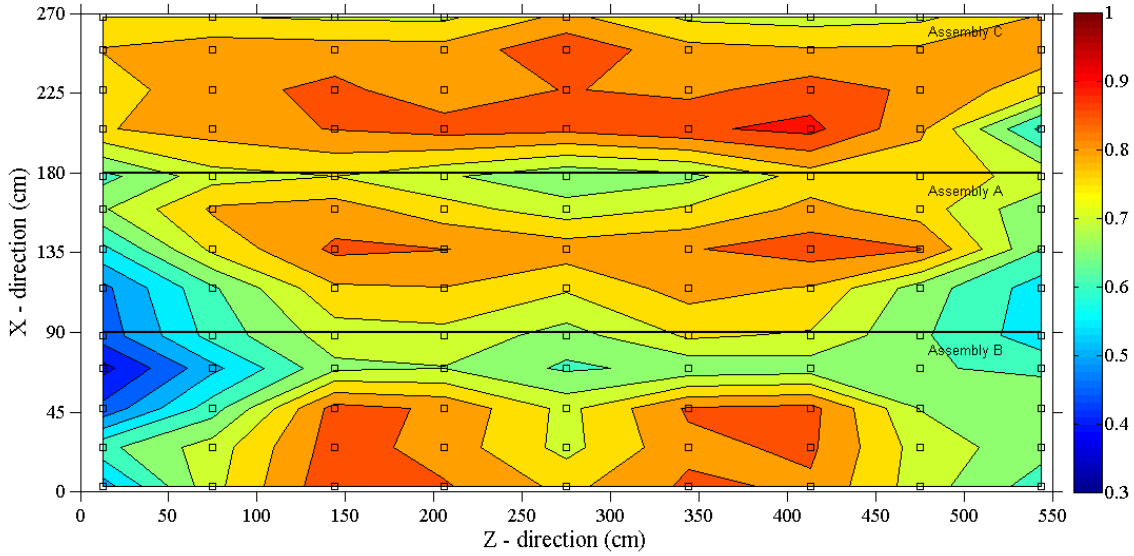

Figure 3-33 Presentation of CoMAC as contour plot for 0<f<200 Hz (the square dots indicate the location of each correlation point)

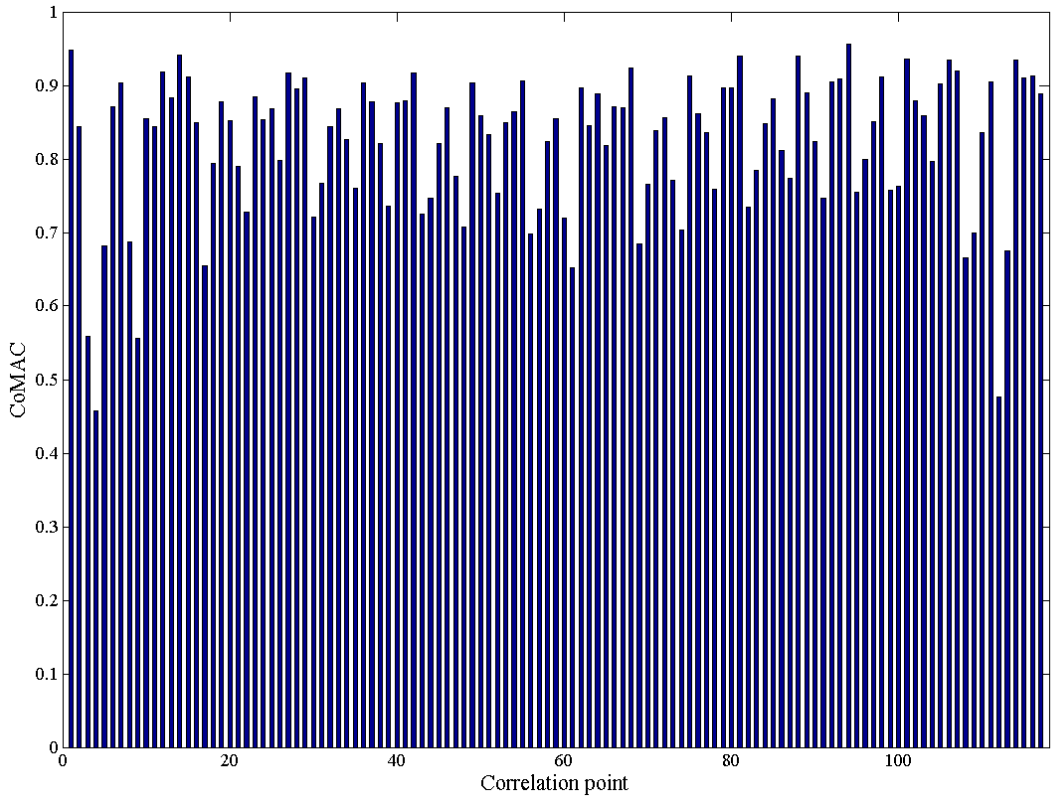

Figure 3-34 CoMAC values of each correlation point for 0<f<100 Hz (out-of-plane displacements)

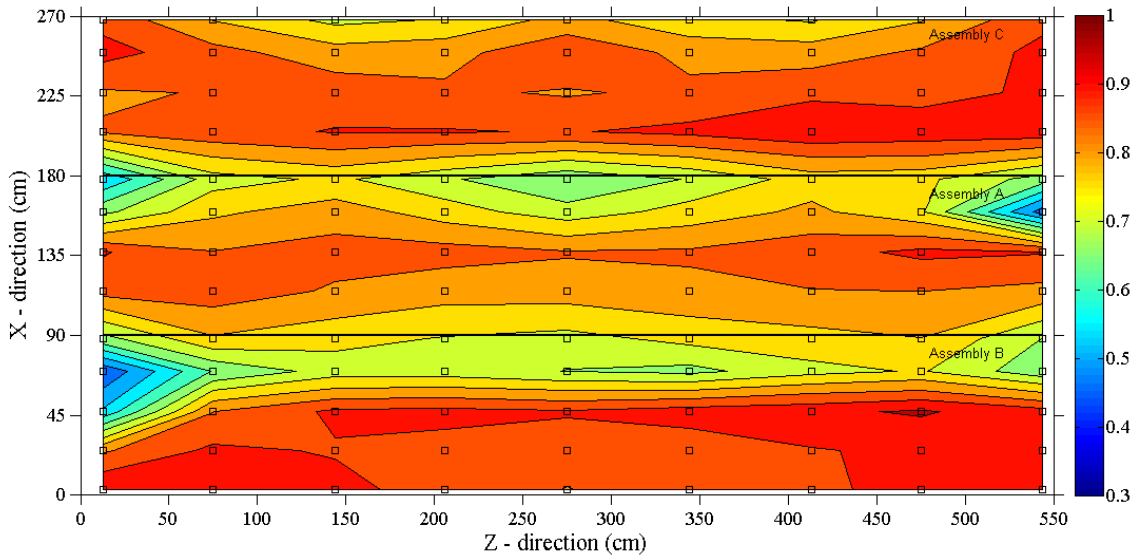

Figure 3-35 Presentation of CoMAC as contour plot for 0<f<100 Hz (the square dots indicate the location of each correlation point)

3.8 Discussion

Finite element models of individual assemblies and a dowelled-joist timber floor formed from three assemblies have been developed in Abaqus. These have been validated successfully against the experimental results. Although each assembly is clearly inhomogeneous in its manufacture, the first attempt at a model assumed a highly-idealised isotropic homogenous plate. The reason for this was to start with the lowest level of complexity and gradually increase the complexity until the required agreement was obtained between the experimental modal analysis and the finite element model. The required agreement was determined in terms of eigen-frequencies as differences less than 10 % and in terms of mode shapes as MAC values over 80 %. The consideration of elastic springs at the position of the vertical edge support revealed the complexity of the boundary conditions used in the experimental situation. It was possible to model the assemblies by using coupling constraints or join connectors at the dowel positions and springs at the supports but the closest agreement was obtained through the use of spring connections at the dowel positions combined with detailed modelling of the boundary conditions (supports) at the two ends of the assemblies. This approach was highly successful for all three assemblies with close agreement in both the mode frequencies and the MAC values.

A finite element model of the dowelled-joist timber floor was formed from the three validated finite element models of the individual assemblies. Twelve out of the fourteen modes below 200Hz, showed close agreement between experimental modal analysis and the finite element model. Due to the validation of the individual assemblies, this validates the modelling of the metal screw connections between assemblies.

3.9 Conclusions

An overview has been given of the experimental work carried out by Rosenheim to determine the material properties of spruce and beech and the dynamic behaviour of individual dowel-connected floor assemblies as well as a dowelled-joist timber floor formed from these assemblies. Both aspects were essential to carry out the development and validation of the finite element models in this thesis.

In this chapter, finite element models have been developed and validated successfully against the experimental modal analysis for (a) individual beech beam, (b) three individual spruce assemblies and (c) a dowelled-joist floor formed from the three assemblies.

A sequence of finite element models of increasing complexity have been assessed to achieve the closest agreement between experimental and finite element eigen-frequencies and mode

shapes. This resulted in the use of spring connections at the dowel positions combined with precise modelling of the boundary conditions (supports) at the two ends of the assemblies. This approach was highly successful for all three assemblies with close agreement in both the mode frequencies and the MAC values.

The main disadvantage of using springs for modelling the dowel connections is that in the output of the eigenvalue analysis many modes are governed by the local response of the springs. These modes are not 'physical' and they were not observed in the experimental procedure.

The application of the coordinate modal assurance criterion indicates that the boundary conditions and the connection zones of the assemblies are complex to model accurately using the finite element method. However, the observed variation in the modal response of nominally identical assemblies means that the pursuit of 'more accurate' models is unlikely to be worthwhile for practical purposes.

Before using the validated finite element model of the dowelled-joist timber floor for the prediction of sound radiation from the floor into a room under point force excitation, it is necessary first to validate the finite element method against a normal mode model for the prediction of sound radiation. This is the objective of the next chapter where a vibroacoustic finite element model is validated against a normal mode model for the prediction of sound radiation from a 140 mm and 180 mm concrete plate into a room under point force excitation.

4. Validation of the finite element method using a normal mode model for sound radiation from a concrete plate into a room

4.1 Introduction

This chapter discusses the validation of the finite element method against a normal mode model for the prediction of sound radiation from a 140mm and 180mm concrete plate (4m x 5m) into a box-shaped room (4m x 5m x 3m). The reason for choosing these two thicknesses is that 140mm is used for vertical transmission suite tests according to ISO 10140 but in Swiss buildings it is common to use 180mm. A finite element model of the plate and the room for fluid-structure interaction was created in Abaqus using structural and acoustic finite elements. Both mode-based and direct-solution steady-state dynamic analysis procedures were investigated during the validation procedure.

4.2 Normal mode model

For a single plate coupled to a room, a normal mode model was developed by Kihlman (1967). Neves e Sousa (2012) modified the model in order to calculate sound pressure level at a position in the room from point force excitation on a simply-supported plate. This method showed reasonable agreement between the measured and predicted sound pressure level for individual excitation and response positions. However, there was an error in the derivation as noted by Hopkins (2011) which meant that the predictions were incorrect for axial and tangential modes. The corrected model was then used by Robinson (2012) to calculate sound radiation from a small concrete plate into a small room.

The corrected version (Hopkins, 2011) results in a transfer function between the pressure in the room at a position with coordinates x, y, z and the force excitation of the plate at a position with coordinates x_s, y_s, given,

$$\frac{p}{F}=\frac{4\omega^2\rho_0}{\pi^2\rho_s V}\left[\sum_{p,q,r=0}^{\infty}\frac{(-1)^r\psi_{p,q,r}(x,y,z)\left[\sum_{m,n=1}^{\infty}\frac{mn[(-1)^{m+p}-1][(-1)^{n+q}-1]\sin\left(\frac{m\pi x_s}{L_x}\right)\sin\left(\frac{n\pi y_s}{L_y}\right)}{\left[{\omega^2}_{m,n}(1+1n)-\omega^2\right](p^2-m^2)(q^2-n^2)}\right]}{\Lambda_{p,q,r}\left({k^2}_{p,q,r}-k^2+2ik\delta_{p,q,r}\right)}\right] \quad (14)$$

where p, q, r are mode constants for the room, m, n are mode constants for the plate, L_x and L_y are the dimensions of the plate and n is the total loss factor of the plate. $\psi_{p,q,r}$ is the eigenfunction for a space with rigid boundaries, $\delta_{p,q,r}$ is the room damping constant, $k_{p,q,r}$ is the room wavenumber and $\omega_{m,n}$ is the angular frequency for simply supported plate mode $f_{m,n}$. $\Lambda_{p,q,r}$ is given by,

$$\Lambda_{p,q,r} = \frac{1}{\varepsilon_p \varepsilon_q \varepsilon_r} \tag{15}$$

where ε_p , ε_q and ε_r are calculated as follows: if p = 0, then ε_p = 1 else ε_p = 2; q = 0, then ε_q = 1 else ε_q = 2; r = 0, then ε_r = 1 else ε_r = 2.

The room wave number is given by,

$$k_{p,q,r} = \pi \sqrt{\left(\frac{p}{L_x}\right)^2 + \left(\frac{q}{L_y}\right)^2 + \left(\frac{r}{L_z}\right)^2} \tag{16}$$

and the room damping constant is given by,

$$\delta_{p,q,r} = \frac{1}{2}\left(\frac{\varepsilon_p\left(\beta_{a,s,x_0} + \beta_{a,s,x_l}\right)}{L_x} + \frac{\varepsilon_q\left(\beta_{a,s,y_0} + \beta_{a,s,y_l}\right)}{L_y} + \frac{\varepsilon_r\left(\beta_{a,s,z_0} + \beta_{a,s,z_l}\right)}{L_z}\right) \tag{17}$$

where β_{a,s,x_0} and β_{a,s,x_l} corresponds to the specific acoustic admittance at x = 0 and x = L_x respectively.

A Matlab code developed for the normal mode model by Professor Carl Hopkins (University of Liverpool) was used for the calculations.

A rectangular room (4.0 m x 5.0 m x 3.0 m) was considered with point force excitation of a rectangular concrete plate (4.0 m x 5.0 m). The harmonic force was applied at a distance that was approximately[1] one-third of the distance along the plate's diagonal (x_s, y_s) = (1.7 m, 1.3 m) and the microphone position was assumed near the corner of the room at (x, y, z) = (0.2m, 0.2m, 0.2m). The material properties from Table 4-1 were used in this code and the frequency resolution was defined to 0.1 Hz.

[1] The force was applied approximately at the one third of the way along the plate's diagonal to try and excite the majority of modes and to be consistent with the finite element model in the next section.

4.3 Finite element model

4.3.1 Description of the model

Figure 4-1 shows the finite element model that was created in Abaqus (Hibbitt et al., 2012) in order to predict the sound radiation from the vibration of a concrete plate (140 mm and 180mm) into a rectangular room due a harmonic force (1-200 Hz). The model consists of two parts: a) a plate (4.0 m x 5.0 m) and b) an acoustic medium (4.0 m x 5.0 m x 3.0 m), that are connected together using tie constraints. This type of constraint is available in Abaqus/Standard and ties all the active degrees of freedom between two surfaces. The plate was assumed to be pinned along the four edges and modelled using shell elements. The acoustic medium of the rectangular room was modelled using acoustic solid elements. The boundary conditions of the acoustic medium were specified in terms of a specific acoustic admittance applied to the six surfaces of the rectangular room.

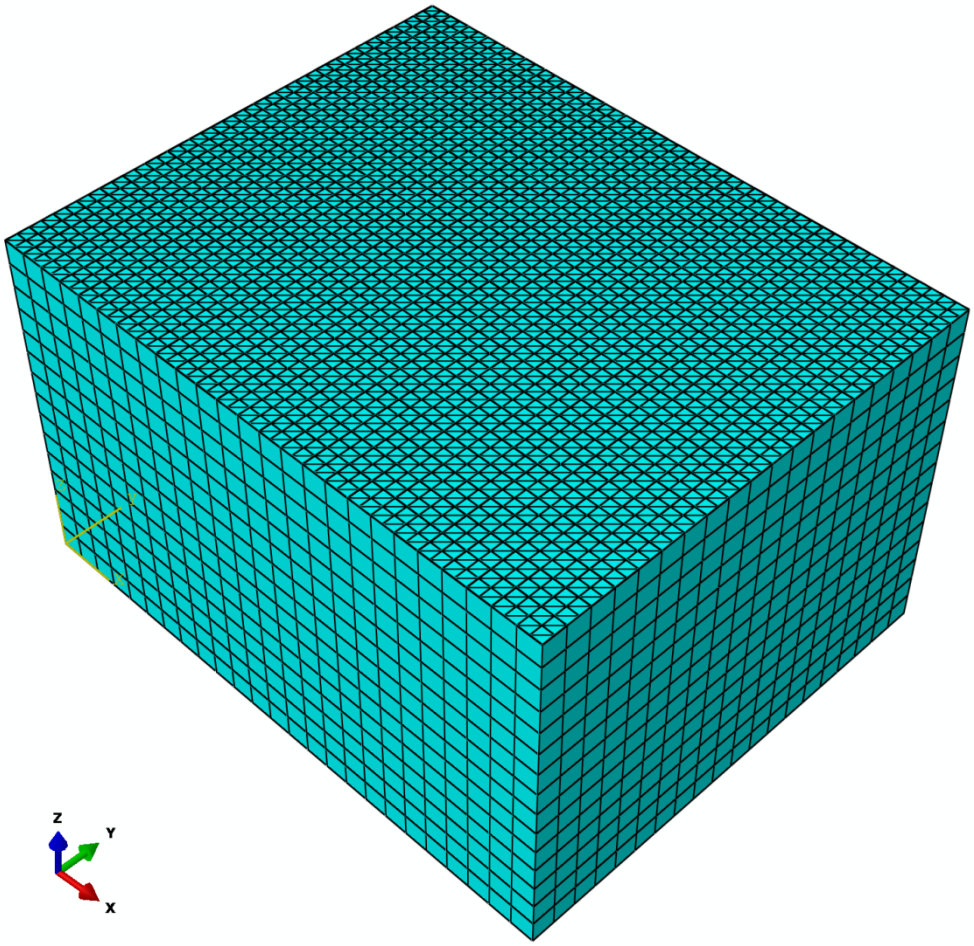

Figure 4-1 Fluid-structure interaction model of the concrete plate (top) and the rectangular room using finite elements

4.3.2 Material properties

Table 4-1 present the material properties that were adopted from the literature (Hopkins, 2007) for the concrete plate and the acoustic medium of the rectangular room. In this chapter only the internal damping of the concrete plate is used in the finite element analyses because the Matlab code for the normal mode model only implements frequency-independent damping.

Table 4-1 Material properties

Concrete		**Room: Acoustic medium**	
Density, ρ [kg/m^3]	2200	Density, ρ [kg/m^3]	1.21
Young's modulus, E [N/m^2]	304973e05	Bulk modulus, K_f [N/m^2]	142355.29
Poisson ratio, v	0.2	Speed of sound in air, c_0 [m/s]	343
Internal damping ratio, ζ [%]	0.25	Acoustic admittance, $\beta_{a,n}$ [m^5/Ns]	3.0897e-05

4.3.3 Meshing

The concrete plate was meshed using the STRI3 shell element (Figure 4-2a) from the element library of Abaqus (Hibbitt et al., 2012). This is a 3-node triangular facet thin shell element with 6 degrees of freedom per node (translations and rotations) and linear interpolation functions that solves thin shell theory using a small-strain approximation.

The use of quadratic elements for this plate was rejected since they increase the computational time without improving agreement with the results of the normal mode model.

The acoustic medium of the rectangular room was meshed using the AC3D8 acoustic solid element (Figure 4-2b) from the element library of Abaqus (Hibbitt et al., 2012). This is an 8-node linear acoustic brick element with one degree of freedom per node (acoustic pressure).

The use of quadratic acoustic elements was rejected after investigation because they significantly increase the computational time whereas they give the same results as the linear acoustic elements. Moreover, the linear acoustic elements offer the advantage of using the specific acoustic admittance as a boundary condition for the room.

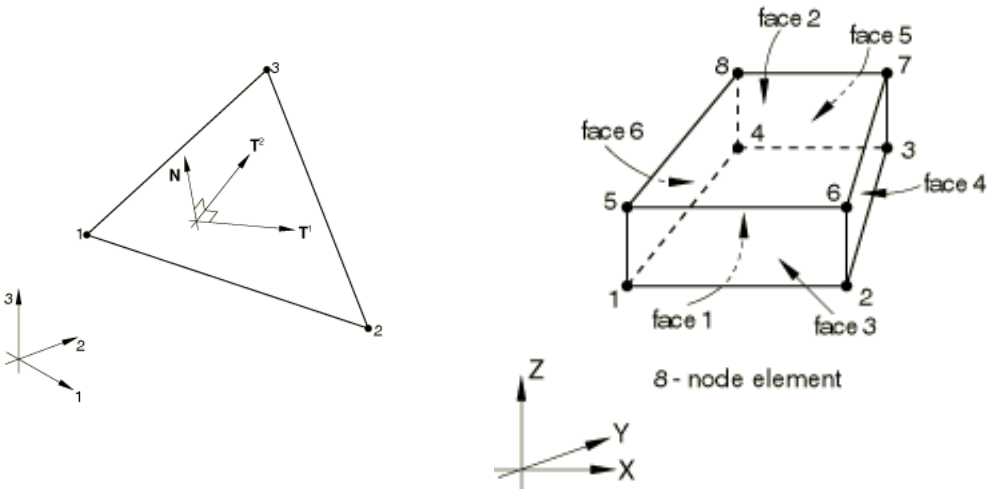

(a) (b)

Figure 4-2 (a) STRI3 3-node linear triangular shell element, (b) AC3D8 8-node linear acoustic brick element (Hibbitt et al., 2012)

According to Lodygowski & Sumelka (2006) for the first order elements (linear interpolation functions), the element dimensions have to be chosen such that the largest dimension is at least six times smaller than the acoustic wavelength at the highest frequency under consideration. Thus, the largest element length in the acoustic mesh, $d_{a,max}$, is given by,

$$d_{a,max} = \frac{\lambda}{6} = \frac{c_0}{6f} \tag{18}$$

where: λ is the wavelength, (m)

c_0 is the phase velocity for sound in air, (m/s)

f is the highest frequency, (Hz)

Since the highest frequency, f, under consideration is 200 Hz and the phase velocity, c_0, for sound in air is equal to 343 m/s, the largest acoustic element length is calculated using equation (18) equal to 0.286 m. In the finite element model the length of each acoustic element was therefore chosen to be 0.2 m as this is a convenient fraction of the room dimensions.

The largest element length in the structural mesh, $d_{S,max}$, is given by,

$$d_{s,max} = \frac{\lambda_B}{6} = \frac{c_{B,p}}{6f} \tag{19}$$

where: λ_B is the wavelength, (m)

$c_{B,p}$ is the phase velocity for a bending wave on a thin plate, (m/s)

f is the highest frequency under consideration, (Hz)

The phase velocity, $c_{B,p}$, for a bending wave on a thin plate is given by Hopkins (2007),

$$c_{B,p} = \sqrt{\frac{2\pi f h c_{L,p}}{\sqrt{12}}} \tag{20}$$

where: $c_{L,p}$ is the phase velocity for a quasi-longitudinal wave on a thin plate, (m/s)

f is the frequency, (Hz)

h is the thickness of the plate, (m)

The phase velocity, $c_{L,p}$, for a quasi-longitudinal wave on a thin plate is given by Hopkins (2007),

$$c_{L,p} = \sqrt{\frac{E}{\rho(1-\nu^2)}} \tag{21}$$

where: E is the Young's modulus of the concrete plate, (N/m^2)

ρ is the density of the concrete plate, (kg/m^3)

ν is the Poisson ratio of the concrete plate

By replacing in (21) the material properties of the concrete plate (Table 4-1) the phase velocity, $c_{L,p}$, for a quasi-longitudinal wave is calculated equal to 3800 m/s.

Using equation (20) the phase velocity, $c_{B,p}$, for a bending wave on a thin plate with thickness, h=180 mm at 200 Hz is calculated to 498 m/s.

Replacing this value in equation (19), the largest structural element length, $d_{s,max}$, was calculated to be equal to 0.415 m. In the finite element model the length of each structural

finite element was chosen to be equal to 0.1 m as this is a convenient fraction of the plate dimensions.

4.3.4 Interaction and boundary condition

The plate was assumed to be pinned along the four edges ($U_X = U_Y = U_Z = 0$). The boundary conditions of the acoustic medium were specified in terms of specific acoustic admittance applied to the six surfaces of the rectangular room. The value of the admittance given in Table 4-1 was divided by the area of each face of the rectangular room in order to transform it to specific acoustic admittance (Table 4-2).

Table 4-2 Specific acoustic admittance, $\beta_{a,s}$, applied to each face of the rectangular room

Surface	Specific acoustic admittance, $\beta_{a,s}$ [m^3/Ns]
3 m x 4 m	2.575e-06
3 m x 5 m	2.060e-06
4 m x 5 m	1.545e-06

The interaction between fluid (air) and structure (concrete plate) was achieved using tie constraints (Figure 4-3). This surface type constraint is available in Abaqus/Standard and ties all the active degrees of freedom between two surfaces even if they have dissimilar mesh refinement. In this model the translational degrees of freedom of the plate were tied to the acoustic pressure degree of freedom of the top surface of the acoustic medium. According to (Hibbitt et al., 2012), in wave propagation problems when a tie constraint is used, the surface with the finer mesh is designated as slave surface. Therefore the top face of the acoustic medium was defined as a *master* surface and the plate was defined as a *slave* surface.

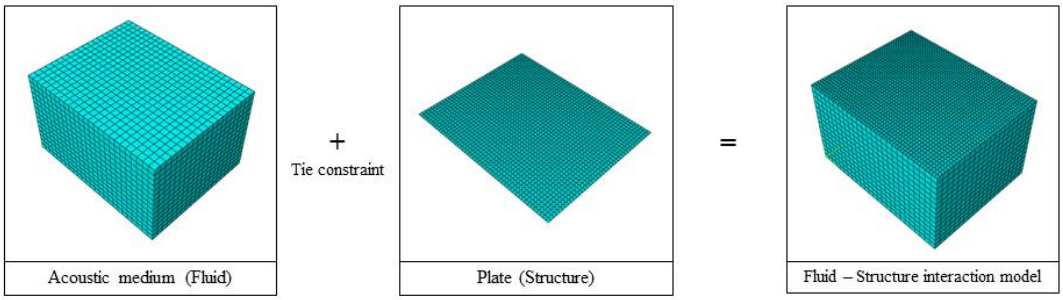

Figure 4-3 Detail of the tie constraint between the acoustic medium and the concrete plate

4.3.5 Force and response positions

A harmonic force with amplitude equal to 1 N at frequencies from 1 to 200 Hz was applied on the concrete plate at the position (x, y) = (1.7 m, 1.3 m). This location was selected to be approximately one-third of the distance along the plate's diagonal in order to excite as many vibration modes as possible (Figure 4-4). It was not possible to apply the force exactly at the one-third of the plate's diagonal due to the chosen element mesh.

The response position for sound pressure was positioned next to the corner of the rectangular room with coordinates (x, y, z) = (0.2 m, 0.2 m, 0.2 m) as all modes have a high response in the corner. A plan view of the response position is given in Figure 4-4.

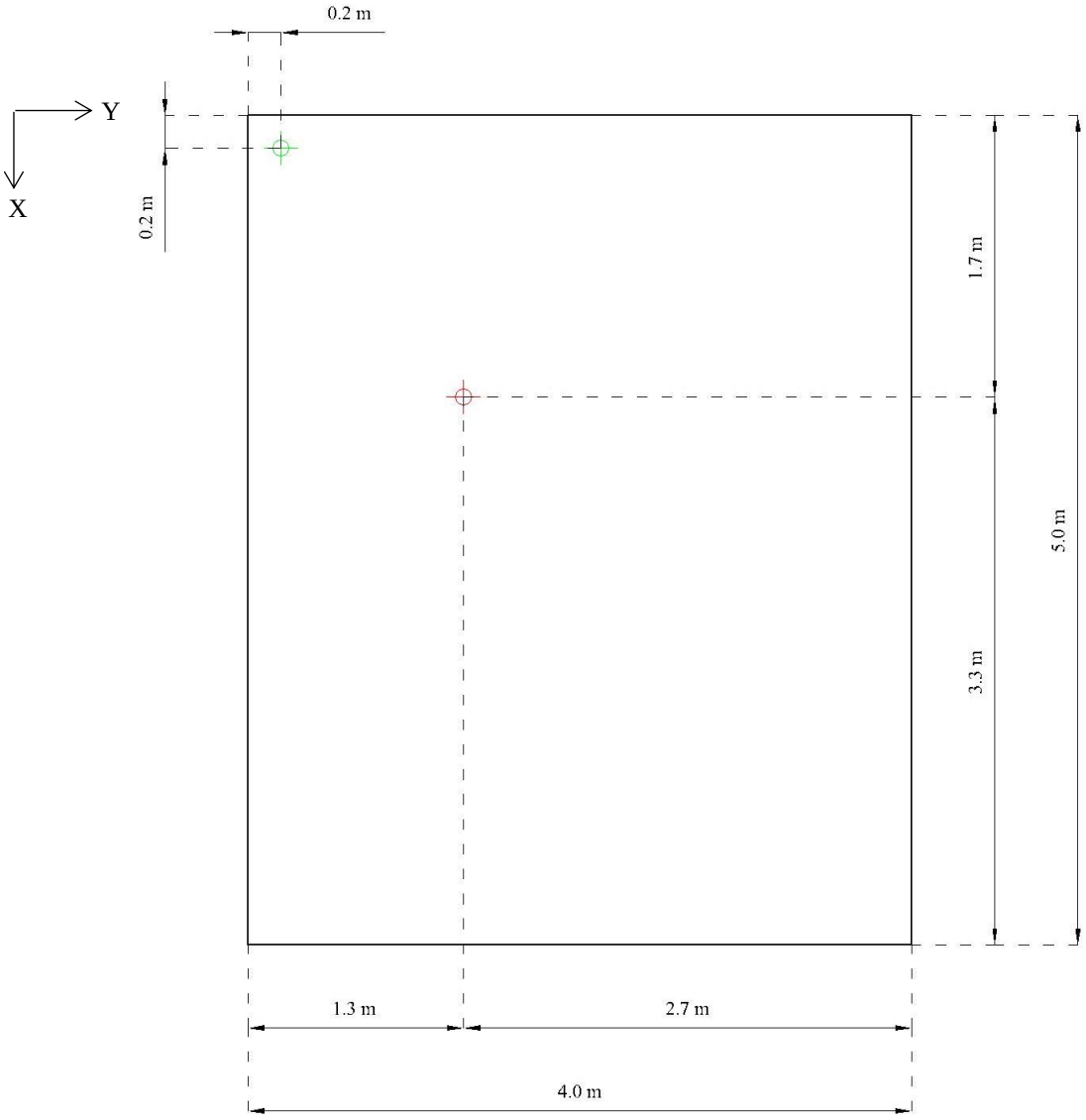

Figure 4-4 Positions of the harmonic force (red point) and the sound pressure response (green point)

4.3.6 Steady-state analysis procedures

4.3.6.1 Direct-solution steady-state dynamic analysis

Table 4-3 shows the properties of the direct-solution steady-state dynamic analyses in this chapter. The frequency range was defined from 1 to 200 Hz with a resolution equal to 0.1 Hz and with linear frequency spacing. The damping was constant and frequency independent equal to ξ=0.25%.

4.3.6.2 Mode-based steady-state dynamic analysis

Table 4-3 shows the properties that were also used for the mode-based steady-state dynamic analyses in this chapter. In order to calculate the response from the 140 mm and the 180 mm concrete plates, 93 and 91 modes were extracted respectively using a preliminary frequency step. At the steady-state modal step, the frequency range was defined from 1 to 200 Hz with resolution equal to 0.1 Hz and with linear frequency spacing. The damping was considered to be frequency-independent and was applied as fraction of the critical damping, ξ, for each mode.

Table 4-3 Direct-solution and mode-based steady-state dynamic analysis properties

Lower frequency [Hz]	Upper frequency [Hz]	Number of points	Frequency spacing type	Damping [%]
1	200	2000	Linear	0.25

4.4 Comparison of finite element method and the normal mode model

4.4.1 140 mm concrete plate

Figure 4-5 compares the results of the direct-solution steady-state finite element analysis and the normal mode model for sound radiation from a 140 mm concrete plate into a rectangular room.

Figure 4-6 compares the results of the mode-based steady-state finite element analysis and the normal mode model for sound radiation from a 140 mm concrete plate into a rectangular room.

In these diagrams, the vertical axis shows the 20log ($|p_{rms}/F_{rms}|$) and the horizontal axis shows the frequency range of the applied harmonic force. p_{rms} stands for the root-mean-square of

the sound pressure calculated near the corner of the room and F_{rms} stands for the root-mean-square of the harmonic force applied approximately at the one third of the plate's diagonal. At the corresponding frequencies on the NMM curve, the purple star symbol indicates the plate modes, the red square symbol indicates the axial room modes, the green triangle indicated the tangential room modes and the blue circle indicates the oblique modes.

In the comparison of the normal mode model and the finite element model, a successful validation requires close agreement in the frequency of the peaks in the sound pressure level response and close agreement in the level of those peaks. Close agreement in the region of the troughs is not critical because in these frequency regions which are outside damping control (i.e. under mass and stiffness control) different results would be expected depending on the type of finite element used. In addition, troughs can occur due to cancellation and the depth of the trough would therefore depend on the amount of significant figures used in both the finite element calculations and the normal mode model. Fortunately it is the peaks in the sound pressure level that are of most interest as these primarily determine the level in frequency bands such as one-third octave bands.

The results of the direct-solution steady-state finite element analysis show close agreement with the normal mode model in terms of the frequency of the peaks in the sound pressure level. However, there are differences in the levels of the peaks and the steady-state direct analysis tends to give higher sound pressure levels (Figure 4-5).

The results of the mode-based steady-state finite element analysis show close agreement with the results of the normal mode model in terms of the frequency of the peaks. Close agreement was achieved in the prediction of the sound pressure levels of the peaks of the first plate mode and the majority of the room modes. For the other plate modes the mode-based steady-state analysis has a tendency to give lower sound pressure levels at the peaks (Figure 4-6). This might partly be due to the fact that the plate damping represents the internal loss factor; hence the peaks have a high Q-factor such that the 0.1Hz frequency resolution of the finite element models is not always sufficient.

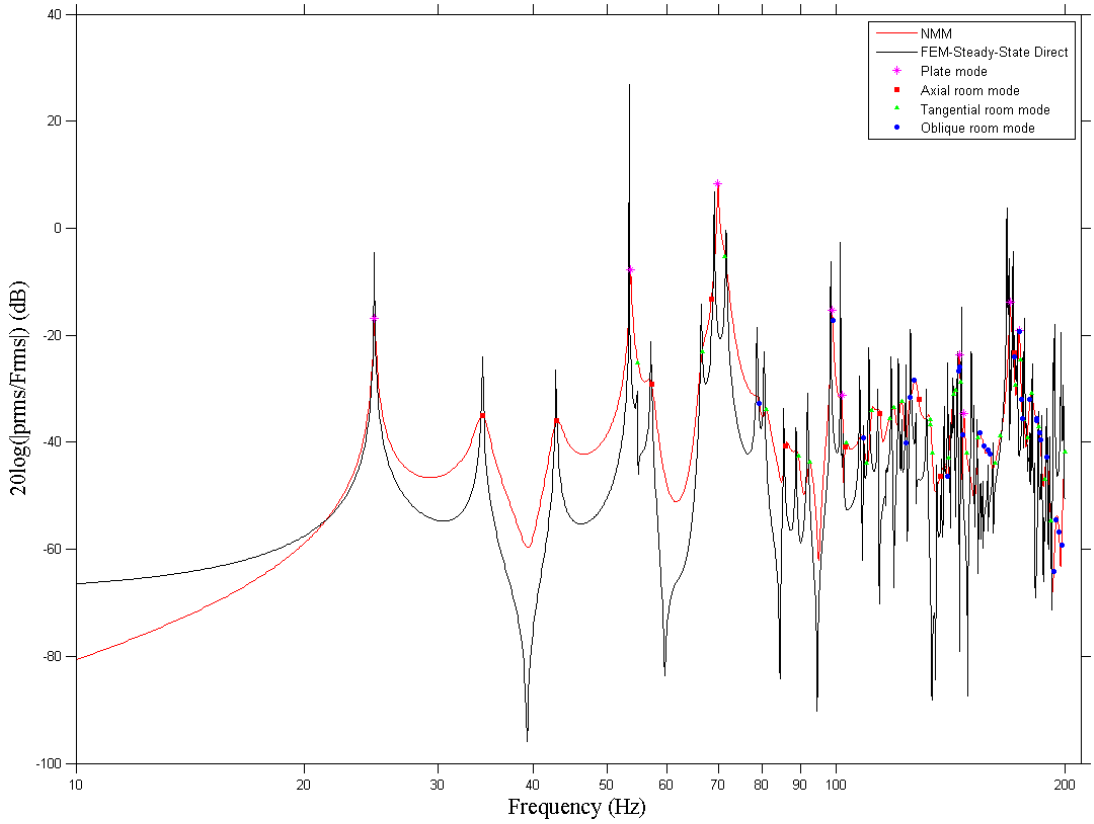

Figure 4-5 Comparison of the direct-solution steady-state analysis and the normal mode model

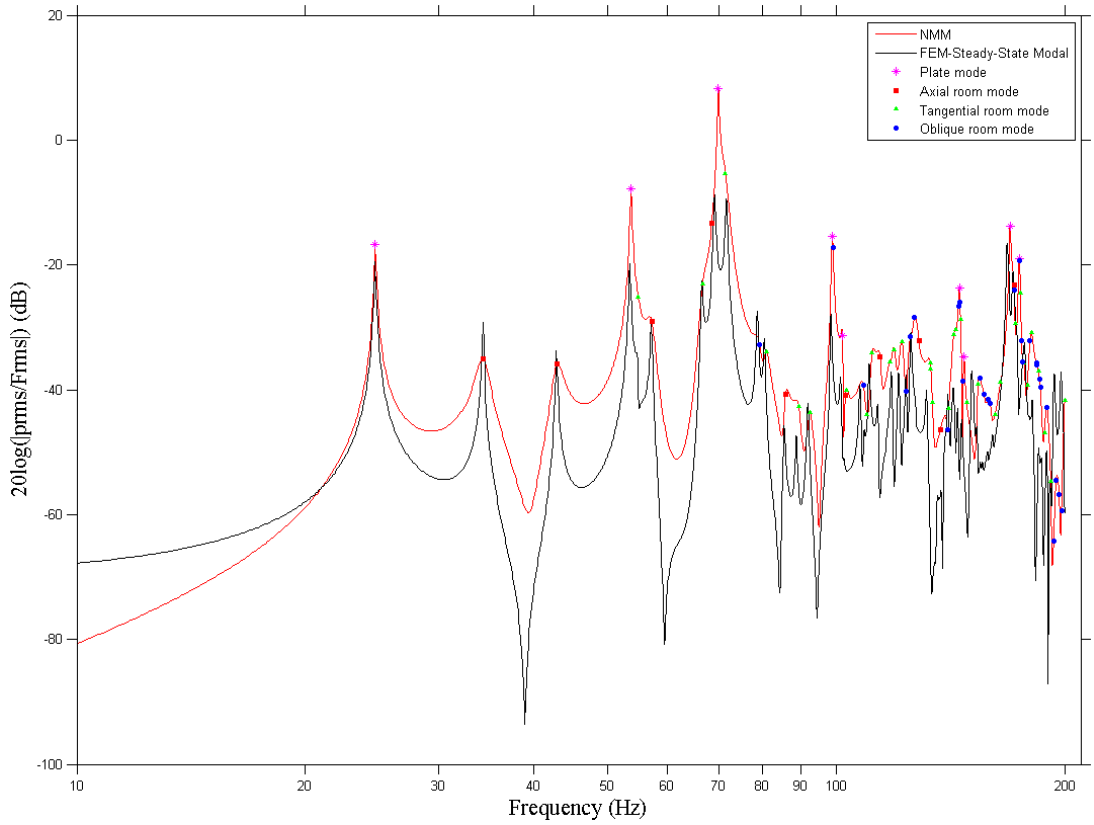

Figure 4-6 Comparison of the mode-based steady-state analysis and the normal mode model

4.4.2 Concrete plate with thickness 180 mm

Figure 4-7 and Figure 4-8 compare the results of the direct-solution and the mode-based steady-state finite element analysis with the results of the normal mode model for sound radiation from a concrete plate with thickness 180 mm into a rectangular room.

The results of the direct-solution steady-state finite element analysis show close agreement with the results of the normal mode model for the frequencies of the peaks in the sound pressure level. There is also close agreement in the predicted levels of the peaks for the plate modes whereas the steady-state direct analysis tends to give higher levels for the peaks of almost all the room modes (Figure 4-7).

The results of the mode-based steady-state finite element analysis show close agreement with the results of the normal mode model in terms of the frequency of the peaks. There is also close agreement in the predicted levels of the peaks for the majority of the room modes whereas the steady-state modal analysis tends to give lower levels for the peaks relating to the plate modes (Figure 4-8).

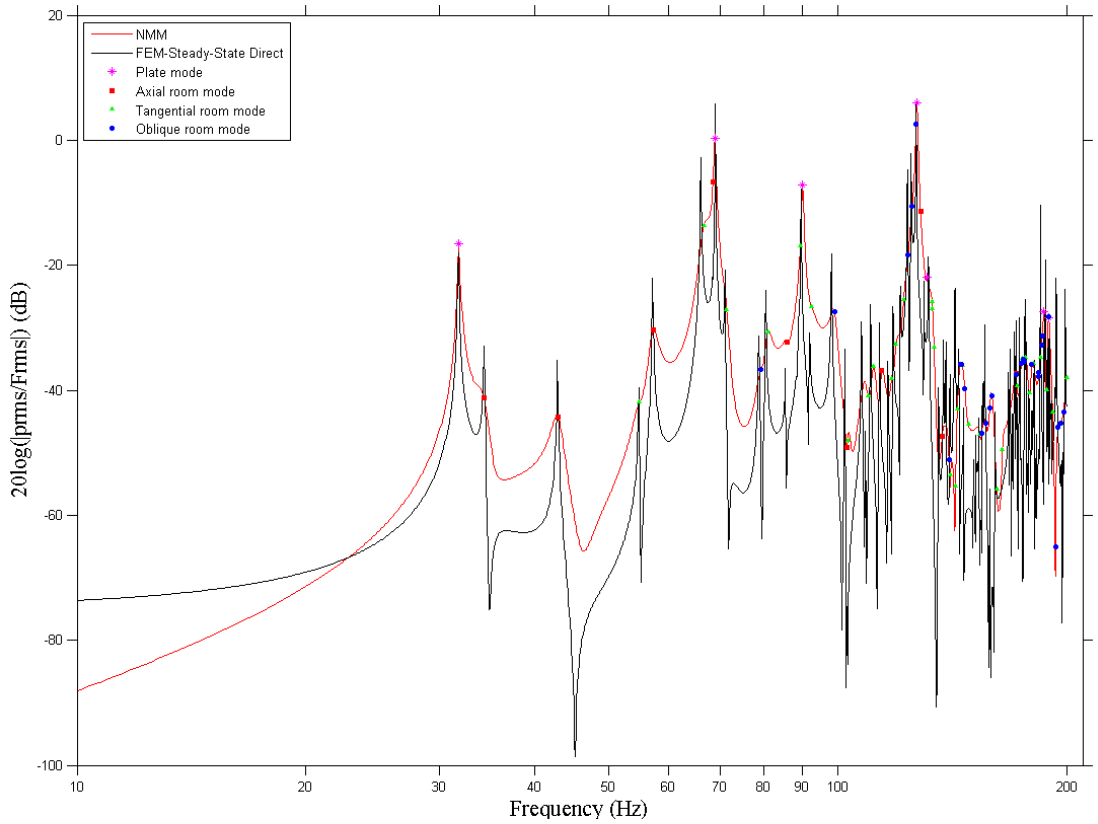

Figure 4-7 Comparison of the direct-solution steady-state analysis and the normal mode model

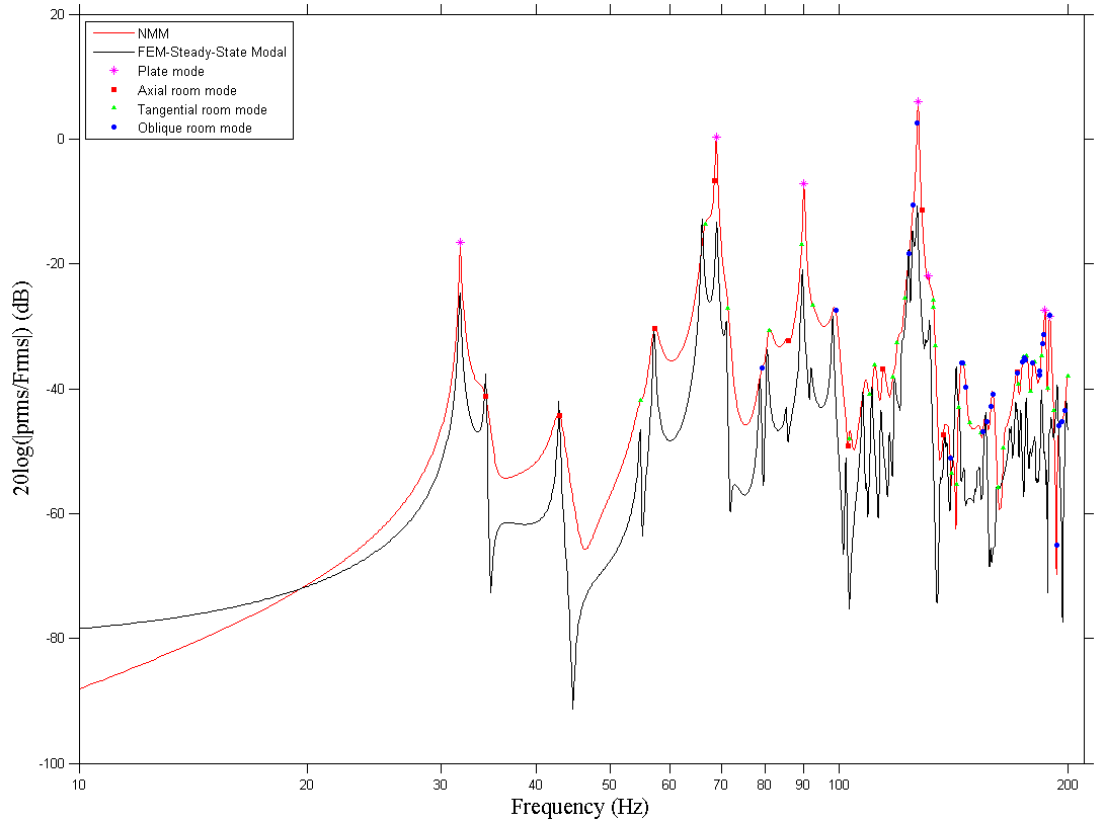

Figure 4-8 Comparison of the mode-based steady-state analysis and the normal mode model

4.5 Discussion

A fluid-structure interaction finite element model was developed in Abaqus using structural and acoustic finite elements and was validated against a normal mode model for sound radiation from a concrete plate into a rectangular room. The validation was made for two concrete plates with different thickness (140mm and 180mm) so that the mode spacing and excitation of the modes differed, and conclusions were not drawn that were specific to one plate. Both mode-based and direct-solution steady- state dynamic analysis procedures were investigated during the validation procedure.

For the 140mm thick concrete plate, both direct-solution and mode-based steady-state analysis were in agreement with the normal mode model in terms of the frequencies of the peaks that occurred in the sound pressure level. Regarding the predicted levels of the peaks, the mode-based steady-state analysis method is slightly more accurate than the direct-solution steady-state analysis method since it successfully predicted the peaks in the sound pressure levels for the first plate mode and almost all the room modes.

For the 180mm thick concrete plate, the direct-solution steady-state analysis predicted the sound pressure levels of the plate modes with higher accuracy whereas the mode-based steady-state analysis predicted the sound pressure levels of the room modes with higher accuracy. Both methods successfully predicted the frequencies of the peaks in the sound pressure level.

4.6 Conclusions

The finite element method has been validated against a normal mode model for sound radiation into a rectangular room from both a 140 mm and 180 mm concrete plate. This used a fluid-structure interaction finite element model that was developed in Abaqus. Linear and quadratic acoustic elements gave similar results whereas the linear structural element STRI3 is the only Abaqus element that can simulate thin plate bending theory to give results that can be compared directly to the normal mode model.

Close agreement has been achieved between the finite element method and the normal mode model in terms of the frequency of the peaks in the sound pressure level; however there are differences in the peak levels. In general, the mode-based steady-state dynamic analysis tends to predict peak levels with higher accuracy than the direct-solution steady-state analysis.

After having validated the finite element method against a normal mode model for the prediction of sound radiation from a plate into a room, the next stage of this thesis is to

develop a vibroacoustic finite element model for a dowelled-joist timber floor in order to predict the sound radiation from the floor into a room under point force excitation on its surface. This is the objective of chapter 5.

5. Prediction of the sound radiation from a dowelled-joist timber floor into a room

5.1 Introduction

This chapter considers the prediction of sound radiation from the dowelled-joist timber floor (4.0 m x 5.0 m) into the box-shaped room (4.0 m x 5.0 m x 3.0 m) using a finite element model that was developed in Abaqus for fluid-structure interaction. It therefore builds upon the validation in Chapter 4 for fluid-structure interaction between a plate and a room using a finite element model. However, implementing fluid-structure interaction is more complex than with the concrete floors because the validated model for the dynamic performance of the dowelled-joist timber floor has 'virtual gaps' between the joists. A solution to this problem is sought through the introduction of a transfer plate.

In this chapter, the response in the room is considered for a number of different positions for point force excitation on the plate. The results are then averaged to represent a more practical assessment; this is because the impact sound insulation of a floor would usually be assessed from the average of different excitation positions. Using this approach, the dowelled-joist timber floor is compared against the 140 mm and 180 mm concrete plates (4.0 m x 5.0 m). However, for the concrete floors, frequency-dependent damping is used that simulate the damping that would occur when they are connected to other walls and floors in a complete building.

5.2 Finite element model of a dowelled-joist timber floor for fluid-structure interaction

5.2.1 Description of the model

Figure 5-1 shows the finite element model that was created in Abaqus (Hibbitt et al., 2012) in order to predict the sound radiation from the vibration of a dowelled-joist timber floor into a rectangular room. The model consists of three parts (Figure 5-2): a) a dowelled-joist timber floor (4.0 m x 5.0 m x 0.2 m), b) a thin transfer plate (4.0 m x 5.0 m) and c) an acoustic medium (4.0 m x 5.0 m x 3.0 m).

Three beam assemblies, each with 22 beams and one beam assembly with 23 beams were joined together using three connection zones to create the dowelled-joist timber floor (see Section 3.7). Each assembly was modelled using 'spring connected beams with elastic supports' (see Section 3.5.6). In each assembly there are 'virtual gaps' between the beams

because each beam was modelled using shell elements along the Y-Z plane (Figure 5-2). These virtual gaps posed no problems for the structural analysis in Chapter 3 but for this fluid-structure interaction problem, a solution is required to 'seal' these gaps whilst maintaining the same dynamic performance of the floor.

The solution was to use a transfer plate. This appears to be a novel solution because no references have yet been found in the literature that uses this approach with sound radiation in finite element models. The transfer plate was a 10 mm thin plate that was modelled using shell elements to transfer the motion from the dowelled-joist timber floor to the acoustic medium (Figure 5-2). The density and the Young's modulus of the plate were selected to be very small in order to guarantee that the plate would not alter the dynamic characteristics of the dowelled-joist timber floor or its interaction with the acoustic medium.

Validation of the approach using the transfer plate is contained in Appendices 1 and 2. Appendix 1 provides evidence that the transfer plate does not change the dynamic response of the dowelled-joist timber floor. Appendix 2 shows that exact agreement was achieved between two vibroacoustic finite element models with and without transfer plate for sound radiation into a room under point force excitation. Therefore it can be concluded that the use of the thin transfer plate between a structure and an acoustic medium does not alter the fluid-structure interaction.

The acoustic medium of the rectangular room was modelled using acoustic solid elements.

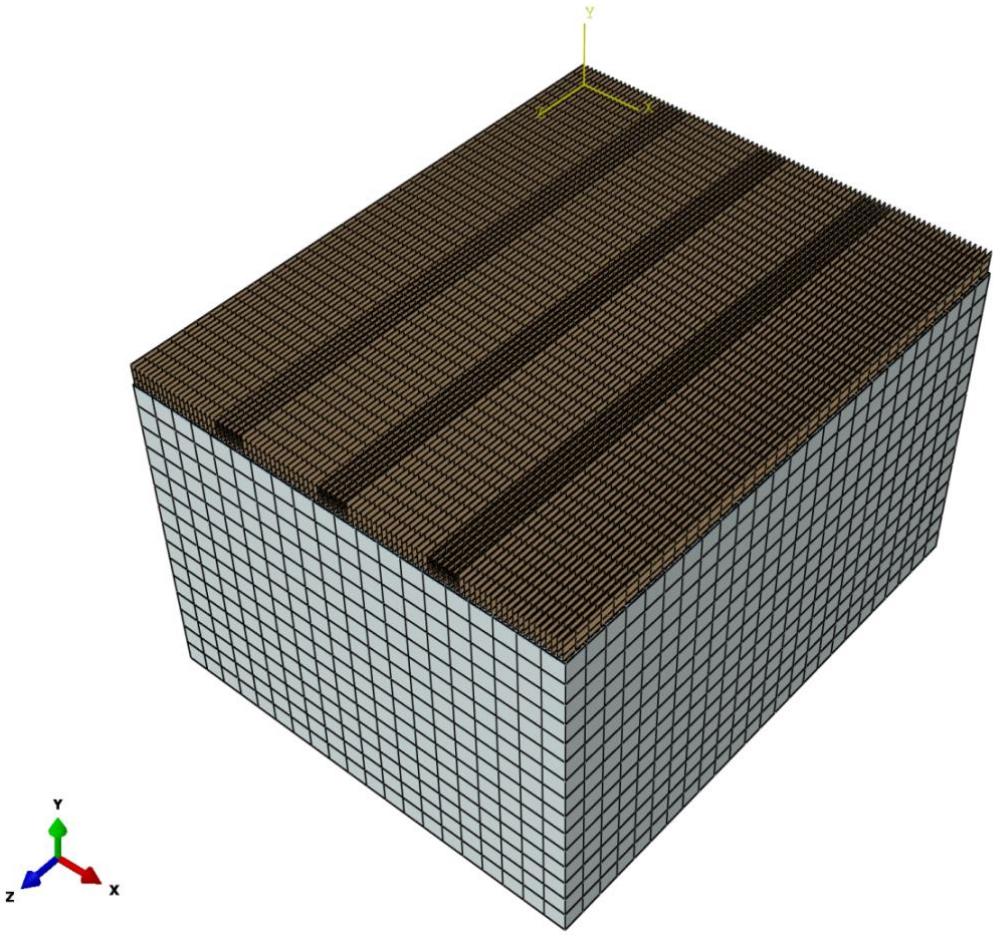

Figure 5-1 Finite element model of the dowelled-joist timber floor and the box-shaped room for fluid-structure interaction

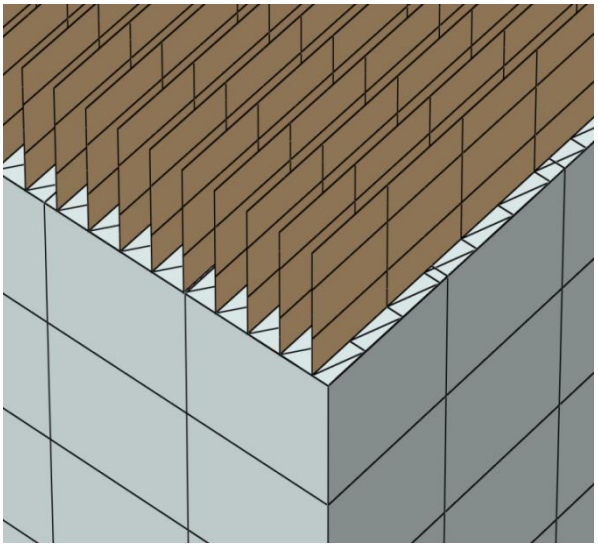

Figure 5-2 Detail of the three parts that form the finite element model: a) Dowelled-joist timber floor (brown colour), b) Thin transfer plate (light grey colour) and c) Acoustic medium (grey colour)

5.2.2 Material properties

Table 5-1 contains the material properties that were used for each component of the finite element model. The density, Young's modulus and Poisson ratio of the dowelled-joist timber floor were defined by the average of the respective quantities from the three individual assemblies of Chapter 3 (Table 3-4). The same method was followed for the definition of the spring stiffness (Table 5-2) as the average stiffness value of the springs of the individual assemblies.

The density of the transfer plate was resulted from the density of the timber floor after applying a reduction factor equal to 10^{-6} to ensure that no additional mass would participate in the model. The Young's modulus of the transfer plate equaled the Young modulus of the timber floor after multiplying by a factor of 10^{-5}. This approach was used to try and ensure that the transfer plate would not add additional stiffness to the dowelled-joist timber floor.

The reduction factors were determined by starting with a factor of 10^{-3} for the density and the Young modulus. These factors were divided by 10 in successive steps until there was no change in the eigen-frequencies of the dowelled-joist timber floor.

The material properties of the acoustic medium remained the same as in Section 4.3.2.

Table 5-1 Material properties

	Dowelled-joist timber floor	**Transfer plate**		**Acoustic medium**
Density, ρ [kg/m^3]	460.23	460.23e-06	Density, ρ [kg/m^3]	1.21
Young's modulus, E [N/m^2]	11189e06	111890	Bulk modulus, K_f [N/m^2]	142355.29
Poisson ratio, v	0.37	0.37	Speed of sound in air, C_0 [m/s]	343
			Acoustic admittance, $\beta_{a,n}$ [m^5/N s]	3.0897e-05

Table 5-2 Spring stiffness

	k_x [N/m]	k_y [N/m]	k_z [N/m]
Dowel springs	10e06	316667	316667
Support springs	-	650000	-

5.2.3 Meshing

5.2.3.1 Element types

The 89 beams that compose the dowelled-joist timber floor were meshed using the quadratic S8R shell element from the element library of Abaqus. The beam-dowel interaction was modelled using the Spring2(S) element whereas the Spring1(S) element was chosen to represent the elastic support conditions.

The thin transfer plate was modelled using the linear triangular STRI3 shell element from the element library of Abaqus. The validation studies of the previous chapter showed that this element show the best behavior in terms of sound radiation.

The acoustic medium of the rectangular room was meshed using the linear AC3D8 acoustic solid element from the element library of Abaqus.

5.2.3.2 Element size

According to Lodygowski & Sumelka (2006) the element dimensions for second order elements (quadratic interpolation functions) have to be chosen such that the largest dimension is at least twelve times smaller than the acoustic wavelength. Thus, the largest element length in the structural mesh of the dowelled-joist timber floor, $d_{s,b,max}$, is given by,

$$d_{s,b,max} = \frac{\lambda_{B,b}}{12} = \frac{c_{B,b}}{12f} \tag{22}$$

where: $\lambda_{B,b}$ is the bending wavelength in a beam, (m)

$c_{B,b}$ is the phase velocity for a bending wave on a beam, (m/s)

f is the highest frequency under consideration, (Hz)

The phase velocity, $c_{B,b}$, for a propagating bending wave on a solid beam is given by Hopkins (2007),

$$c_{B,b} = \sqrt[4]{\frac{4\pi^2 f^2 c_{L,b}^2 I_b}{S}} \tag{23}$$

where: $c_{L,b}$ is the phase velocity for a quasi-longitudinal wave on a solid beam, (m/s)

f is the higher frequency under consideration, (Hz)

I_b is the moment of inertia about the strong axis of the beam, (m^4)

S is the area of the cross-section of the beam, (m^2)

The phase velocity, $c_{L,b}$,for a quasi-longitudinal wave on a solid beam is given by Hopkins (2007),

$$c_{L,b} = \sqrt{\frac{E}{\rho}} \tag{24}$$

where: E is the Young's modulus, (N/m^2)

ρ is the density, (kg/m^3)

The highest frequency of interest is 200Hz. By replacing all the known variables in equations (22), (23) and (24) the largest structural element length in each beam of the dowelled-joist timber floor, $d_{s,b,max}$,was calculated to be equal to 0.25 m. However, the quadrilateral elements that were used for the modelling of the dowelled-joist timber floor were chosen to have a maximum size of 0.125 m in the Z – direction to simplify the modelling based on the floor dimensions.

By replacing in equations (19), (20) and (21) the material properties of the 10 mm transfer plate, the largest structural element length in the transfer plate, $d_{s,p,max}$, was found equal to 0.205 m. However, the triangular elements that were used for the modelling of the transfer plate were chosen to have a maximum size of 0.0625 m in the Z – direction and 0.045 m in the X – direction for finite element modelling reasons.

The largest acoustic element length, $d_{a,max}$, was calculated in the previous chapter (see Section 4.3.3) equal to 0.286 m. Therefore the length of each acoustic element was chosen to be 0.2 m.

5.2.4 Interaction and boundary conditions

The support conditions of the dowelled-joist timber floor were described in detail in Section 3.5.6. The boundary conditions of the acoustic medium were defined in terms of specific acoustic admittance applied to the six surfaces of the rectangular room (Table 4-2).

The thin transfer plate was attached to the dowelled-joist timber floor using multi point beam constraints (Figure 5-3). This type of constraint is available in Abaqus/Standard (Hibbitt et al., 2012) and constrains the displacement and rotation of each *slave* node to the displacement and rotation of one *control* point. In order to make the transfer plate follow the motion of the dowelled-joist timber floor, each node of the transfer plate was defined as a *slave* and paired with one *control* point on the dowelled-joist timber floor.

The interaction between the acoustic medium and the transfer plate was achieved using tie constraints (Figure 5-3). It is reminded that this type of constraint ties all the active degrees of freedom between two surfaces even if they have dissimilar mesh refinement. The top face of the acoustic medium was defined as a *master* surface and the transfer plate was defined as a *slave* surface.

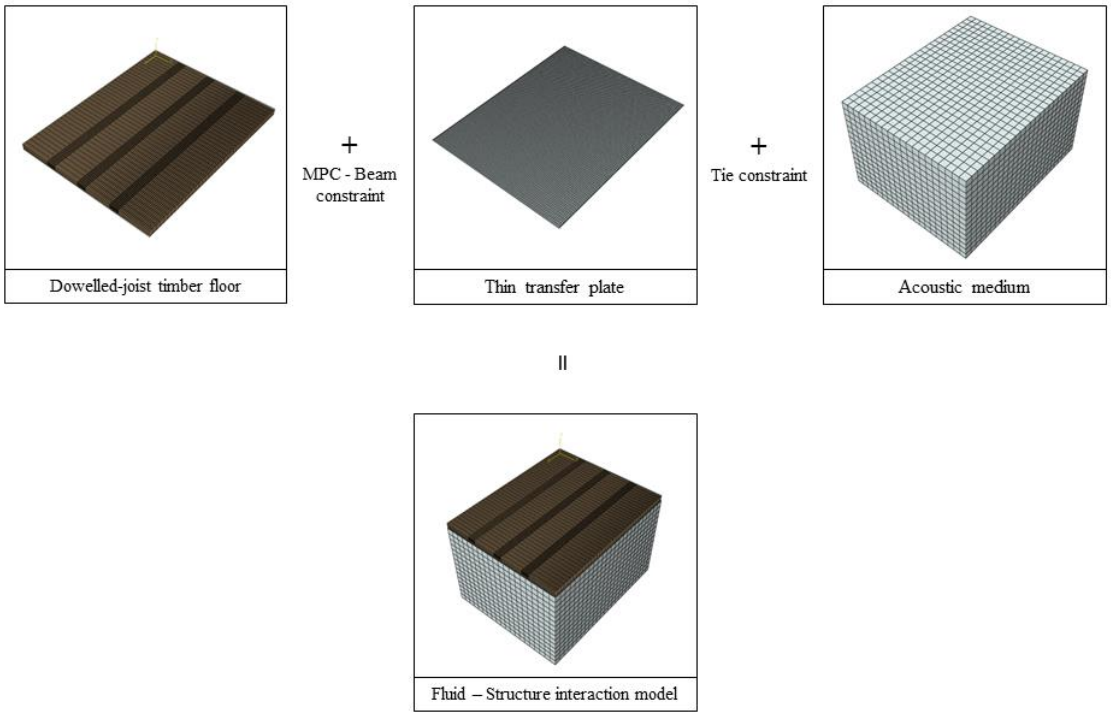

Figure 5-3 Detail of the interaction between the parts of the finite element model for fluid-structure interaction

5.3 Prediction of sound radiation from a dowelled-joist timber floor into a rectangular room

5.3.1 Force and response positions

A total of five different excitation positions were used on the dowelled-joist timber floor. A harmonic force with amplitude equal to 1 N and frequencies from 1 to 200 Hz was applied at one of the five excitation positions in each model that was solved (Figure 5-4). The excitation positions were selected to be at a distance ≥0.5 m from the boundaries and ≥1.0 m from each other.

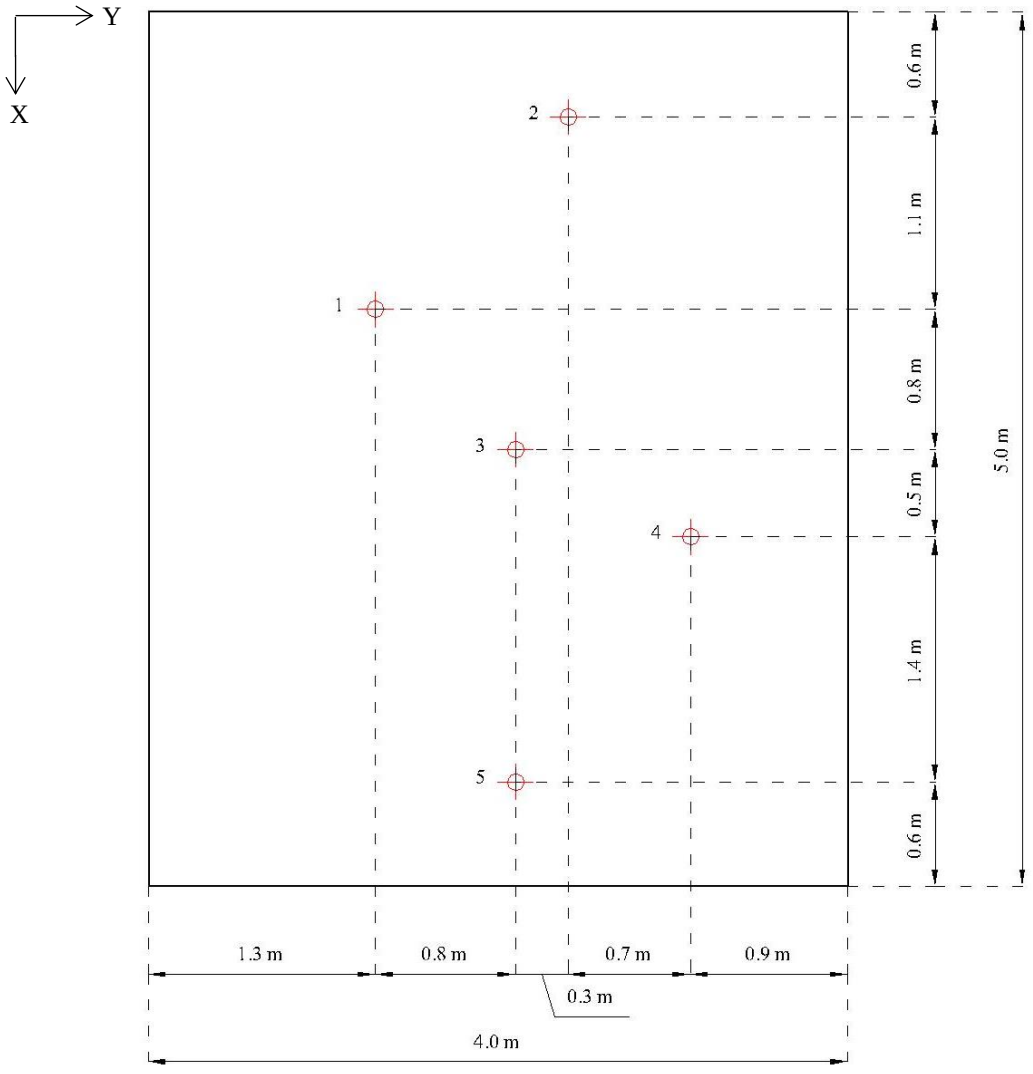

Figure 5-4 Positions of the five harmonic forces

For each excitation force, the sound pressure was determined at all nodes forming the acoustic medium (8190 nodes) except the nodes that are tied to the transfer plate. The mean-square pressure, $\left(p^2{}_{rms}\right)_{average}$, was calculated according to,

$$\left(p^2{}_{rms}\right)_{average} = \frac{1}{N_{nodes}} \sum_{i=1}^{N_{nodes}} p^2{}_{rms} \tag{25}$$

where p_{rms} is the root mean square sound pressure which is equal to $\frac{|p|}{\sqrt{2}}$ (where p is the complex peak pressure) and N_{nodes} is the number of the nodes to be used to determine an average value for the acoustic medium.

5.3.2 Mode-based steady-state dynamic analysis

Table 5-3 shows the properties of the mode-based steady-state dynamic analyses. For the calculation of the response, 303 modes were extracted using a preliminary frequency step. At the steady-state modal step, the frequency range was defined from 1 to 200 Hz with resolution equal to 0.1 Hz and with logarithmic frequency spacing.

Table 5-3 Mode-based steady-state analysis properties

Lower frequency [Hz]	Upper frequency [Hz]	Number of points	Frequency spacing type
1	200	2000	Logarithmic

The damping was applied using the fraction of the critical damping, ξ, for each of the 303 modes (Figure 5-5). 'Non-physical' modes that were governed by the local response of the springs resulting in significant in-plane motion, and were not observed in the experimental modal analysis, were excluded from the analysis by assigning a damping ratio equal to unity (Figure 5-6). In Appendix 3, some examples are given of mode shapes that were excluded from the mode-based steady-state dynamic analysis. For the remaining 92 modes, the damping ratio was defined according to the experimental procedure as shown in Table 5-4.

Table 5-4 Damping ratio, ξ of the 92 modes

Mode	Loss factor, η	Damping ratio, ξ
Fundamental	0.02	0.01
Elsewhere	0.14	0.07

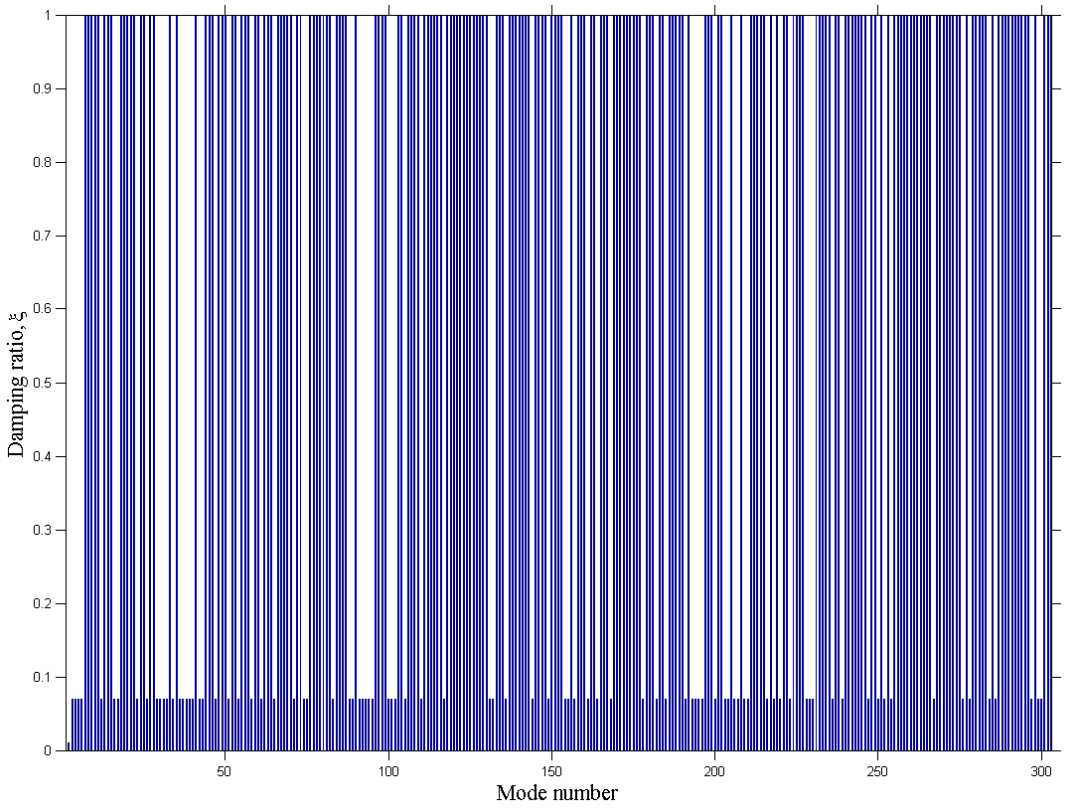

Figure 5-5 Damping ratio, ξ of the 303 extracted modes

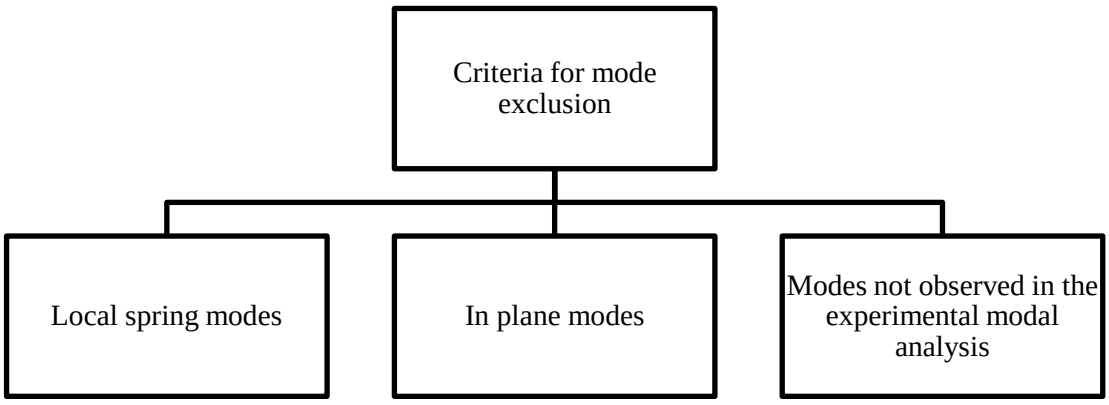

Figure 5-6 Criteria for the exclusion of the modes from the analysis

5.3.3 Sound radiation results

Figure 5-7 shows the transfer function results for the dowelled-joist timber floor in one-third octave bands. The vertical axis shows the $10\log\left[\left(p^2{}_{rms}\right)_{average}/F^2{}_{rms}\right]$ and the horizontal axis shows the centre frequencies for the one-third octave bands. Each thin line in the graph corresponds to the response from a different excitation force and the thick dashed blue line corresponds to the average of the responses from the five different force positions.

For all the force positions the highest sound pressure level was achieved in the 16 Hz band which corresponds to the lowest frequency mode of the floor. At this frequency, the highest sound pressure level occurred with force position 3 which is close to the center of the floor. In one-third octave bands from 1 Hz to 50 Hz, the higher sound pressure response occurred in the room with excitation at the force positions 1, 3 and 4 whereas from 63 Hz to 200 Hz the highest sound pressure occurred with force positions 2 and 5.

Table 5-5 show the maximum difference in dB between the five different force positions for the bands with frequency equal and over 16 Hz. The maximum difference between the five different force positions is 10.6 dB at the band with centre frequency 100 Hz

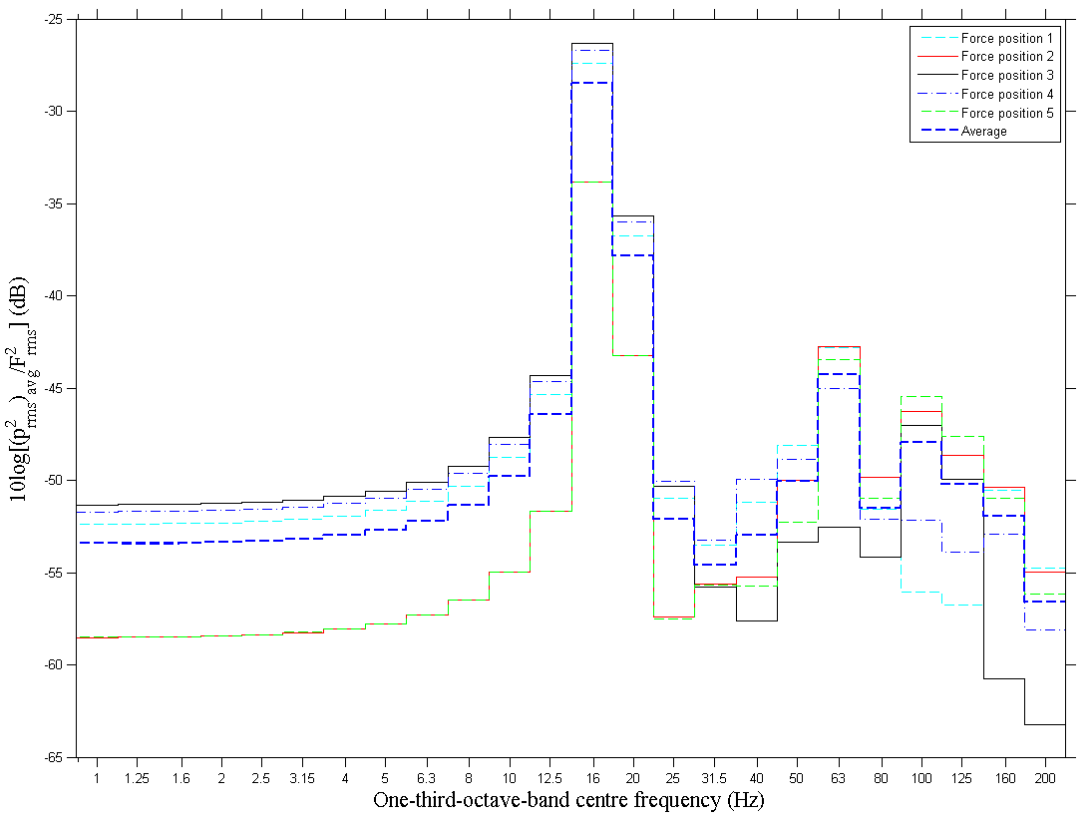

Figure 5-7 Transfer function results for the dowelled-joist timber floor

Table 5-5 Maximum difference between the five force positions

Frequency (Hz)	16	20	25	31.5	40	50	63	80	100	125	160	200
Maximum difference (dB)	7.5	7.5	7.4	2.5	7.7	5.2	9.8	4.3	10.6	9.1	10.4	8.4
Force positions	3-2	3-2	4-5	4-3	4-3	1-3	2-3	2-3	5-1	5-1	2-3	1-3

5.4 Prediction of sound radiation from a 140 mm and a 180 mm concrete plate into a rectangular room

5.4.1 Force and response positions

In order to compare the sound radiation from a dowelled-joist timber floor with the sound radiation from a 140 mm and a 180 mm concrete plate (see Section 4.3), the force and response positions that were described in Section 5.3.1 were adopted for the analyses in this section.

5.4.2 Mode-based steady-state dynamic analysis

Table 5-6 shows the properties of the mode-based steady-state dynamic analyses. In order to calculate the response from a 140 mm and a 180 mm concrete plate, 93 and 91 modes were extracted respectively using a preliminary frequency step. At the steady-state modal step, the frequency range was defined from 1 to 200 Hz with resolution equal to 0.1 Hz and with logarithmic frequency spacing.

Table 5-6 Mode-based steady-state analysis properties

Lower frequency [Hz]	Upper frequency [Hz]	Number of points	Frequency spacing type
1	200	2000	Logarithmic

In contrast to Chapter 4, the damping was defined as frequency-dependent to represent a fully-connected concrete floor in a building (rather than accounting for only the internal losses as was done in Chapter 4 to help identify the peaks in the transfer function). The damping was applied as fraction of the critical damping, ξ, for each mode (Figure 5-8 and Figure 5-9). It was calculated by Hopkins (2007),

$$\xi = \frac{\eta}{2} = \frac{1}{2}\left(0.005 + \frac{1}{\sqrt{f}}\right) \tag{26}$$

where η is the loss factor and f is the frequency (Hz).

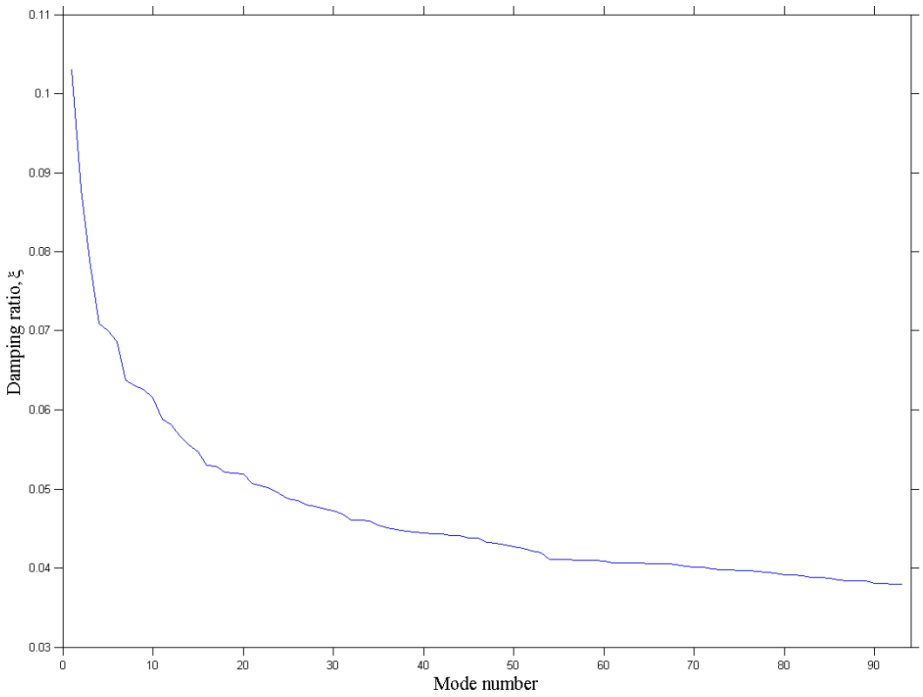

Figure 5-8 Concrete plate (140 mm) - Damping ratio, ξ for the 93 extracted modes

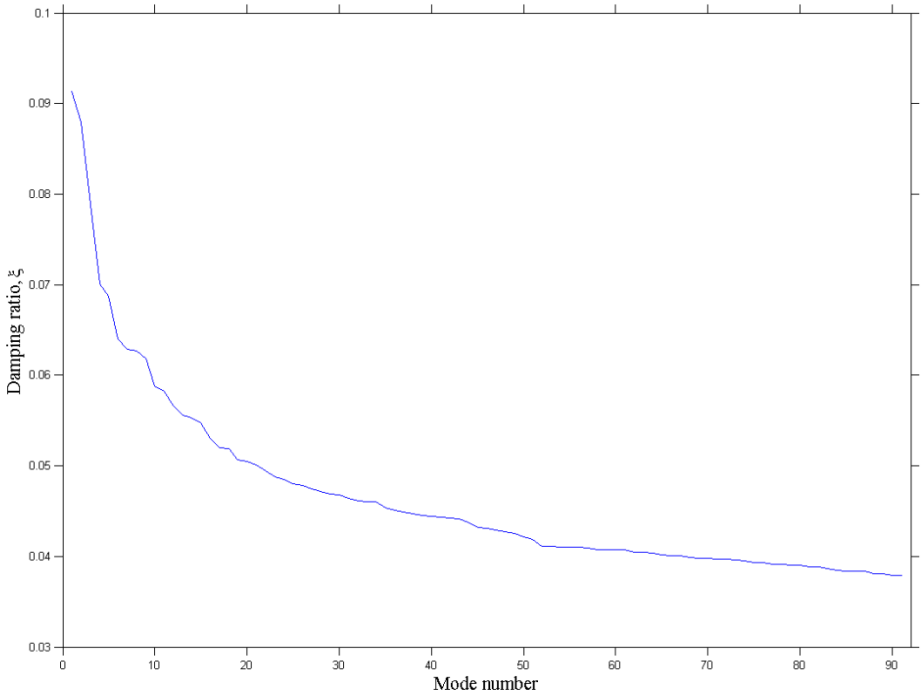

Figure 5-9 Concrete plate (180 mm) - Damping ratio, ξ for the 91 extracted modes

5.4.3 Sound radiation results

Figure 5-10 and Figure 5-11 show the transfer function results for the 140 mm and the 180 mm concrete plates in one-third octave bands.

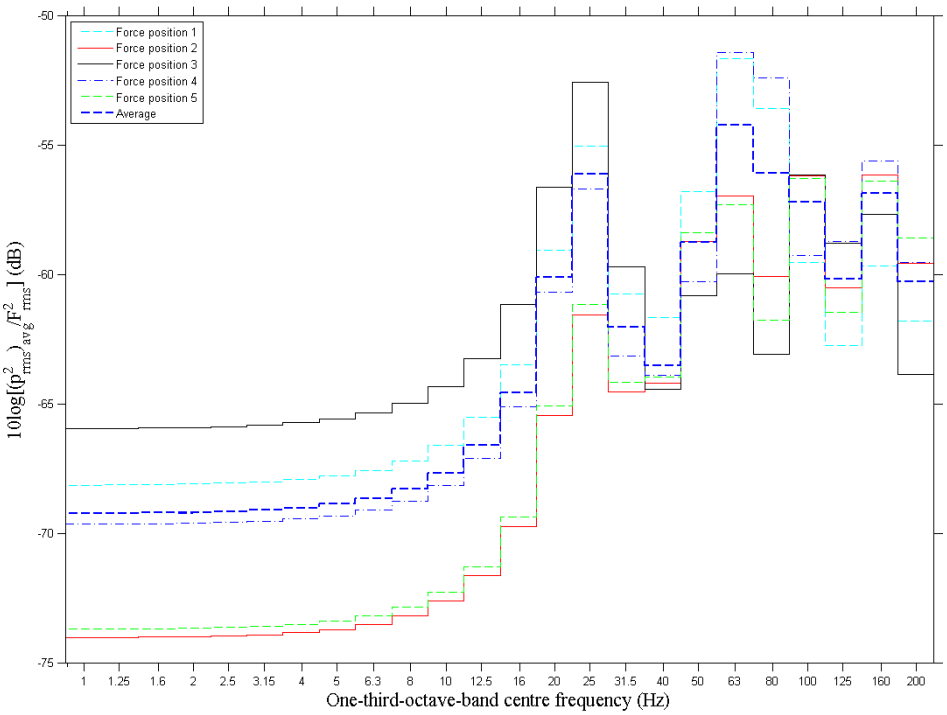

Figure 5-10 Transfer function results for the 140mm concrete plate

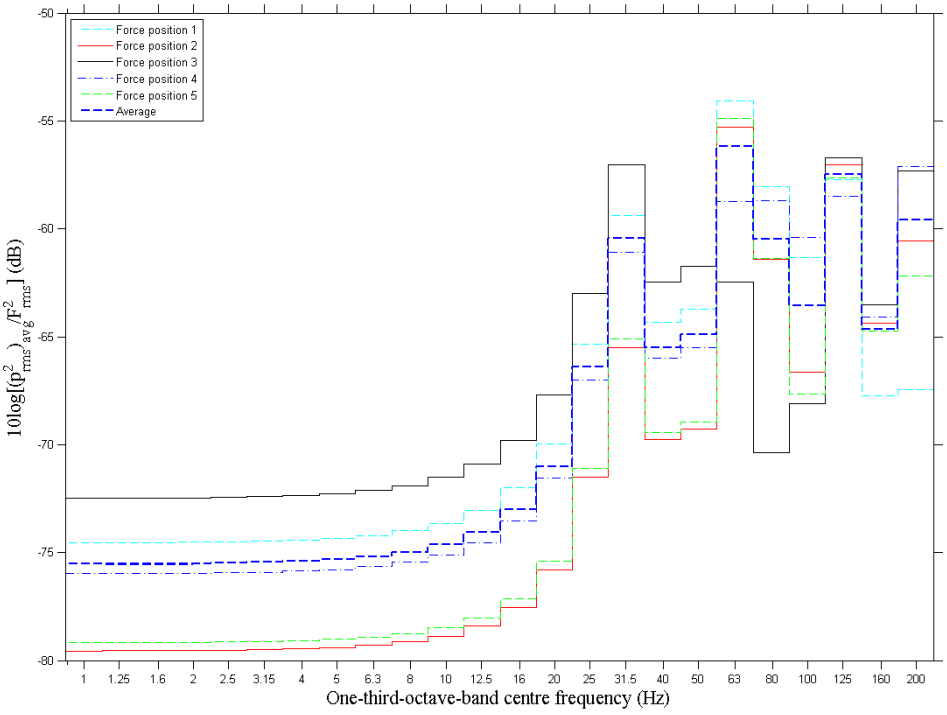

Figure 5-11 Transfer function results for the 180mm concrete plate

For the same applied force, the 140 mm concrete plate produces higher sound pressure than the 180 mm concrete plate. For both plates the highest sound pressure occurs in the 63 Hz band.

Table 5-7 and Table 5-8 show for the 140 mm and 180 mm concrete plate respectively the maximum difference in dB between the five different force positions for the bands with frequency equal and over 16 Hz. For the 140 mm concrete plate, the maximum difference between the five different force positions is 10.7 dB at 80 Hz.

Table 5-7 Maximum difference between the five force positions (140 mm concrete plate)

Frequency (Hz)	16	20	25	31.5	40	50	63	80	100	125	160	200
Maximum difference (dB)	8.6	8.8	9.0	4.8	2.7	4.0	8.3	10.7	3.4	4.0	4.0	2.3
Force positions	3-2	3-2	3-2	3-2	1-3	1-3	1-3	4-3	3-1	4-1	4-1	4-1

For the 180 mm concrete plate, the maximum difference between the five different force positions is 12.3 dB at 80 Hz.

Table 5-8 Maximum difference between the five force positions (180 mm concrete plate)

Frequency (Hz)	16	20	25	31.5	40	50	63	80	100	125	160	200
Maximum difference (dB)	7.7	8.1	8.5	8.5	7.3	7.5	8.4	12.3	7.7	1.8	4.2	10.4
Force positions	3-2	3-2	3-2	3-2	3-2	3-2	1-3	1-3	4-3	3-4	3-1	4-1

5.5 Comparison of the dowelled-joist timber floor with the 140 mm and 180 mm concrete plates

Comparison of the dowelled-joist timber floor and the 140 mm and 180 mm concrete plates is carried out here, but one must be careful in the interpretation of the results. The reason for this is that in FEM, a force is applied without any impedance associated with this force source. This is different to the situation with a footstep or the ISO tapping machine that is used to measure impact sound insulation. For this reason it is not possible to identify to state which floor has the highest or lowest impact sound insulation.

Figure 5-12 compares the dowelled-joist timber floor and the 140 mm and 180 mm concrete plates in terms of the transfer function. In Figure 5-12 each line shows the average sound pressure levels from the five force positions expressed in one-third octave bands. The main conclusion that can be drawn from this is that compared to the concrete floors the dowelled-joist floor has significant radiation around the 16Hz band and that a prominent feature such as this does not occur with the concrete floors.

Future work will need to consider how to use the FEM model to make a fair comparison between the different floors, possibly by adjusting the input force.

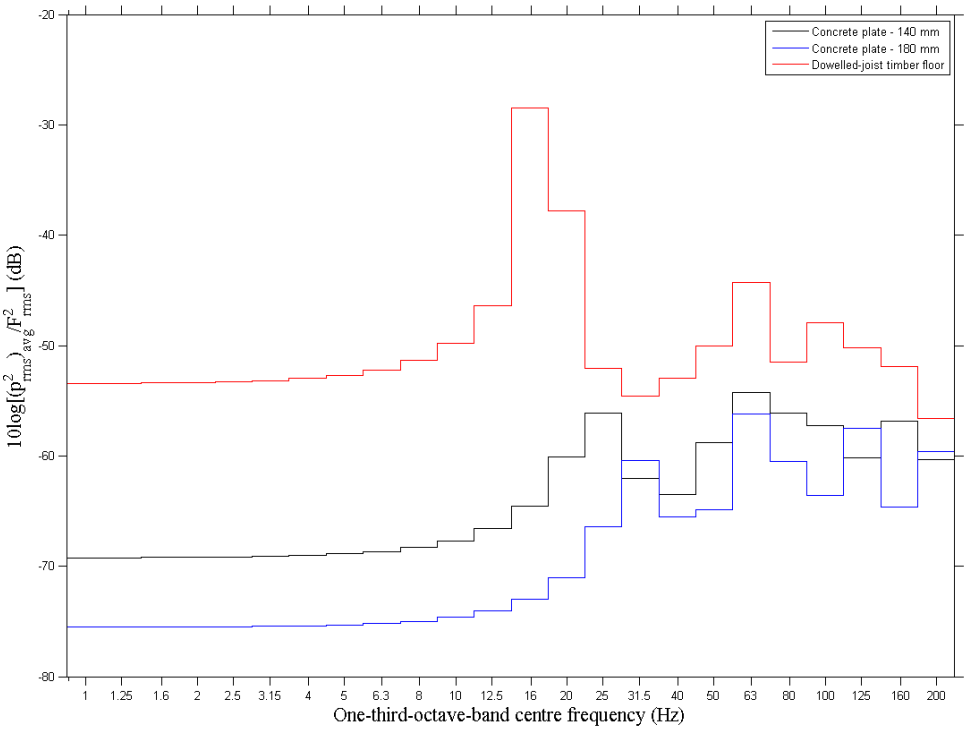

Figure 5-12 Comparison of the dowelled-joist timber floor with the 140 mm and 180 mm concrete plates

5.6 Conclusions

A finite element model has been developed in Abaqus for the prediction of sound radiation from a dowelled-joist timber floor into a rectangular room. In order to accommodate a finite element model of the dowelled-joist floor which had ‘virtual gaps’ between the joists it was necessary to introduce a ‘transfer plate’ to transfer the motion from the dowelled-joist timber floor to the acoustic medium. This approach appears to be novel as no mention of it has been found in the literature. Use of this transfer plate was validated in terms of both vibration and sound radiation.

Compared to the concrete floors the dowelled-joist floor has significant sound radiation around the 16Hz band (the lowest eigen-frequency) and this prominent feature does not occur with the concrete floors. Future work will need to assess whether this is likely to be an issue in a real building when the floor is combined with a floating floor and a ceiling.

6. Conclusions

6.1 Findings

Finite element models for structural response have been developed and validated against experimental modal analysis for (a) individual beam, (b) three individual assemblies and (c) a dowelled-joist floor formed from the three assemblies. A sequence of finite element models of increasing complexity have been developed and assessed in order to achieve the closest agreement with experimental modal analysis for both eigen-frequencies and mode shapes. This resulted in the use of spring connections at the dowel positions combined with precise modelling of the boundary conditions at the two ends of the assemblies. This approach was highly successful for all three assemblies with close agreement in both the eigen-frequencies and the MAC values.

For sound radiation into a rectangular room, a finite element method for fluid-structure interaction has been validated against a normal mode model with both a 140 mm and 180 mm concrete plate. The linear structural element STRI3 is the only Abaqus element that can simulate thin plate bending theory for direct comparison with the normal mode model although the linear and quadratic acoustic elements give similar results. Close agreement was observed between the finite element method and the normal mode model for the frequency of the peaks in the sound pressure level; however there are differences in the peak levels. It was found that the mode-based steady-state dynamic analysis has an advantage over the direct-solution steady-state analysis as it predicts the peak levels with higher accuracy.

A finite element model was then developed to predict sound radiation from a dowelled-joist timber floor into a rectangular room. Two issues needed to be addressed for this complex timber floor. The first concerned the finite element model for the dynamic response of the dowelled-joist floor which used springs at the dowel positions. These springs introduced spurious modes in the eigenvalue analysis that do not correspond to modes observed in the experimental modal analysis. Therefore when this model was used for fluid-structure interaction it was necessary to suppress the effect of these modes through the use of a damping ratio of unity. The second issue concerned the ‘virtual gaps’ between the joists. This made it necessary to introduce a ‘transfer plate’ to transfer the motion from the dowelled-joist timber floor to the acoustic medium. This approach appears to be novel as no mention of it has been found in the literature. Use of this transfer plate was validated in terms of both vibration and sound radiation. Compared to the concrete floors the dowelled-joist floor has significant sound radiation around the 16Hz band (the lowest eigen-frequency)

and this prominent feature does not occur with the concrete floors. Future work will need to assess whether this is likely to be an issue in a real building when the floor is combined with a floating floor and a ceiling.

6.2 Further work

The application of the coordinate modal assurance criterion showed the complex dynamic response of the connection zones in the dowelled-joist timber floor. It would be beneficial to examine the contribution of the connection zones in the dynamic behavior and the radiated sound from the dowelled-joisted timber floor system. One possibility could be to develop two vibroacoustic finite element models of the dowelled-joist timber floor with two and four connection zones respectively and compare the sound radiation results with the results in Chapter 5.

Future work could also implement frequency-dependent damping in the normal mode model so that a comparison could be made with the finite element model for sound radiation from the concrete floors using damping that simulates the in situ total loss factor.

This thesis has validated the model of the dowelled-joist timber floor and developed procedures that can be used to assess the radiated sound into a room by averaging multiple excitation points. The next step is to develop a calculation method that can simulate the force applied by the ISO tapping machine on these different floors to allow a fair comparison of the impact sound insulation of the dowelled-joisted timber floor and the concrete floors. Following this there is potential to investigate methods to reduce the sound radiation from the dowelled-joist timber floor with a ceiling or a floating floor which could also be modelled using the approach to FEM that was developed in this thesis.

References

Blevins, R. D., 1995. *Formulas for Natural Frequency and Mode shape*. s.l.:Krieger Publishing Company.

Chopra, A. K., 2006. *Dynamics of Structures.* 3rd ed. New Jersey: Prentice Hall.

Dahl, K. B., 2009. *Mechanical Properties of Clear Wood from Norway Spruce, Doctotal theses*. Trondheim: Norwegian University of Science and Technology.

de Silva, C. W., 2005. *Vibration and shock handbook.* 1st ed. Boca Raton: Taylor & Francis.

Ewins, D. J., 2000. Model Validation: Correlation for updating. *Sadhana,* 25(3), pp. 221-234.

Fahy, F. & Gardonio, P., 2007. *Sound and Structural Vibration.* 2nd ed. Amsterdam: Elsevier.

Friswell, M. I. & Mottershead, J. E., 1995. *Finite Element Model Updating in Structural Dynamics.* 1st ed. Dordrecht: Kluwer Academic Publishers.

Getzner, 2012. *Sylomer, SR450.* [Online] Available at: http://www.getzner.com

Heylen, W. & Avitabile, P., 1998. *Correlation Considerations - Part 5: Degree of freedom correlation techniques.* Santa Barbara, California, Society for Experimental Mechanics.

Hibbitt, D., Karlsson, B. & Sorensen, P., 2012. *Abaqus 6.12 Documentation and User Manual.*. Providence, Rhode Island, USA: Dessault Systemes Simulia Corp..

Hopkins, C., 2007. *Sound Insulation.* 1st ed. Amsterdam: Elsevier/Butterworth-Heinemann.

Hopkins, C., 2011. *Derivation for a point-excited plate coupled to a box-shaped space [letter]* [Personal communication] (9 December 2011).

Hutton, D. V., 2004. *Fundamentals of Finite Element Analysis.* 1st ed. New York: McGraw-Hill .

Khennane, A., 2013. *Introduction to Finite Element Analysis Using MATLAB and Abaqus.* 1st ed. Boca Raton: CRC Press, Taylor & Francis Group.

Kihlman, T., 1967. Sound radiation into a rectangular room. Applications to airborne sound transmission in buildings. *Acustica,* Volume 18, pp. 11-20.

Lodygowski, T. & Sumelka, W., 2006. Limitations in application of finite element method in acoustic numerical simulation. *Journal of Theoretical and Applied Mechanics,* 44(4), pp. 849-865.

Mac Donald, B. J., 2013. *Practical Stress Analysis with Finite Elements.* 2nd ed. Dublin: Glasnevin Publishing.

Petyt, M., 2010. *Introduction to finite element vibration analysis.* 2nd ed. New York: Cambridge University Press.

Robinson, M. K., 2012. *Prediction of sound and vibration response using Transient Statistical Energy Analysis. PhD Thesis.* Liverpool: University of Liverpool.

Simmons, C., Hagberg, K. & Backman, E., 2011. *Acoustical Performance of Apartment Buildings - Resident's Survey and Field Measurements* , Borås: SP Technical Research Institute of Sweden.

Appendices

Appendix 1 – Validation of the transfer plate in terms of vibration

Two finite element models of the dowelled-joist timber floor, with and without transfer plate, were compared in terms of eigenfrequencies and mode shapes (Figure A-1and Figure A-2) to ensure that the use of the transfer plate does not change the dynamic characteristic of the floor.

The results of the eigenvalue analysis show that the two models have perfect agreement in terms of eigenfrequencies for all the corresponding mode pairs (45) in the range from 0 to 200 Hz (Figure A-3). In addition, the application of the modal assurance criterion for the 15 first mode pairs (Table A-1) shows perfect correlation in terms of mode shapes. As result, it was validated the use of transfer plate does not alter the dynamic characteristics of the dowelled-joist timber floor.

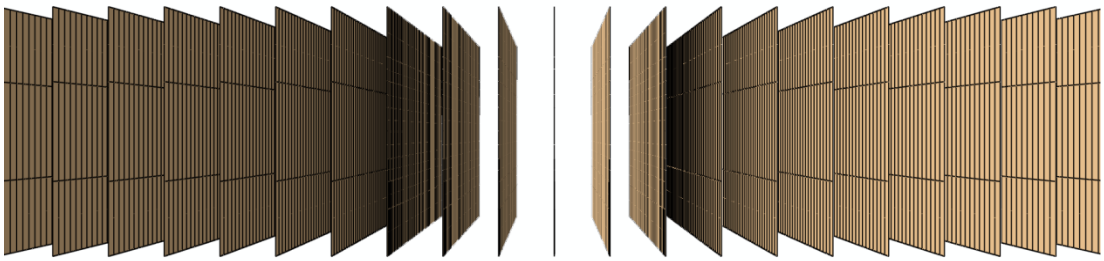

Figure A-1 Finite element model of the dowelled-joist timber floor without transfer plate

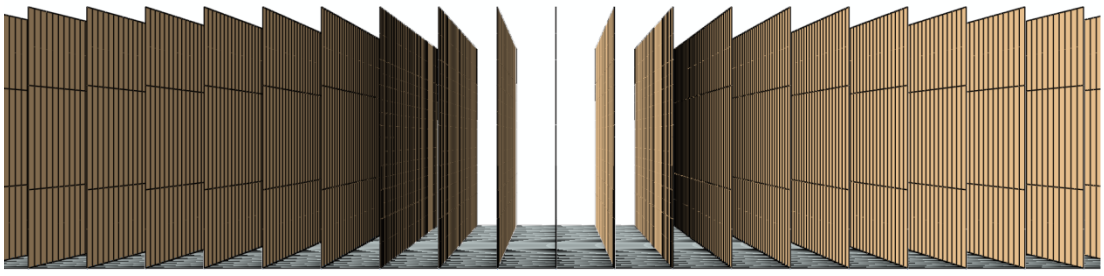

Figure A-2 Finite element model of the dowelled-joist timber floor with transfer plate

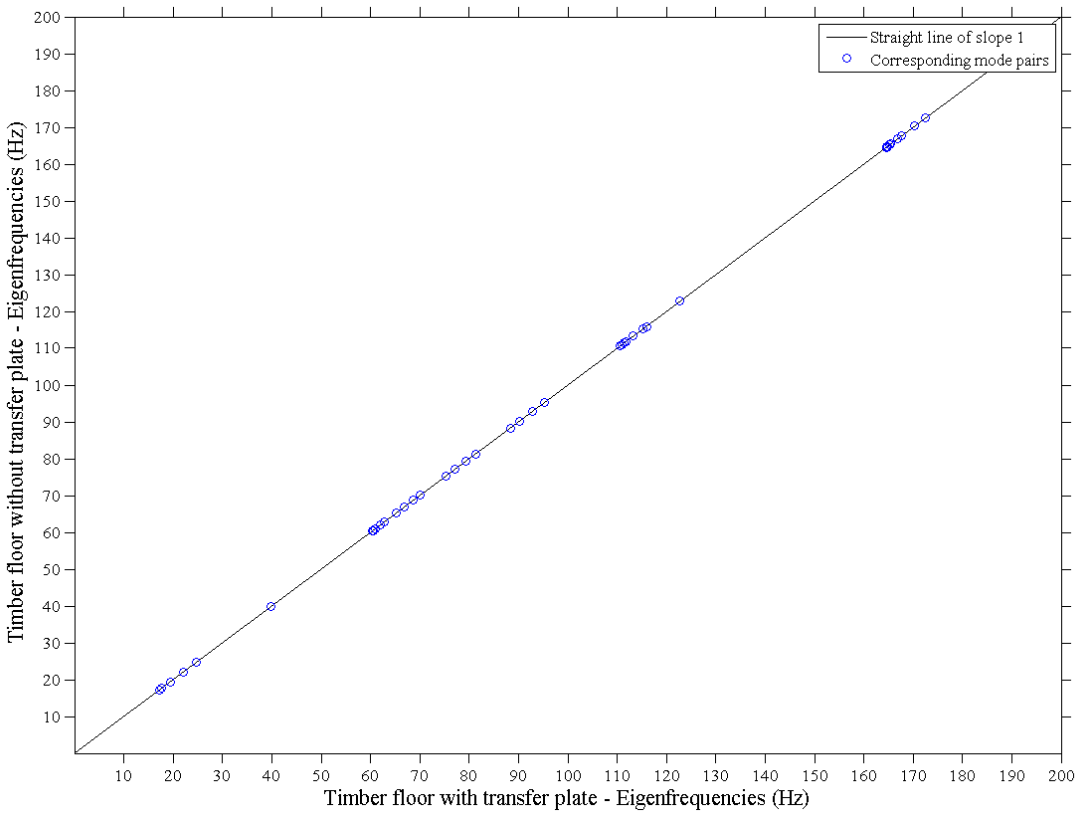

Figure A-3 Comparison of the eigenfrequencies for 41 corresponding mode pairs

Table A-1 Mode shape visual inspection for the first 15 mode pairs

Timber floor without transfer plate	Timber floor with transfer plate	MAC [%]
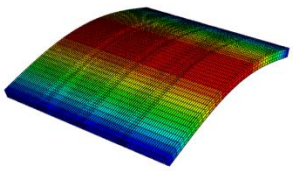	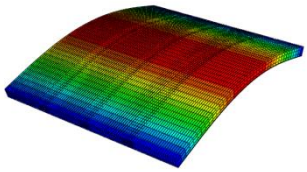	*Perfect correlation in terms of frequencies and mode shapes*
Mode 1: 17.141 Hz	Mode 1: 17.141 Hz	100
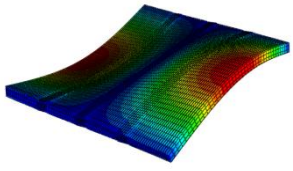	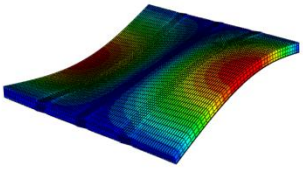	*Perfect correlation in terms of frequencies and mode shapes*
Mode 2: 17.728 Hz	Mode 2: 17.728 Hz	100

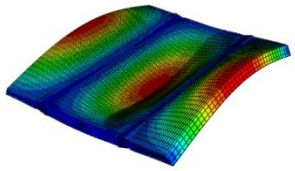	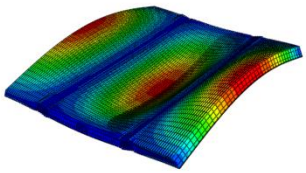	*Perfect correlation in terms of frequencies and mode shapes*
Mode 3: 19.425 Hz	Mode 3: 19.425 Hz	100
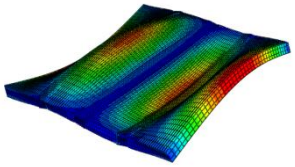	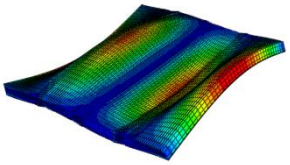	*Perfect correlation in terms of frequencies and mode shapes*
Mode 4: 20.088 Hz	Mode 4: 22.089 Hz	100
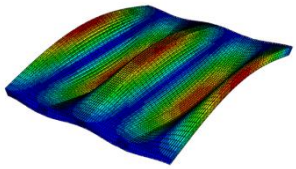	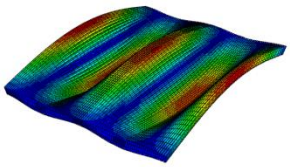	*Perfect correlation in terms of frequencies and mode shapes*
Mode 5: 24.62 Hz	Mode 5: 24.623 Hz	100
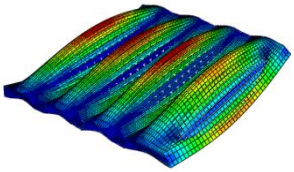	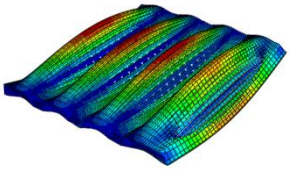	*Perfect correlation in terms of frequencies and mode shapes*
Mode 6: 39.749 Hz	Mode 6: 39.757 Hz	100
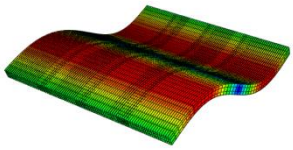	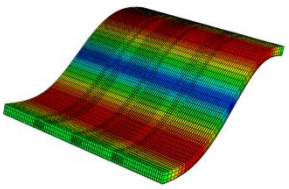	*Perfect correlation in terms of frequencies and mode shapes*
Mode 7: 60.297 Hz	Mode 7: 60.297 Hz	100
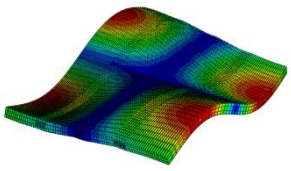	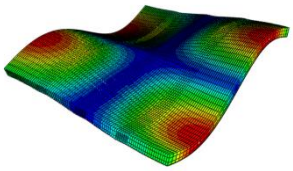	*Perfect correlation in terms of frequencies and mode shapes*
Mode 8: 60.493 Hz	Mode 8: 60.493 Hz	100

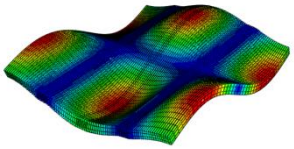	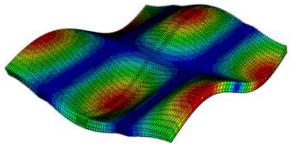	*Perfect correlation in terms of frequencies and mode shapes*
Mode 9: 61.067 Hz	Mode 9: 61.067 Hz	100
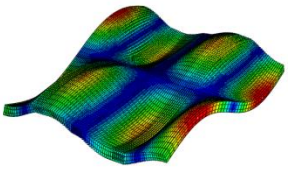	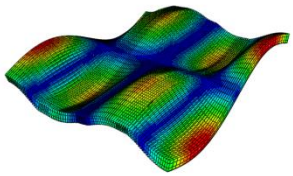	*Perfect correlation in terms of frequencies and mode shapes*
Mode 10: 61.966 Hz	Mode 10: 61.967 Hz	100
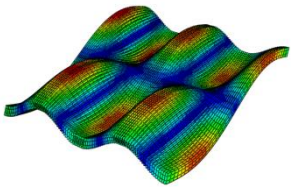	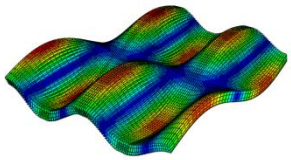	*Perfect correlation in terms of frequencies and mode shapes*
Mode 11: 62.811 Hz	Mode 11: 62.812 Hz	100
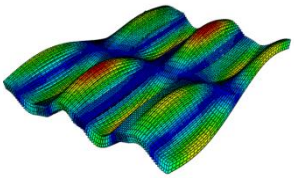	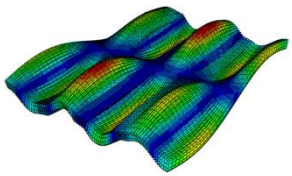	*Perfect correlation in terms of frequencies and mode shapes*
Mode 12: 65.186 Hz	Mode 12: 65.188 Hz	100
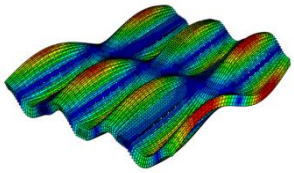	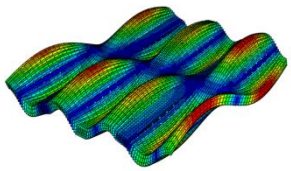	*Perfect correlation in terms of frequencies and mode shapes*
Mode 13: 66.91 Hz	Mode 13: 66.913 Hz	100
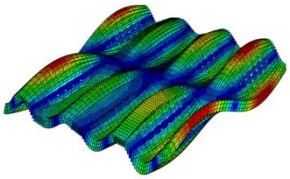	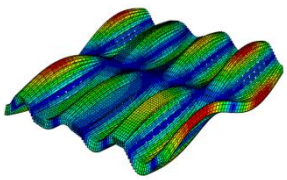	*Perfect correlation in terms of frequencies and mode shapes*
Mode 14: 68.72 Hz	Mode 14: 68.723 Hz	100

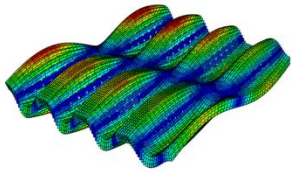	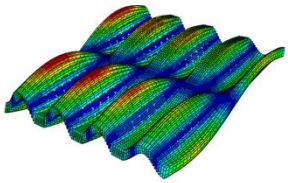	*Perfect correlation in terms of frequencies and mode shapes*
Mode 15: 70.094 Hz	Mode 15: 70.098 Hz	100

Appendix 2 – Validation of the transfer plate in terms of sound radiation

To validate the use of the transfer plate for sound radiation the finite element model for the 140 mm concrete plate from Section 4.3 was used. A comparison is made of this model without and with a thin transfer plate between the concrete plate and the acoustic medium as shown in Figure A-4. Tie constraints were used for the interaction of the transfer plate with the concrete plate and with the acoustic medium (Table A-2). The material properties of the concrete plate (see Section 4.3.2) were adopted also for the transfer plate but by applying reduction factors for the density (a factor of 10^{-6}) and the Young modulus (a factor of 10^{-5}). The force position and sound pressure positions were the same as in Section 4.3.5.

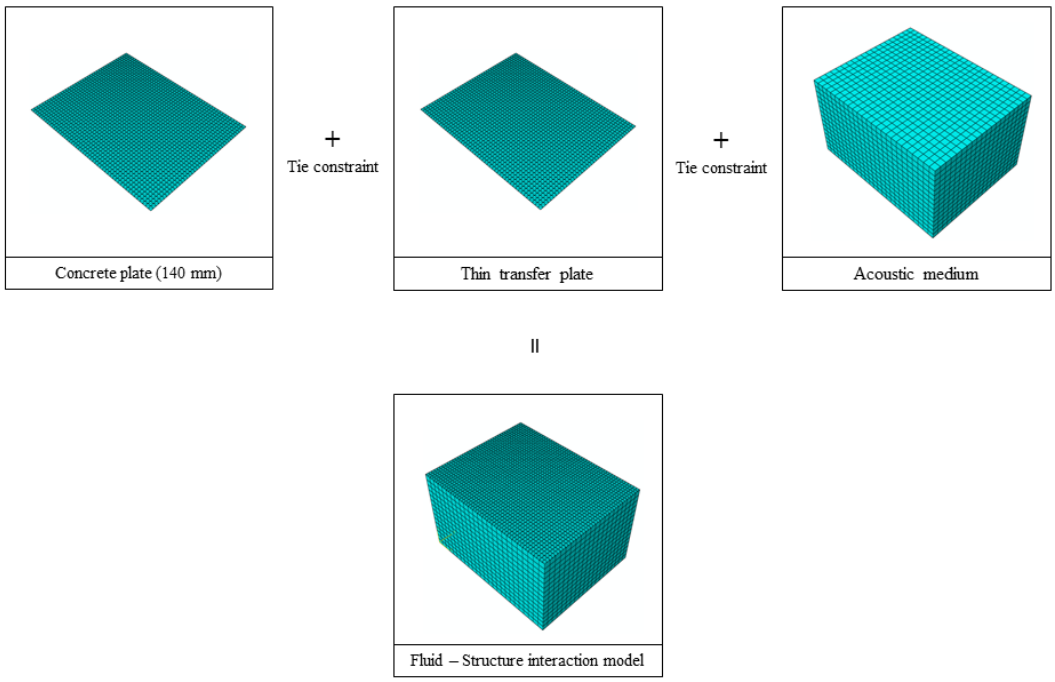

Figure A-4 Finite element model for the validation of the transfer plate in terms of sound radiation

Table A-2 Tie constraint dependencies between the parts of the finite element model

	Master	Slave
Concrete plate – Transfer plate	Concrete plate	Transfer plate
Transfer plate – Acoustic medium	Acoustic medium	Transfer plate

Figure A-5 shows the results of the mode-based steady-state analysis for the two finite element models with and without transfer plate (see Section 4.4.1). Exact agreement was achieved between the two models thus; therefore it can be concluded that the use of the thin transfer plate between a structure and an acoustic medium does not alter the fluid-structure interaction.

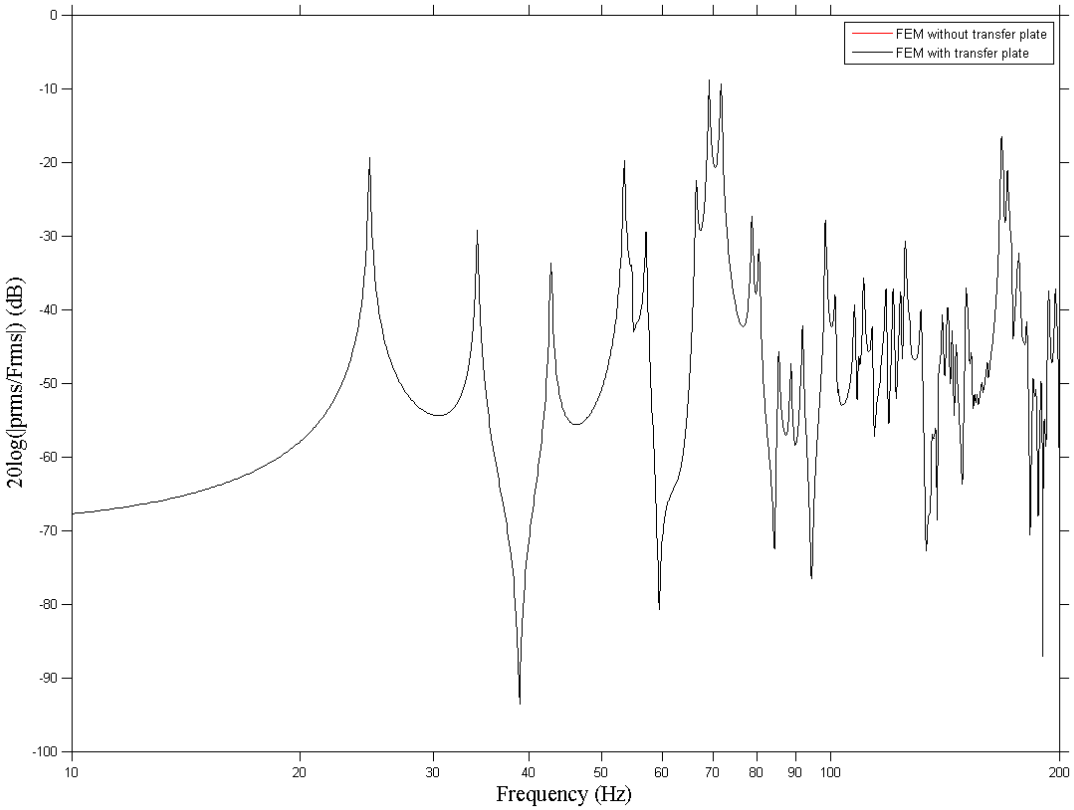

Figure A-5 Comparison of two finite element models, with and without transfer plate, in terms of acoustic pressures near the corner of the rectangular room (0.2 m, 0,2 m, 0.2 m)

Appendix 3 – Modes excluded from the mode-based steady-state dynamic analysis

Figure A-6 - Figure A-9 show three representative examples of the modes that were not included in the mode-based steady state analysis because they were not observed in the experimental modal analysis.

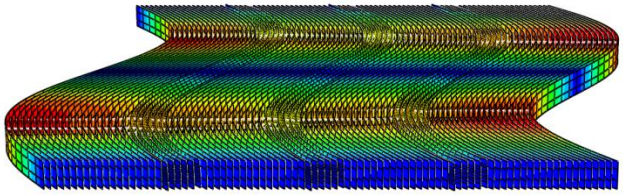

Figure A-6 In plane mode 1

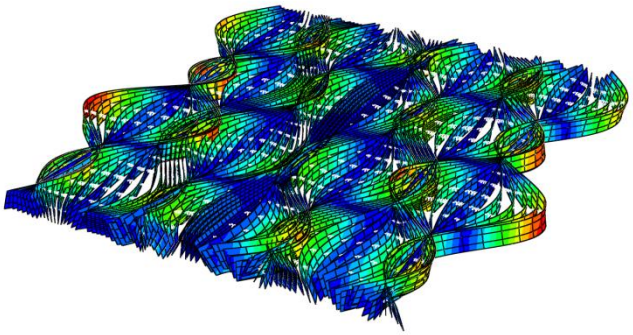

Figure A-7 In plane mode 2

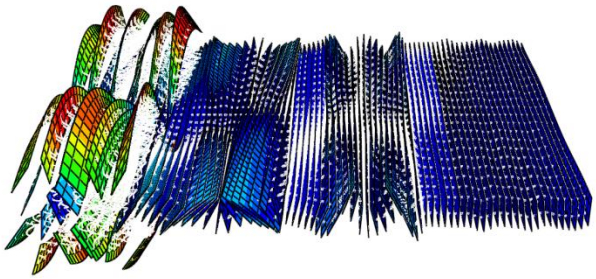

Figure A-8 Local spring mode 1

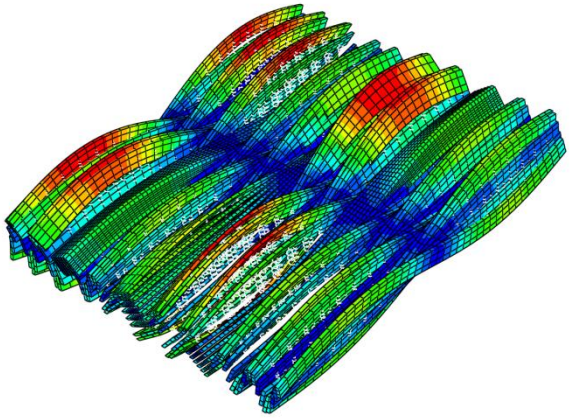

Figure A-9 Local spring mode 2